THE PLASTIC DEFORMATION OF CRYSTALLINE MATERIALS SUBJECTED TO CONSTANT RATE CONDITIONS.

BY

Manohar Lal Aggarwal

A thesis submitted to the School of Graduate Studies in partial fulfilment of the requirements for the degree of Master of Applied Science in Mechanical Engineering at the University of Ottawa.

December, 1972

ABSTRACT

A theoretically rigorous expression, derived from the fundamental equation of rate processes was utilized to describe the yield phenomenon in crystalline materials. The constant strain rate and the constant stress rate conditions were analyzed and the effects of the various parameters influencing the stress-strain characteristics in the yield region were studied.

The widely differing yield behaviour of materials in the constant strain rate condition has been rationalized in terms of the shape and height of the energy barrier. The investigation was carried out over a wide temperature range where the activation volume was varied from 1 b^3 to 10^4 b^3 and the activation energy up to 2.5 eV, the highest physically reasonable values. The yield stress was observed to be a sensitive function of the temperature at activation volumes less than about 10^2 b^3 and the temperature sensitivity was relatively weak for larger activation volumes. The yield drop was found to have a maximum in the intermediate temperature range while it vanished at very low and very high temperatures.

In constant stress rate tests, the initial density of mobile dislocations and the work-hardening rate were observed to have significant effects on the yield region characteristics.

ACKNOWLEDGEMENT

The author is greatly indebted to Dr. A.S. Krausz, under whose supervision this research project was carried out, for his valuable suggestions, critical discussions and constant encouragement.

He also wishes to express his sincere thanks to the National Research Council of Canada and the Department of Mechanical Engineering, University of Ottawa, for the financial support in the form of Research and Teaching Assistantships. The courtesies extended by the personnel of the Computing Centre of the University of Ottawa are highly appreciated.

The help and encouragement from his colleagues, Mr. H.S. Raina and Mr. A.T. Chetty in particular, are gratefully acknowledged.

TABLE OF CONTENTS

LIST OF FIGURES

LIST OF TABLES

NOMENCLATURE

A	Area of cross-section of the specimen.
A'	Constant defined in Eqn. (2.14).
b	Burgers vector.
d	Length of the dislocation loop involved in activation.
E	Elastic modulus of material.
ΔE	Activation energy.
ΔE_W	Energy supplied by the applied stress.
F	Applied force.
g_i	Degree of degeneracy of the ith energy level.
H	Work-hardening coefficient.
h	Planck's constant.
K	Combined spring constant of the specimen and testing machine.
K'	Spring constant of the testing machine.
k	Boltzmann constant.
k	Rate constant.
L	Length of the specimen.
ℓ	Distance between two obstacles.
m'	Mass of a complex.
n'	Stress exponent in the equation $v = v_o(\tau_{eff}/\tau_o')^{n'}$.
n	Quantum number.
P	Probability.
Q	Partition function.
R	Rate of reaction.
S	Crosshead speed.

Str	Structure.
T	Absolute temperature.
t	Time.
V	Activation volume.
v	Dislocation velocity.
$\bar{v}_c$	Average velocity of the complexes over a barrier.
v_o	Constant in the equation $v = v_o(\tau_{eff}/\tau_o')^{n'}$.
x	Distance covered by the dislocation in overcoming the energy barrier.
y	Crosshead displacement.

GREEK LETTERS

α	Geometrical factor.
β	Dislocation multiplication factor.
δ	Width of the activated state.
$\dot{\gamma}$	Shear strain rate.
γ	Total shear strain.
γ_{po}	Initial shear strain.
γ_{py}	Yield point strain.
ν_o	Frequency of atoms at 0^oK.
ρ	Density of the complexes or dislocations.
ρ_m	Mobile dislocation density.
ρ_o	Initial mobile dislocation density.
κ	Transmission coefficient.

τ Shear stress.

τ_a Applied shear stress.

$\dot{\tau}$ Applied stress rate.

τ_o Yield stress at 0^oK.

τ_o' Constant in the equation $v = v_o(\tau_{eff}/\tau_o')^{n'}$.

τ_y Yield stress.

τ_{yl} Lower yield stress.

τ_{yu} Upper yield stress.

SUBSCRIPTS

b Backward movement of the dislocations.

e Elastic component of strain.

f Forward movement of the dislocations.

p Plastic component of strain.

SUPERSCRIPTS

‡ Activated state.

r Reactant state.

CHAPTER 1

INTRODUCTION

The conspicuous difference between the stress-strain characteristics of mild steel and copper has attracted the interest of engineers and scientists for well over a hundred years. It is only in the last twenty years, however, that some progress has been made in the understanding of the physical cause of this difference. In the early sixties a method was developed by Gilman and Johnston (1,2) for the analysis of the initial region of stress-strain and creep curves utilizing the observed microscopic and macroscopic behaviour of LiF. This approach was later applied to the investigation of the deformational behaviour of metals by Hahn (3) and Cottrell (4). The earlier studies (1,2) were based on an empirical knowledge of the deformation parameters. Later, Gilman and Johnston (5) proposed a semi-empirical model for the analysis of the plastic properties of crystalline materials. While this type of analysis lead to important conclusions they should be replaced by a rigorous theory.

It is necessary to emphasize here that the model representing the plastic behaviour of a certain material has limited applicability unless it can be correlated with the properties associated with the atomic level. It is the purpose of the present study to base the analysis of the flow

behaviour on a rigorous theory derived from quantum statistical mechanics and to obtain information on the mechanism of plastic deformation. The theory thus describes the deformational behaviour in terms of physical quantities, namely, activation energy and activation volume, the characteristic parameters of a flow process.

A peculiarity encountered in the plastic deformation process of crystalline materials is the yield phenomenon observed in stress-strain tests. This phenomenon is of great theoretical interest and technological importance. For instance, in cold forming operations, the plastic deformation associated with localized yielding results in markings on the metal surface, commonly known as stretcher strains. While in the forming of some components these irregularities are of little concern, in the manufacturing of others, for example, motor car bodies, aircraft fuselages, the stretcher strains make it difficult to achieve the high degree of surface finish required prior to painting. The procedures required in consequence of this effect make the production more complicated involving heating and prestraining as well. In certain other engineering processes such as overspeeding of rotor disks and shrink fitting, etc., the body is intentionally stressed beyond the yield regions. It is therefore important that the widely different yield behaviour exhibited by various materials and the dependence of yield on the temperature, rate of deformation and other metal forming variables be rationalized and understood on a rigorous theoretical basis.

1.1 Plastic Stress-Strain Behaviour

Under the effect of external loads, crystalline materials exhibit large plastic flow preceded by a relatively small elastic strain. The elastic stress-strain behaviour of most materials can be described by simple mathematical relations. Plastic deformation, however, is a complex process because it is controlled by several factors.

The equation of state relating the four major variables of plastic deformation, namely, shear stress τ, shear strain rate $\dot{\gamma}$, temperature T, and structure is described as (6,7)

$$\dot{\gamma} = f(\tau, T, Str) \tag{1.1}$$

The plastic process can therefore be described if this functional form is known. Eqn. (1.1), in principle, describes the stress-strain relation for any mode of plastic deformation.

To establish Eqn. (1.1), it is necessary to understand the process of plastic deformation from a consideration of the structural changes which take place at the atomic level during the process. The plastic deformation in crystalline materials occurs by one atomic plane gliding over another in a definite crystallographic direction. The slip does not occur as a rigid body translation but by the discrete movement of rows of atoms progressing by one lattice distance in succession. The process is associated with breaking and

establishing of atomic bonds across the slip plane. The boundary between the slipped and unslipped areas of a slip plane is called a dislocation.

Plastic deformation is thus the consequence of dislocation motion which essentially is an atomic phenomenon. A physical understanding of the plastic flow process can, therefore, be derived only from a study of the laws which control the behaviour of an ensemble of atoms.

The atoms in a crystal structure are always in random thermal vibration about their equilibrium positions with amplitudes increasing with temperature. The effect of the applied stress on these thermal fluctuations is to increase the probability of the atoms attaining higher energy levels. The interatomic forces are, thus, overcome under this joint effort as the dislocation moves across the crystal bringing about a permanent shape change.

The dislocation glide in the crystal structure encounters obstacles to its motion. These obstacles may arise when the dislocation passes through the strain field of others, when it approaches solute atoms and vacancies, the intersection with precipitated secondary phases, and other effects (8). The lattice is distorted due to the presence of these obstacles. The size of an obstacle is defined by the extent of the disturbed lattice region. An obstacle is thus essentially an atomic configuration associated with an energy greater than the work that can be performed by the applied stress.

The energy field encountered by a moving dislocation is shown in Fig. (1.1). The energy level ΔE_W due to the applied stress is high enough to carry the dislocation, $\perp$, over the periodic energy field of the crystal lattice and over other small obstacles. It is stopped, however, at a barrier where the energy level is higher than ΔE_W. The dislocation can overcome the barrier only when the atomic rearrangement and the energy correspond to that associated with the activated state, $\ddagger$. The energy difference $(\Delta E^{\ddagger} - \Delta E_W)$ necessary for the process has to be supplied by the thermal energy of the crystal. Depending upon the amplitude of thermal fluctuations, the dislocation waits in front of the barrier until the combined effect of stress and thermal energy, through random movements, is sufficient to move the dislocation across the barrier. The process of dislocation movement from one side of the energy barrier to the other depends on the statistical thermodynamic probabilities. The dislocation mobility is, in consequence, controlled by the stress-biased thermally activated process of overcoming the energy barriers. Once an obstruction is overcome, the dislocation moves at a high velocity until it encounters another obstacle. The time to travel the distance between the energy barriers is small compared to the time it has to wait in front of a barrier. The rate of deformation is therefore described by the rate at which an obstruction to flow is cleared.

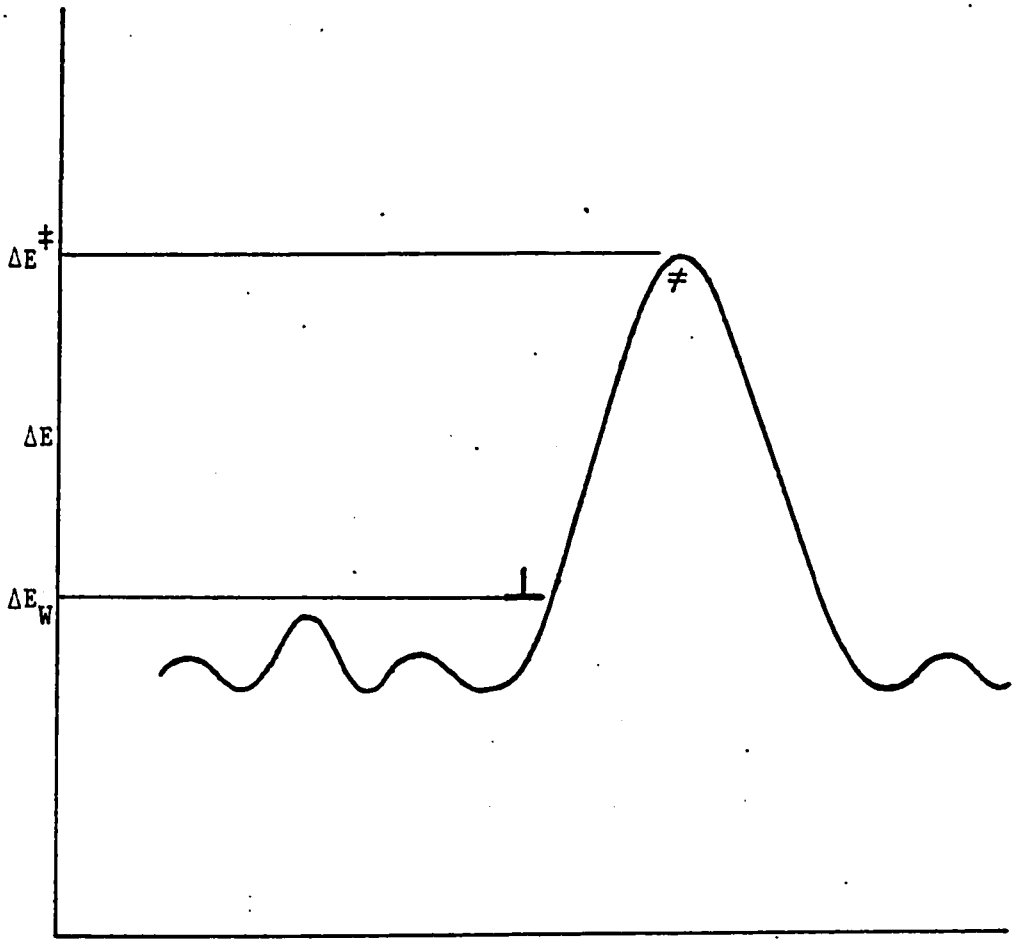

Fig. 1.1 The energy field encountered by a moving dislocation

Considering now that the dislocation velocity is controlled by thermal activations and affected by the applied stress, the functional dependence is expressed as

$$v = v(\tau, T, Str) \tag{1.2}$$

The movement of dislocations is related to plastic shear strain rate, $\dot{\gamma}_p$, by Orowan's equation (9) as

$$\dot{\gamma}_p = \alpha\, b\, \rho_m\, v(\tau, T, Str) \tag{1.3}$$

where b is the Burgers vector, ρ_m is the density of mobile dislocations and α is a geometrical factor.

Eqn. (1.3) describes fully the time dependent flow in crystalline materials. A stress-strain curve is obtained from this equation by describing the dislocation density and the velocity functions. Eqn. (1.3) was used by Gilman and Johnston (1,2) and other investigators (3,4,10) for the theoretical analysis of the yield phenomenon observed in constant strain rate tests. These studies utilized an empirical relation between the dislocation velocity, v, and the effective shear stress, τ_{eff}, expressed as

$$v = v_o(\tau_{eff}/\tau'_o)^{n'} \tag{1.4}$$

where v_o, τ'_o and n' are experimental parameters. Eqn. (1.4) leads to valuable information on the stress dependence of the yield behaviour.

Another empirical equation

$$v = c_1 \tau_{eff}^{n'} \exp(-c_2/T) \tag{1.5}$$

and a semi-empirical equation

$$v = c_3 \exp(-c_4/\tau_{eff}) \exp(-c_5/T) \tag{1.6}$$

was also proposed (5) to represent the temperature dependence of the dislocation velocity. In equations (1.5) and (1.6) the effect of temperature is expressed only partly in an explicit manner because the parameters c_1 to c_5 and n' are empirical values and depend on the temperature (11,12). In fact, a series of constants obtained by data fitting are meaningless in terms of the atomic processes associated with plastic deformation. For a good understanding of the thermally activated flow, its analysis should be based on thermodynamic probabilities and the laws of quantum statistical mechanics.

The present investigation utilizes a rigorous expression for dislocation velocity and replaces the empirical equations (1.4), (1.5) and (1.6).

1.2 Analytical Approach to Derive the Dislocation Velocity Expression

From the phenomenological description of section (1.1) it is established that the dislocation movement is a thermally activated process. Furthermore, the dislocation as well as the obstacles are essentially atomic configurations by which

the lattice is distorted in these regions. The energy of these atomic configurations depends on the amount of the lattice distortion. This means that in order to overcome the obstacle, the complex of atoms delineating the dislocation must first acquire an energy $\Delta E^{\ddagger}$ (Fig. 1.1) necessary for the process. The phenomenon can be conceived by visualizing that a dislocation held in front of a barrier passes from the reactant state 1 (Fig. 1.2) to the product state 2 by going through an activated state $\ddagger$. Because this passage is associated with the breaking and establishing of atomic bonds, the process of plastic flow is identical to a chemical reaction (13). The analytical approach to derive an expression for the dislocation velocity is therefore based essentially on the rate theory of chemical kinetics.

The Rate Theory Model (14,15)

The rate at which the complexes of atoms in state 1 (Fig. 1.2) cross over the barrier is described as

$$R = \frac{\bar{v}_c}{\delta} \rho^{\ddagger} \tag{1.7}$$

where $\bar{v}_c$ = average velocity of the complexes over the barrier.

δ = length associated with the activated state.

$\rho^{\ddagger}$ = number of complexes within the distance δ.

The probability, P, of having local energy fluctuations equal to a magnitude $\Delta E^{\ddagger}$ is given by the Maxwell-Boltzmann distribution (15) as

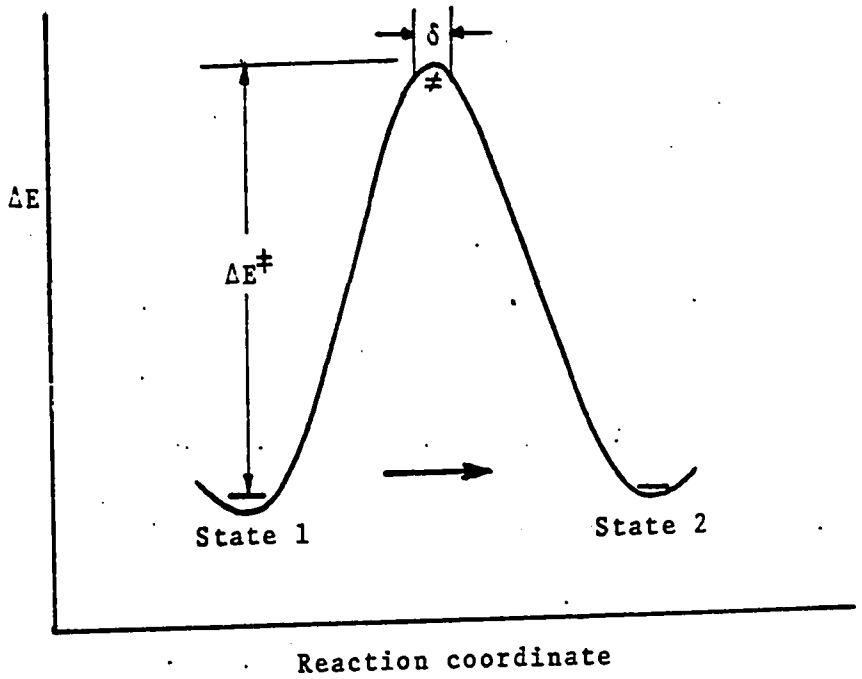

Fig. 1.2 Potential energy curve for the reaction

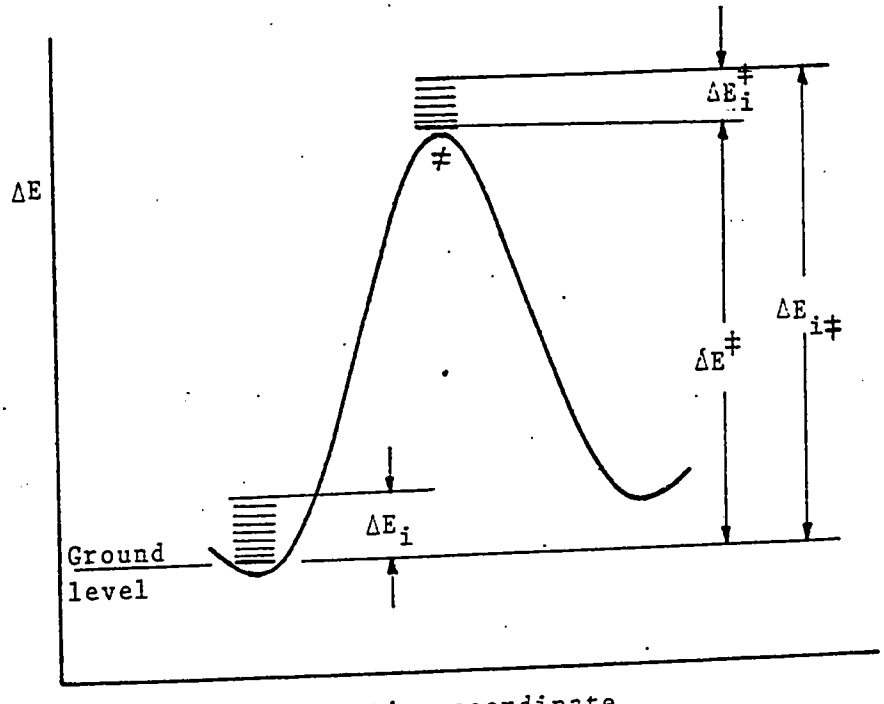

Fig. 1.3 Diagram shows the energy associated with each state

$$P(\Delta E^{\ddagger}) = \text{const. } \exp(-\Delta E^{\ddagger}/kT)$$

For one degree of freedom along the reaction path

$$\Delta E^{\ddagger} = \frac{1}{2} m' v_c^2$$

where m' is the mass of the complex and v_c is the velocity with which it crosses the barrier. The probability of having velocity in an infinitesimal range v_c and $v_c + dv_c$ is, therefore,

$$P(v_c) = \text{const. } \exp(-m'v_c^2/2kT)\ dv_c$$

The average velocity in the forward direction is (14)

$$\bar{v}_c = \frac{\int_0^{\infty} v_c \exp(-\frac{m' v_c^2}{2kT})\ dv_c}{\int_{-\infty}^{\infty} \exp(-\frac{m' v_c^2}{2kT})\ dv_c}$$

$$= (\frac{kT}{2\pi m'})^{1/2}$$

From Eqn. (1.7) the rate of reaction becomes

$$R = (\frac{kT}{2\pi m'})^{1/2} \frac{\rho^{\ddagger}}{\delta}$$

$$= \rho_r k \qquad (1.8)$$

where ρ_r is the number of complexes in state 1 taking part in the process and k is the rate constant. If $\rho_r = 1$, then $R = k$. Thus k is defined as the rate of a single, elementary, process. From Eqn. (1.8)

$$k = \frac{R}{\rho_r}$$

$$= \left(\frac{kT}{2\pi m}\right)^{1/2} \frac{1}{\delta} \frac{\rho^{\ddagger}}{\rho_r} \qquad (1.9)$$

It has been assumed by Eyring (14) that the complexes in state 1 are in equilibrium with those in the activated state. For such a system the number of complexes are proportional to the total partition function (p.f) of the state

$$\frac{\rho^{\ddagger}}{\rho_r} = \frac{Q_{\ddagger}}{Q^r}$$

where $Q_{\ddagger}$ = p.f of the activated complexes referred to the ground level of the initial state (Fig. 1.3).

and Q^r = p.f. of the reactants.

If g_i is the degree of degeneracy of the ith energy level, then from Fig. (1.3)

$$\frac{Q_{\ddagger}}{Q^r} = \frac{\sum_{i\ddagger} g_i \exp\left(-\frac{\Delta E_{i\ddagger}}{kT}\right)}{\sum_i g_i \exp\left(-\frac{\Delta E_i}{kT}\right)}$$

$$= \exp\left(-\frac{\Delta E^{\ddagger}}{kT}\right) \frac{\sum_{i\ddagger} g_i \exp\left(-\frac{\Delta E_i^{\ddagger}}{kT}\right)}{\sum_i g_i \exp\left(-\frac{\Delta E_i}{kT}\right)}$$

or $$\frac{Q^{\ddagger}}{Q^r} = \frac{Q_c^{\ddagger}}{Q^r} \exp(-\frac{\Delta E^{\ddagger}}{kT}) \qquad (1.11)$$

where $Q_c^{\ddagger}$ is the complete partition function of the activated complexes. Because the activated complexes behave in the same manner as the normal ones, except along the reaction coordinate, the p.f for the activated state is

$$Q_c^{\ddagger} = Q_t\ Q_r\ Q_e\ Q_t^*\ Q_v^*$$

$$= Q^{\ddagger}\ Q_t^*$$

where Q_t = translational p.f.

Q_r = rotational p.f.

Q_e = electronic p.f.

Q_t^* = translational p.f. for the vibrational degree of freedom along the reaction coordinate.

Q_v^* = vibrational p.f. without the degree of freedom in the direction of the reaction coordinate.

and $Q^{\ddagger}$ = the p.f. of the activated complexes obtained by omitting Q_t^* from $Q_c^{\ddagger}$.

The degree of freedom associated with the partition function Q_t^* is the rigorous equivalent of what hitherto has been called the reaction coordinate. The translational energy corresponding to the motion of the complexes in this direction is

$$\Delta E_t = \frac{n^2 h^2}{8\ \delta^2\ m'}$$

where n is the quantum number and h is Planck's constant. The corresponding partition function is, therefore,

$$Q_t^* = \sum \exp\left(-\frac{n^2h^2}{8\delta^2\, m' kT}\right)$$

Because the translational energy levels are closely spaced, their distribution can be regarded as continuous. Replacing the summation by integration and integrating from 0 to ∞, one gets

$$Q_t^* = \left(\frac{2\pi\, m' kT}{h^2}\right)^{1/2} \delta$$

Thus

$$Q_t^{\ddagger} = Q^{\ddagger} \left(\frac{2\pi\, m' kT}{h^2}\right)^{1/2} \delta \qquad (1.12)$$

which gives the complete partition function for the activated state. Substituting for $Q_c^{\ddagger}$ in Eqn. (1.11) and combining with (1.10), one gets

$$\frac{\rho^{\ddagger}}{\rho_r} = \frac{Q^{\ddagger}}{Q^r} \left(\frac{2\pi\, m' kT}{h^2}\right)^{1/2} \delta \exp\left(-\frac{\Delta E^{\ddagger}}{kT}\right)$$

Eqn. (1.9) can, therefore, be rewritten as

$$k = \frac{kT}{h} \frac{Q^{\ddagger}}{Q^r} \exp\left(-\frac{\Delta E^{\ddagger}}{kT}\right) \qquad (1.13)$$

which describes the rate constant for a thermally activated process controlled by a single characteristic energy barrier.

If ℓ is the average distance travelled by the dislocation after each activation, the velocity of the process is

$$v = \ell \frac{kT}{h} \frac{Q^{\ddagger}}{Q^{r}} \exp\left(-\frac{\Delta E^{\ddagger}}{kT}\right) \qquad (1.14)$$

A correction must, however, be applied to this expression due to the probability that (i) not every complex reaching the top of the barrier is converted into products; (ii) a reactant may form products without actually passing over the barrier - the so called quantum mechanical tunnelling phenomenon (14).

Eqn. (1.14), in effect, is then modified as

$$v = \kappa \ell \frac{kT}{h} \frac{Q^{\ddagger}}{Q^{r}} \exp\left(-\frac{\Delta E^{\ddagger}}{kT}\right) \qquad (1.15)$$

where κ, the correction factor, is called the transmission coefficient, and is usually assumed to be unity for crystalline materials.

Under the action of the applied stress the height of the energy barrier is reduced. If ΔE_W is the contribution due to the stress acting on the dislocation, the apparent height will be (Fig. 1.4)

$$= \Delta E^{\ddagger} - \Delta E_W$$

Experimental studies (13,16) show that ΔE_W can be assumed to be a linear function of stress expressed as

$$\Delta E_W = V \tau_{eff}$$

where V is the activation volume and τ_{eff} is the effective shear stress acting on the dislocation. From Eqn. (1.15) one gets

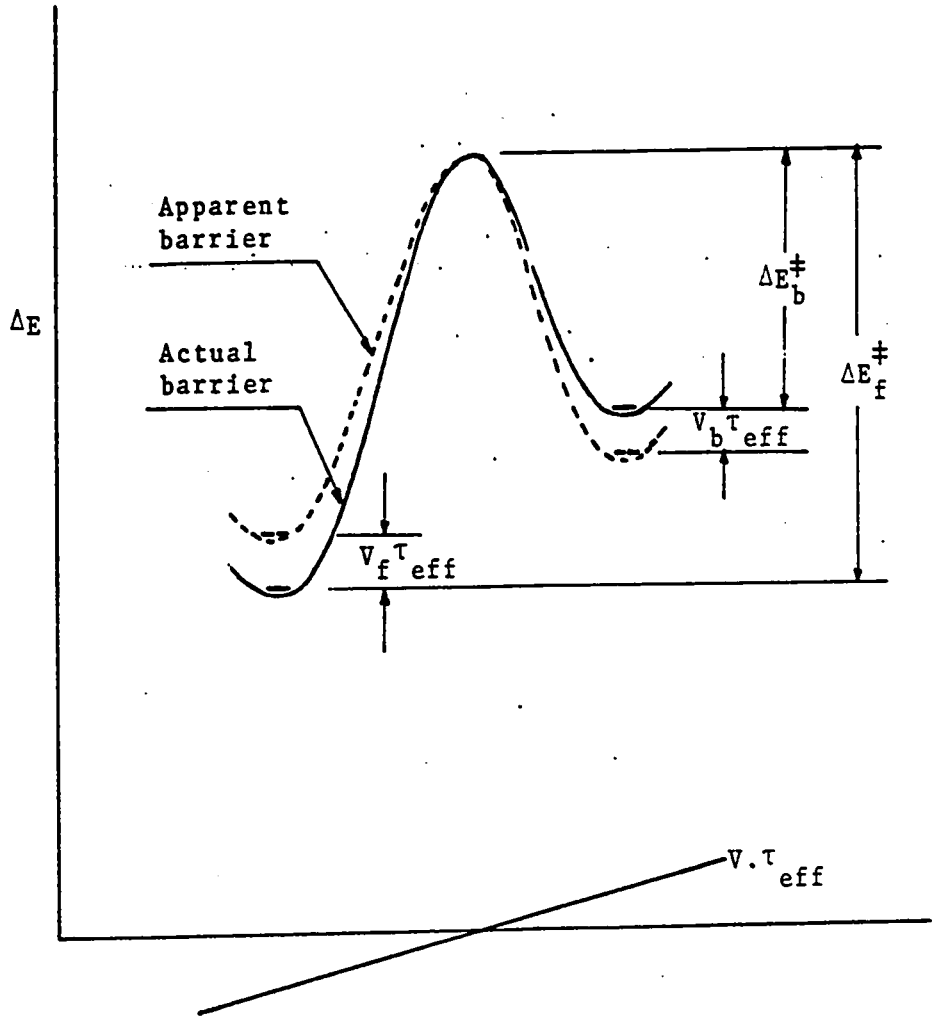

Fig. 1.4 Actual and the apparent shapes of an energy barrier

$$v = \kappa \ell \frac{kT}{h} \frac{Q^{\ddagger}}{Q^{r}} \exp\left(-\frac{\Delta E^{\ddagger} - V \tau_{eff}}{kT}\right)$$

which describes the velocity of the dislocations moving in the direction of the applied stress. A finite probability must, however, be allowed for the backward movement of the dislocations (13). If subscripts f and b denote the quantities associated with the forward and the backward movements respectively, the following expression is obtained for the dislocation velocity

$$v = \kappa_f \ell_f \frac{kT}{h} \frac{Q_f^{\ddagger}}{Q_f^{r}} \exp\left(-\frac{\Delta E_f^{\ddagger} - V_f \tau_{eff}}{kT}\right)$$

$$- \kappa_b \ell_b \frac{kT}{h} \frac{Q_b^{\ddagger}}{Q_b^{r}} \exp\left(-\frac{\Delta E_b^{\ddagger} + V_b \tau_{eff}}{kT}\right) \qquad (1.16)$$

where as illustrated by Fig. (1.4), the effect of stress is to increase the apparent height of the barrier in the backward direction. In addition, the quantities κ_f, ℓ_f, $Q_f^{\ddagger}$, Q_f^{r}, $\Delta E_f^{\ddagger}$ and V_f may or may not be equal to those for the reverse movement. Also these parameters being independent of the stress and the temperature, the expression describes the dislocation velocity in terms of well defined physical quantities and as an explicit function of the temperature.

Referring back to the empirical expression for dislocation velocity (Eqn. 1.4), the stress exponent n' can be shown to be a sensitive function of the stress and the

temperature (11). Fig. (1.5) illustrates its strong dependence on temperature as calculated from Eqn. (1.16), when n' is taken as the minimum slope in the practical region of log v vs. log τ_{eff} plot. The experimental measurements (12) shown in Fig. (1.6) depict a behaviour consilient to that predicted by the Rate Theory.

In a series of investigations, Krausz (11,13) has shown that the two term rate expression (Eqn. 1.16) describes fully the stress and the temperature dependence of the dislocation velocity for a number of crystals, for example, NaCl, Ge, Si, LiF, Al, etc. Rohde and Pitt (16) concluded that this theory represents exactly their experimental data for dislocation velocities in Ni single crystals. In a study on thermally activated flow in Ge, Van Bueren (17) obtained an identical expression. It was also found to explain well the phenomena of stress and strain relaxation (18,19) in single as well as in polycrystalline materials. A similar approach was used by Hahn, Ree and Eyring (20), Krausz and Eyring (21), and many other investigators (22,23) to represent the macroscopic deformation behaviour of metals, minerals and polymers.

Equation (1.16) can, therefore, be used with confidence for the present study to analyze the yield region characteristics of various crystalline materials.

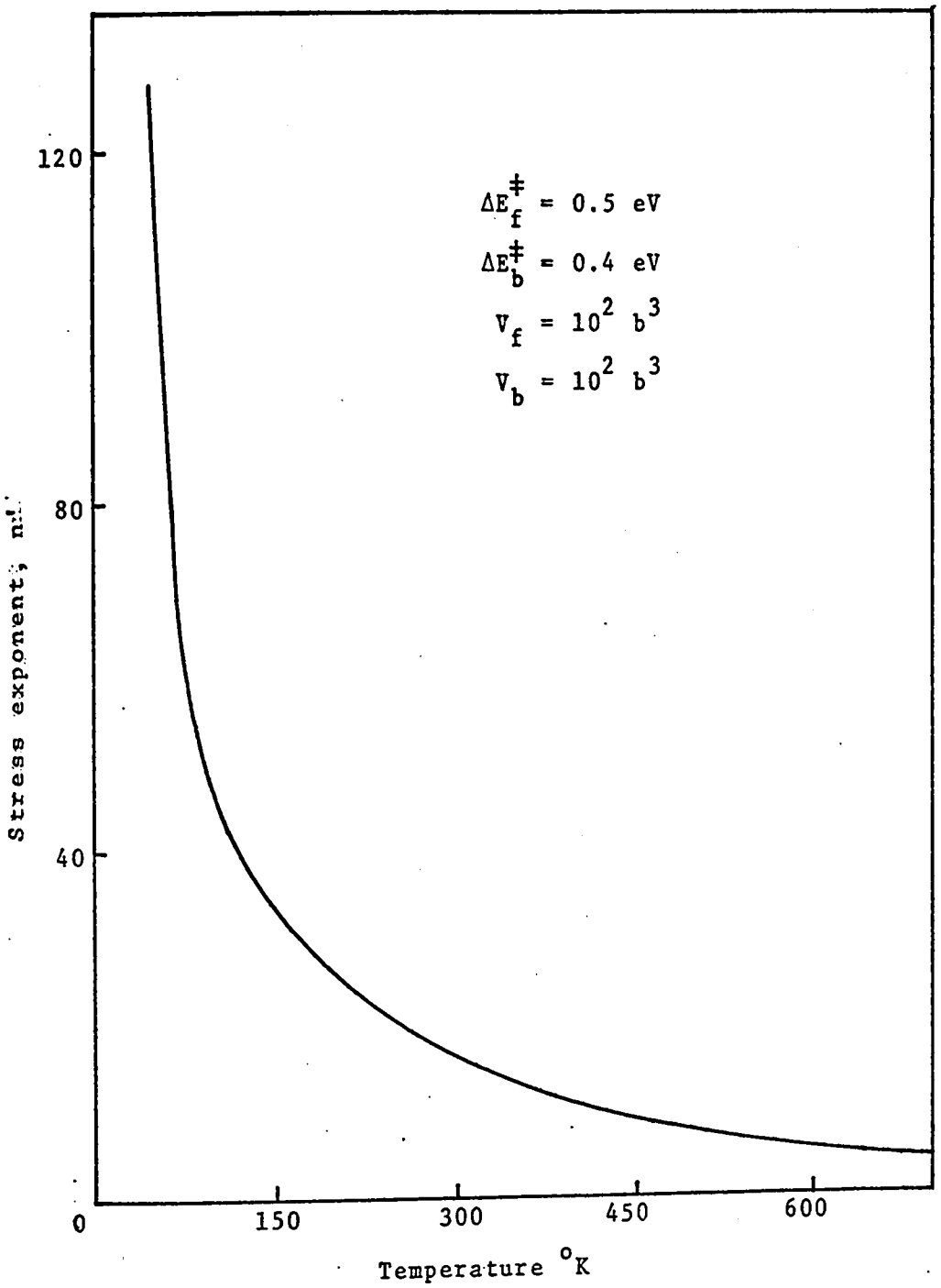

Fig. 1.5 The temperature dependence of the stress exponent, n', as calculated from Eqn. (1.16)

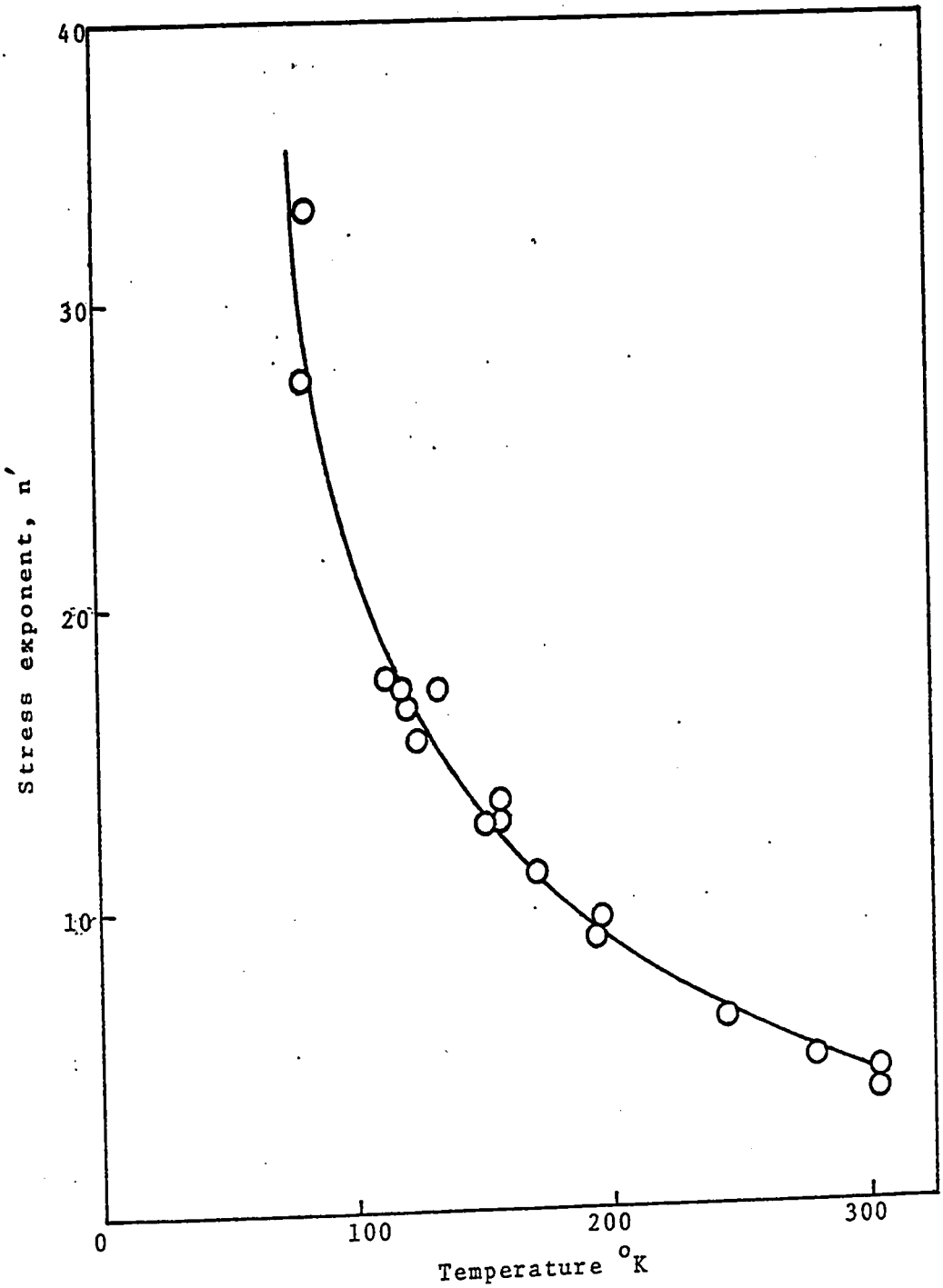

Fig. 1.6 Experimental results for the temperature dependence of the stress exponent, n', measured in iron (12)

CHAPTER 2

THE ANALYSIS OF YIELD BEHAVIOUR

If ρ_m dislocations with Burgers vector b are moving with an average velocity v, then their contribution to the plastic shear strain rate can be expressed as (9)

$$\dot{\gamma}_p = \alpha\, b\, \rho_m\, v \tag{2.1}$$

where α is a geometrical factor. The mobile dislocation density ρ_m, present in the crystal, increases as the material deforms plastically. Measurements with many crystalline materials, for example, LiF (1,2), Fe (3) and Ge (24), etc., have shown that at small plastic strains ($\gamma_p < 0.1$) the variation is linear, and can be expressed approximately as

$$\rho_m = \beta\, \gamma_p$$

where β is the dislocation multiplication factor. Values of the parameter β calculated from recent density measurements (25) are summarized in Table 2.1. In order to extend the description of ρ_m to the smallest strains, the extrapolation stated as

$$\rho_m = \rho_o + \beta\, \gamma_p \tag{2.2}$$

is assumed to be valid (3) for all test conditions. In the above equation, ρ_o is the mobile dislocation density initially present in the crystal.

Table 2.1 Dislocation Multiplication Factor, β (25)

Material	$\beta(10^9/cm^2)$
Ag	230
Al	80
Cu (monocrystal)	100
Cu (polycrystal)	50
Fe (coarse grain, 100μ)	80
Fe (fine grain, 15μ)	200
Fe (3% Si)	200
Ge	1
InSb	0.7
LiF	1
Ni	1
Mo	8
Ta	80
U	90
V	1,000
	400
	500

Combining equations (1.16), (2.1) and (2.2) we get

$$\dot{\gamma}_p = \alpha\, b\, (\rho_o + \beta\, \gamma_p)\Big[\kappa_f\, \ell_f\, \frac{kT}{h}\, \frac{Q_f^{\ddagger}}{Q_f^{r}}\, \exp\Big(-\frac{\Delta E_f^{\ddagger} - V_f\, \tau_{eff}}{kT}\Big)$$

$$- \kappa_b\, \ell_b\, \frac{kT}{h}\, \frac{Q_b^{\ddagger}}{Q_b^{r}}\, \exp\Big(-\frac{\Delta E_b^{\ddagger} + V_b\, \tau_{eff}}{kT}\Big)\Big] \qquad (2.3)$$

Eqn. (2.3) describes the plastic behaviour of crystalline materials in general for any deformation process. An experimental curve that a testing machine should give can be described by this equation by solving it under the deformation conditions imposed on the test specimen. The yield phenomena observed in stress-strain tests may be understood from this expression as follows. Consider the straining of a crystal at a constant rate containing only a single dislocation. The dislocation must move at a fixed velocity to allow the crystal to deform at a specific rate. Because of the relation between stress and velocity, the stress is specified by the required velocity of the dislocation. If the number of dislocations increases to ρ_m, their velocity should decrease in the inverse proportion of the density. A smaller stress is required to move the dislocations at this lower velocity. The stress therefore drops exhibiting an upper yield point. As the material elongates at a lower stress, the density of dislocations increases, causing a hindrance to the motion of one another. This phenomenon is called work-hardening. To maintain the motion of dislocations at a given velocity, the applied stress in turn should rise again. The point at which the stress-strain curve begins to ascend is the lower yield stress.

A different mode of testing, i.e., constant stress rate test, where the material is subjected to a continuously

increasing stress, a drop in the velocity of dislocations is not possible. At the beginning of yielding, the dislocations are forced to move at a faster rate under the imposed stress conditions. The material, therefore, undergoes rapid elongation as it continues to yield until the effects of work-hardening dominate the flow behaviour and thus resulting in a decreased deformation rate.

The yield phenomenon in crystalline materials is, therefore, the result of an increase in the number of mobile dislocations at the start of plastic flow. It is also necessary that there should be at least a small number of mobile dislocations present initially so that multiplication can occur. The condition of the initial mobile dislocation density is zero will not be considered in the present analysis. Furthermore, the analysis excludes any other yield mechanism such as, twinning, geometric softening and work-softening (4).

Equation (2.3) is valid for both the constant strain rate and constant stress rate conditions. While the atomic processes associated with deformation under either of these test conditions are identical, their experimental behaviours show different apparent characteristics. It is, therefore, logical to discuss the methods used in analyzing these experimental results separately.

2.1 The Analysis of Constant Strain Rate Tests

Experimentally, the constant strain rate condition is usually approximated by conducting the tests at a constant crosshead speed, S. If y is the crosshead displacement at time t

$$dy/dt = S = \text{constant}$$

The total crosshead movement is the sum of the elastic deformation of the machine and the specimen y_e, and the plastic deformation of the specimen y_p, thus

$$\begin{aligned} y &= S \cdot t \\ &= y_e + y_p \\ &= F/K + y_p \end{aligned} \tag{2.4}$$

where F is the applied force and K is the combined spring constant of the specimen and the machine elements, defined as

$$\frac{1}{K} = \frac{1}{K'} + \frac{L}{AE} \tag{2.5}$$

This relation may be understood by referring to Fig. (2.1) where K' is a spring constant representing the elastic response of the deforming fixture, and E, L and A are, respectively, the elastic modulus, length and cross-section of the specimen.

Following Halsey, White and Eyring (26) and Johnston (2) the relation between the plastic shear strain and the applied shear stress τ_a is described by the following equation

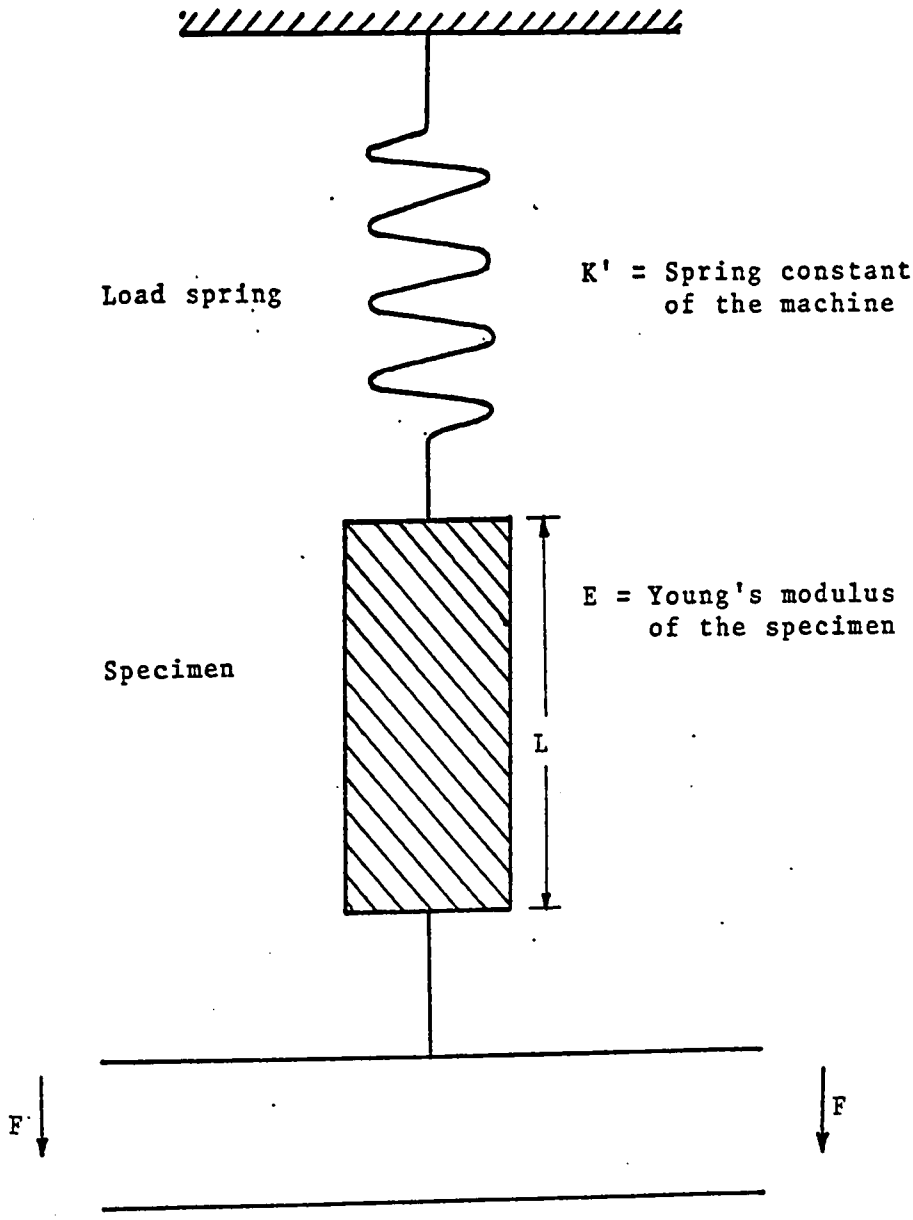

Fig. 2.1 Schematic representation of the elastic elements of a deforming system

$$\gamma_p = (y - \frac{2A}{K} \tau_a)/L$$

In this expression the shear force is assumed to be one half of the applied force.

The plastic strain rate is, therefore,

$$\dot{\gamma}_p = \frac{S}{L} (1 - \frac{2A}{K} \frac{d\tau_a}{dy}) \tag{2.6}$$

The combination of equations (2.3) and (2.6) describes the dependence of the applied stress on the crosshead displacement as

$$\frac{d\tau_a}{dy} = C - D[C(y + \frac{L\rho_o}{\beta}) - \tau_a][A_f T \exp(-\frac{\Delta E_f^{\ddagger} - V_f \tau_{eff}}{kT}) - A_b T \exp(-\frac{\Delta E_b^{\ddagger} + V_b \tau_{eff}}{kT})] \tag{2.7}$$

where $C = K/2A$

$D = \alpha b \beta/S$

$$A_f = \kappa_f \ell_f \frac{k}{h} \frac{Q_f^{\ddagger}}{Q_f^r}$$

$$A_b = \kappa_b \ell_b \frac{k}{h} \frac{Q_b^{\ddagger}}{Q_b^r}$$

and $\tau_{eff} = \tau_a - \tau_i$

$= \tau_a - H\gamma_p$

where the internal stress τ_i is assumed to be a linear function of strain and H is the work-hardening coefficient.

Eqn. (2.7) is a reformulation of the strain rate Eqn. (2.3) incorporating the constant strain rate condition imposed on the specimen. The dependence of the yield behaviour on the parameters ρ_o, K, β and H was analyzed by Gilman and Johnston utilizing the empirical model (1,2). The calculated results were in good agreement with their measurements on LiF. The effect of temperature, however, has never been analyzed before. It is now expressed in a fully explicit manner by the above differential equation. This relation contains, in addition, the activation energies $\Delta E_f^{\ddagger}$, $\Delta E_b^{\ddagger}$ and the activation volumes V_f, V_b as structural parameters, and hence the effect on the yield behaviour due to each of these can be analyzed. Solutions can be obtained for the various levels of these activation parameters, characterizing the size and shape of the energy barrier encountered by a dislocation during its motion.

2.2 Temperature Dependence of the Yield Behaviour

To analyze the effect of temperature on the upper yield stress and the lower yield stress, we use the condition that at these points the applied stress has a local maximum and minimum so that

$$d\tau_a/dy = 0 \tag{2.8a}$$

or from Eqn. (2.6) .

$$\dot{\gamma}_p = S/L \tag{2.8b}$$

i.e., the applied strain rate equals the plastic strain rate. Eqn. (2.7) combined with conditions (2.8a,b) describes the temperature dependence of the yield stress, τ_y, expressed as

$$\frac{S}{L} = \alpha\, b(\rho_o + \beta\, \gamma_{py})[A_f\, T \exp(-\frac{\Delta E_f^{\ddagger} - V_f\,(\tau_y - H\,\gamma_{py})}{kT}) - A_b\, T \exp(-\frac{\Delta E_b^{\ddagger} + V_b(\tau_y - H\,\gamma_{py})}{kT})] \tag{2.9}$$

where γ_{py} is the plastic strain at the yield point.

Because Eqn. (2.9) cannot be solved in closed form, the differential Eqn. (2.7) was integrated numerically to determine the temperature dependence of the yield-point characteristics. A typical set of stress-strain curves computed from this equation over a temperature range is represented in Fig. (2.2). The numerical values assigned to the various parameters are given in Table (2.2)**. The behaviour predicted by the present analysis was found to be in good agreement with the experimental results shown in Fig. (2.3).

Figures (2.2) and (2.3) illustrate a sensitive dependence of the yield behaviour on the temperature. Though some of the curves in these figures appear to exhibit a sharp

---

**Unless otherwise specified, these same values for the various parameters are used in all the calculations that follow.

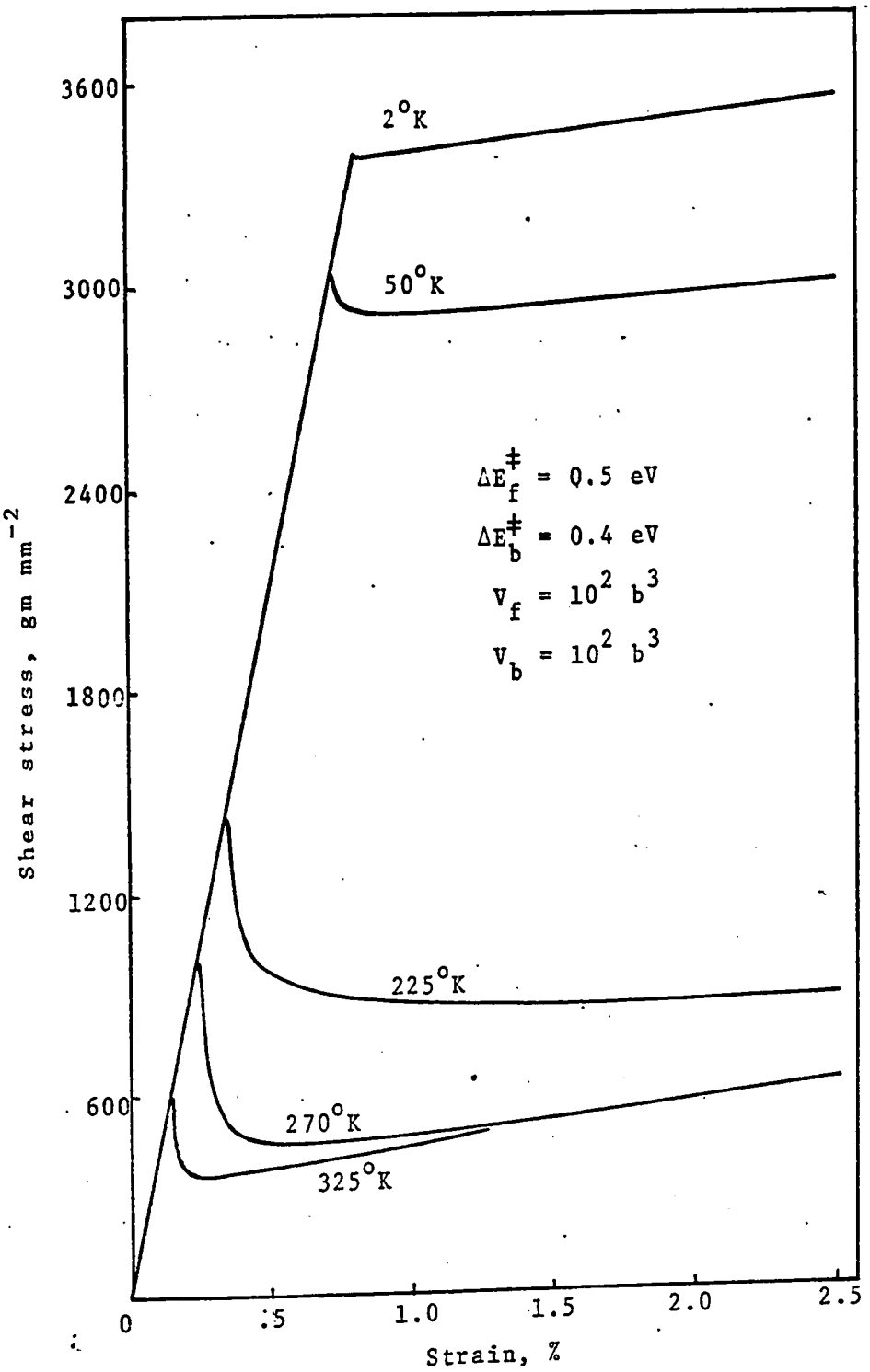

Fig. 2.2 The temperature dependence of the yield point characteristics calculated from Eqn. (2.7)

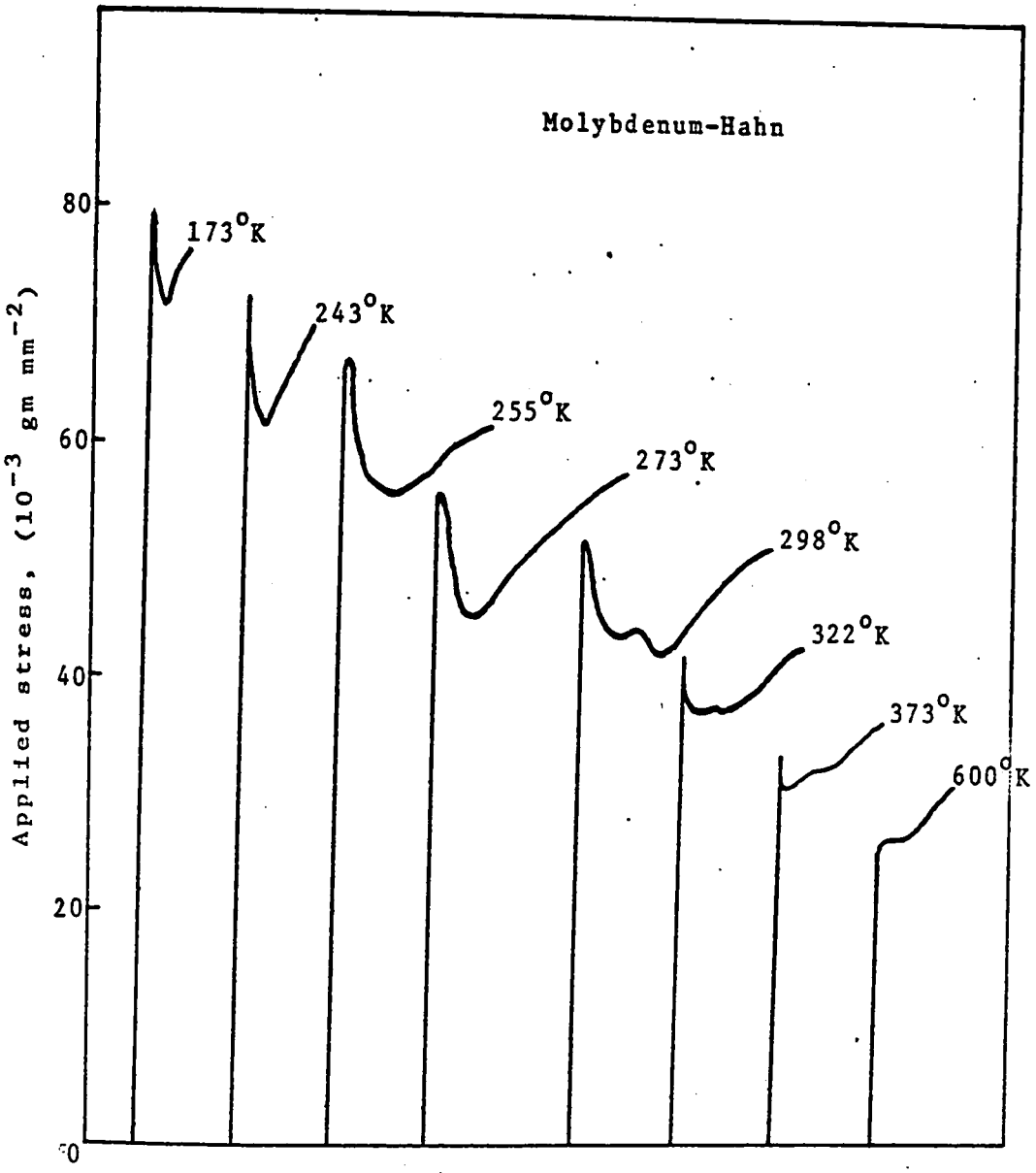

Fig. 2.3 Experimentally observed yield behaviour on molybdenum

Table 2.2 Numerical Values Assigned to Various Parameters in Present Calculations

α	2.0
b	2.9×10^{-8} cm
β	10^{9} disl cm^{-2}
S	2.12×10^{-3} cm sec^{-1}
L	14.02 mm
A	12.50 mm^{2}
ρ_o	10^{2} disl cm^{-2}
H	10^{2} gm mm^{-2} 1% γ_p^{-1}
$\dot{t}$	50.0 gm mm^{-2} sec^{-1}
K = E	7.40×10^{5} gm mm^{-2}
$\kappa_f = \kappa_b$	1.0
$\ell_f = \ell_b$	10.0 b
$Q_f^{\ddagger}/Q_f^{r} = Q_b^{\ddagger}/Q_b^{r}$	1.0

upper yield point, the calculations show that the change of slope does not result abruptly, but occurs smoothly under the condition of continuously increasing mobile dislocations density. A rounded yield point can be shown for all these curves if replotted on an appropriate scale. The extent of rounding seems to depend also on the amount of stress drop between the upper and the lower yield points. These details are not explicit in these figures but will be apparent in

some of the later curves that assume different shapes of the energy barriers (see Fig. 2.8a, b, for instance).

The upper and the lower yield stresses obtained from the above theoretical results are represented in Fig. (2.4). The behaviour is comparable to the experimental observations of many investigators (27-31) as indicated in Fig. (2.5).

In a study on the effect of temperature on the yield stress, Orowan (32) derived the following relation

$$\tau_y = A - B\sqrt{T}$$

where A and B are constants. An examination of the experimental data, however, indicates that the dependence can be better described by the transcendental form of function represented by Eqn. (2.9).

In the low temperature range, Fig. (2.4) indicates an approximately linear dependence of the yield stress on the temperature. This behaviour can be understood easily in terms of Eqn. (2.9) as explained in the following section.

Low Temperature Analysis

At low temperatures the available thermal energy is obviously low and therefore the applied stress has to be high. The backward movement of dislocations under high forward stresses is assumed to be negligible. Eqn. (2.9), in effect, describes the yield stress as

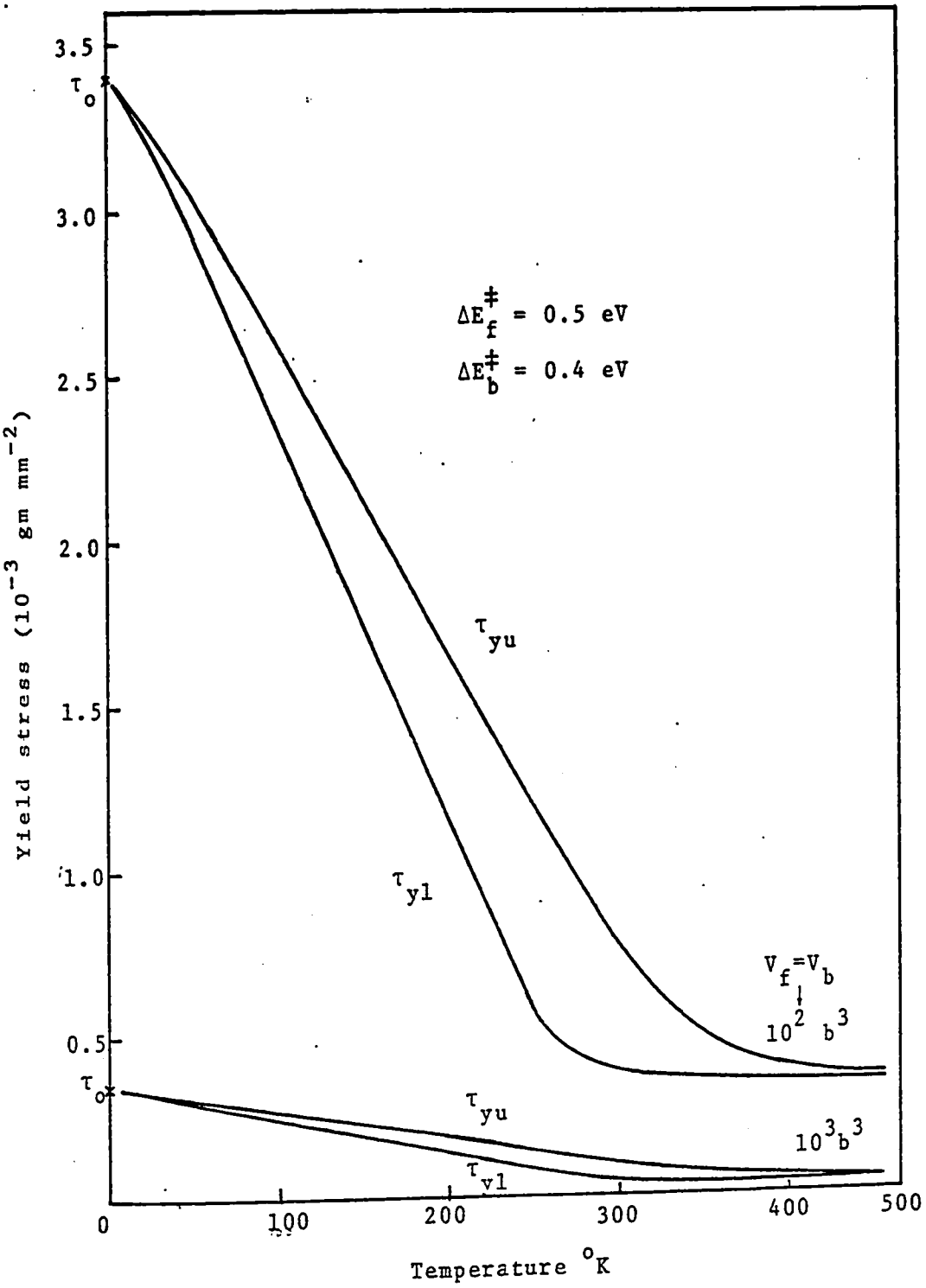

Fig. 2.4 The upper and lower yield stresses as the function of temperature

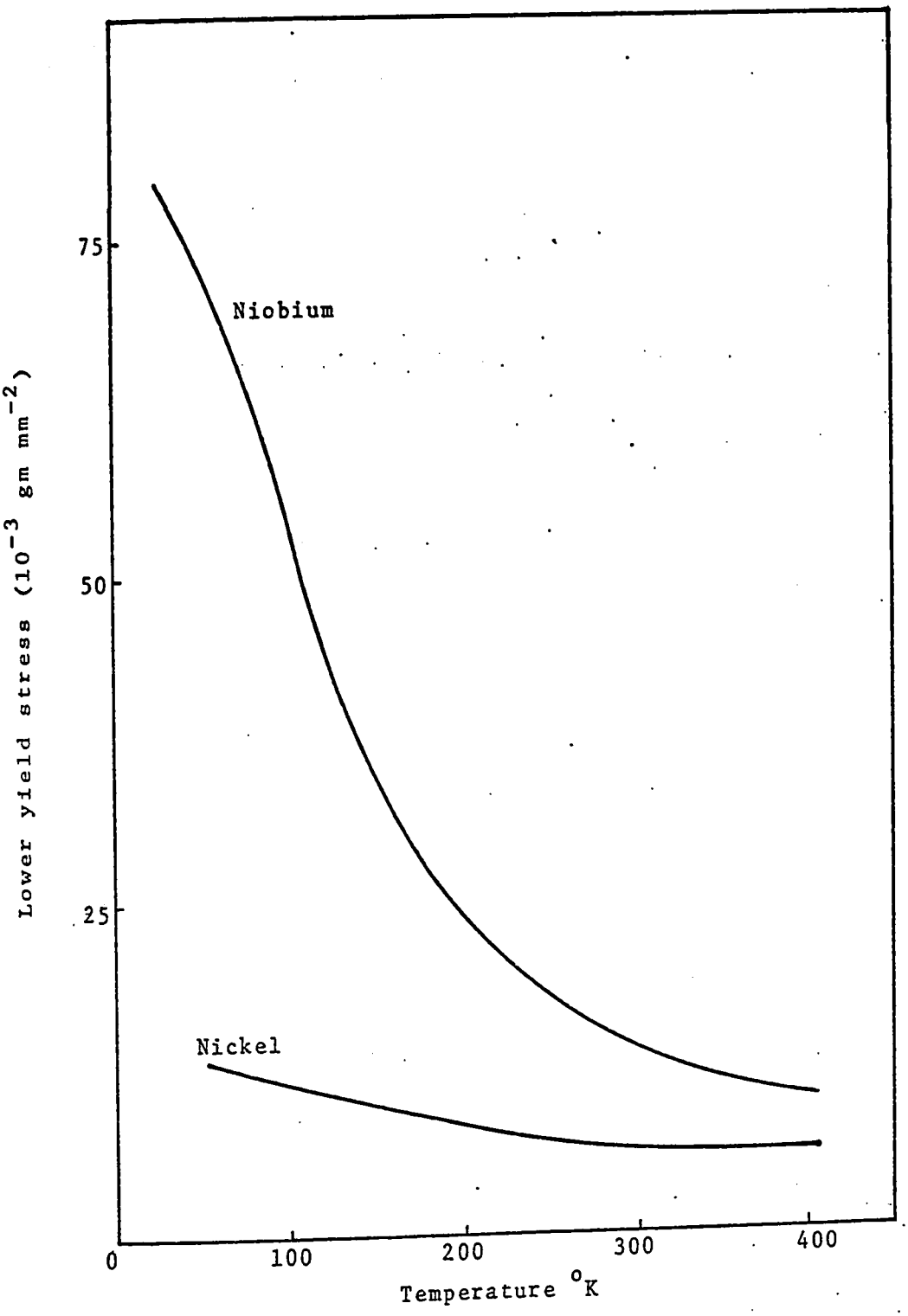

Fig. 2.5 The temperature dependence of the lower yield stress measured in niobium and nickel (27)

$$\tau_y = \tau_i + \frac{\Delta E_f^{\ddagger} - kT \ln \left(\kappa_f \ell_f \frac{kT}{h} \frac{Q_f^{\ddagger}}{Q_f^{r}} \frac{\alpha b \rho_m L}{S}\right)}{V_f} \qquad (2.10)$$

which shows that the temperature dependence of the yield stress is governed by the term T ln T. Except close to $0^{\circ}K$, the function T is more sensitive than ln T, which will consequently result in an approximately linear variation of the yield stress with temperature as has been shown in Fig. (2.4).

Eqn. (2.10) can be used also to predict the yield behaviour at absolute zero. From the quantum mechanical system considered in the present study it is known that (15)

$$\frac{kT}{h} = \frac{1}{2} \nu_o \qquad (2.11)$$

where ν_o is the frequency with which the atoms in the dislocation structure vibrate at $0^{\circ}K$. Combining Eqns. (2.10) and (2.11), the resulting expression with T = 0 gives

$$\tau_o = \tau_i + \Delta E_f^{\ddagger}/V_f$$

which would be the yield stress at the absolute zero temperature. The curves in Fig. (2.4) will, therefore, meet the stress axis at the finite value τ_o, marked in the figure.

Using the results obtained for the upper yield stress, τ_{yu}, and the lower yield stress, τ_{yl}, the percent yield drop defined as

$$(\tau_{yu} - \tau_{yl})/\tau_{yl} \times 100$$

was calculated and the results are shown in Fig. (2.6). The figure illustrates that the yield drop has a maximum in the intermediate temperature range and vanishes both at very low and very high temperatures. The experimental results obtained by Worthington (28) on mild steel (Fig. 2.7a) and by Hahn (3) on molybdenum (Fig. 2.7b) show a similar behaviour. The yield drop decreases in the low temperature range and vanishes on high temperature side, in agreement with the predictions of the present analysis.

2.3 Effect of the Activation Parameters

A. The Effect of Backward Activation Energy

The symmetry of the energy barrier seems to have the greatest effect on the yield behaviour of materials. The calculated stress-strain curves for various forms of energy barriers are shown in Fig. (2.8a,b) in which all the parameters except $\Delta E_b^{\ddagger}$ were kept constant. Fig. (2.9) represents the variation of the percent yield drop as a function of temperature, calculated for a range of backward activation energy values. It is seen that for values of $\Delta E_b^{\ddagger} = \Delta E_f^{\ddagger}$, these curves exhibit pronounced yield drops and for $\Delta E_b^{\ddagger} << \Delta E_f^{\ddagger}$ the drop is negligible. An examination of the activation parameters obtained from direct dislocation mobility studies (Table 2.3) indicates that the stress-strain measurements by Patel (33) on silicon (Fig. 2.10) and by Lucke and Lange (34)

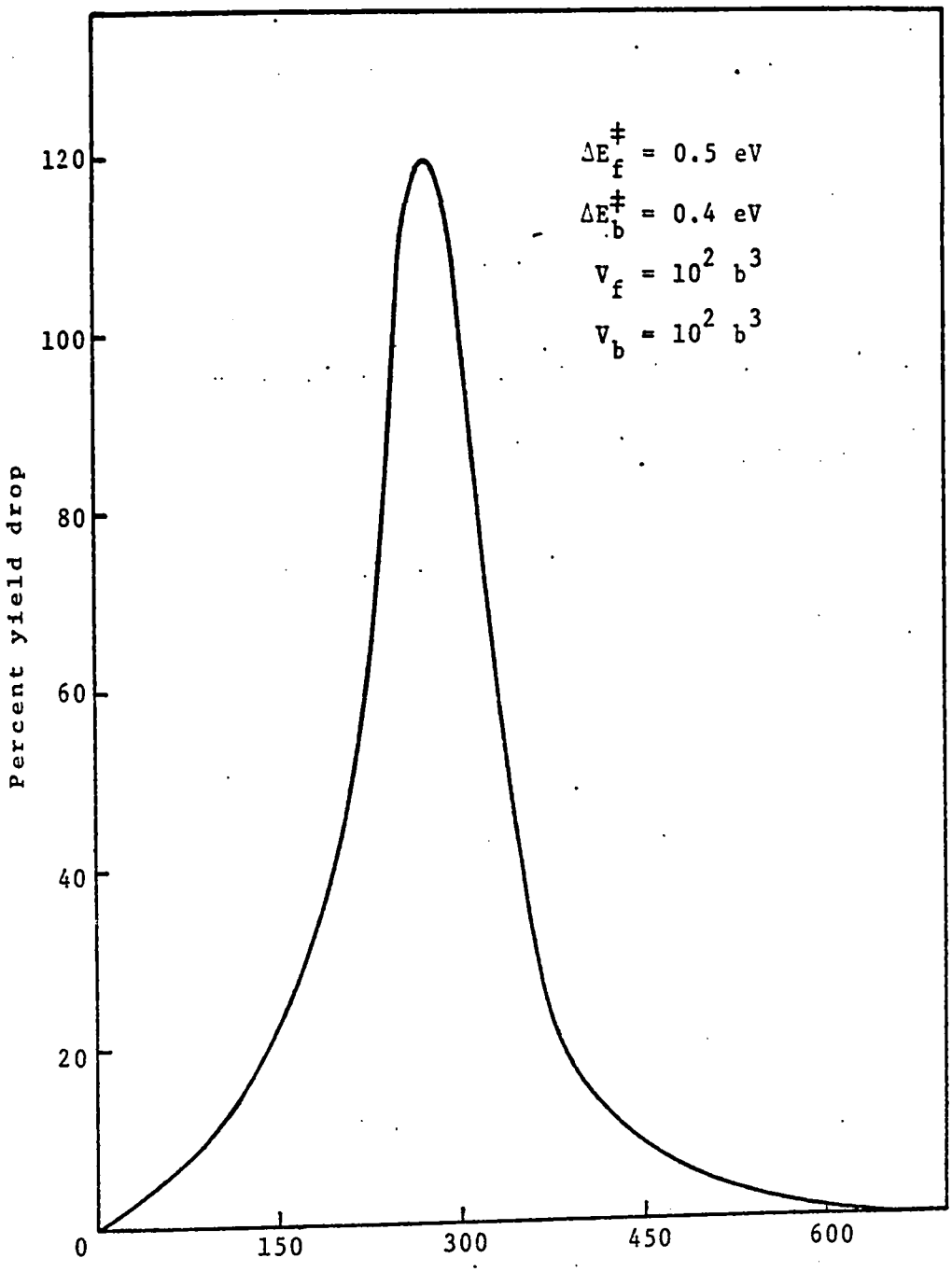

Fig. 2.6 Temperature dependence of the percent yield drop calculated using the results of Fig. (2.4)

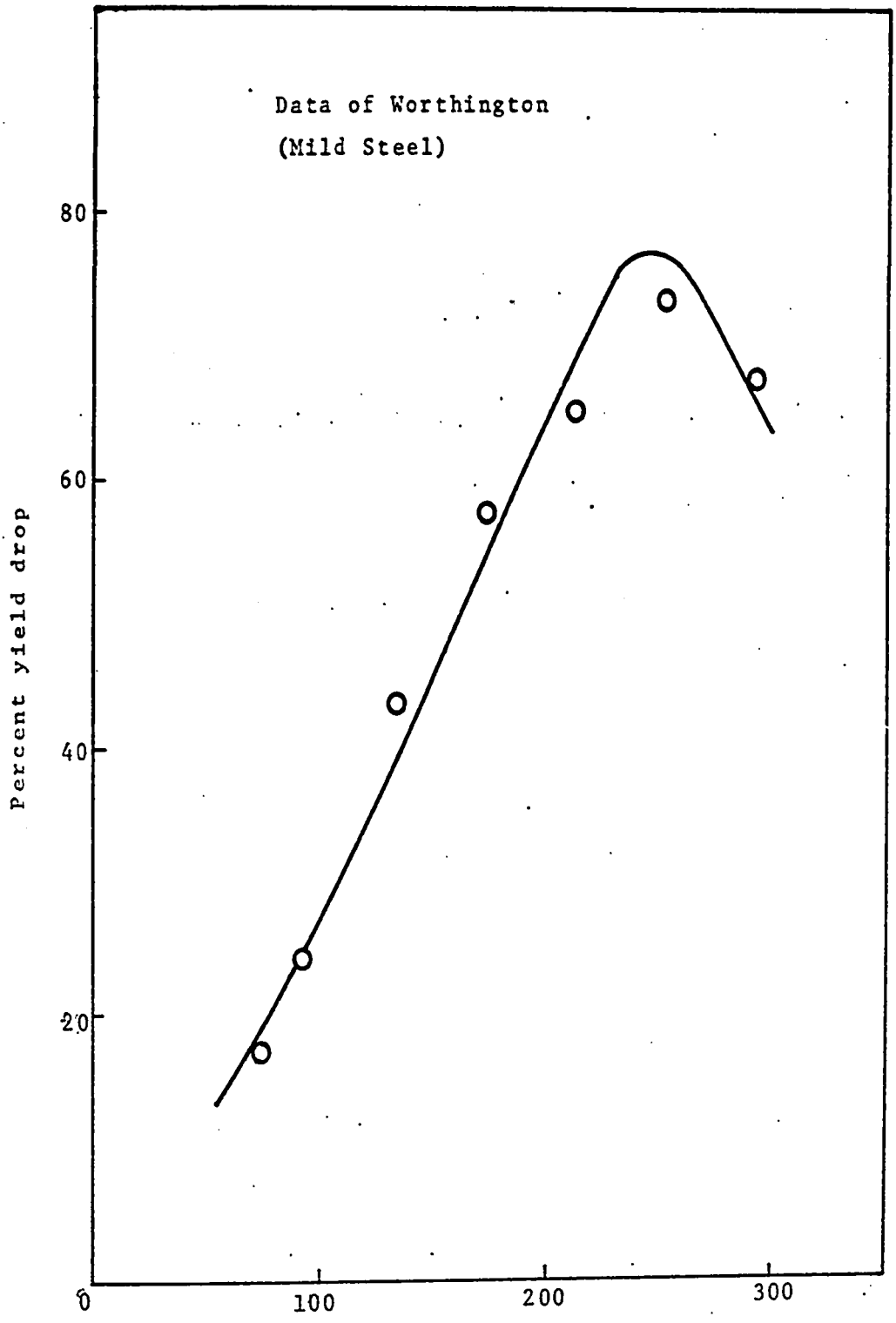

Fig. 2.7a The yield drop as a function of temperature measured in mild steel (28)

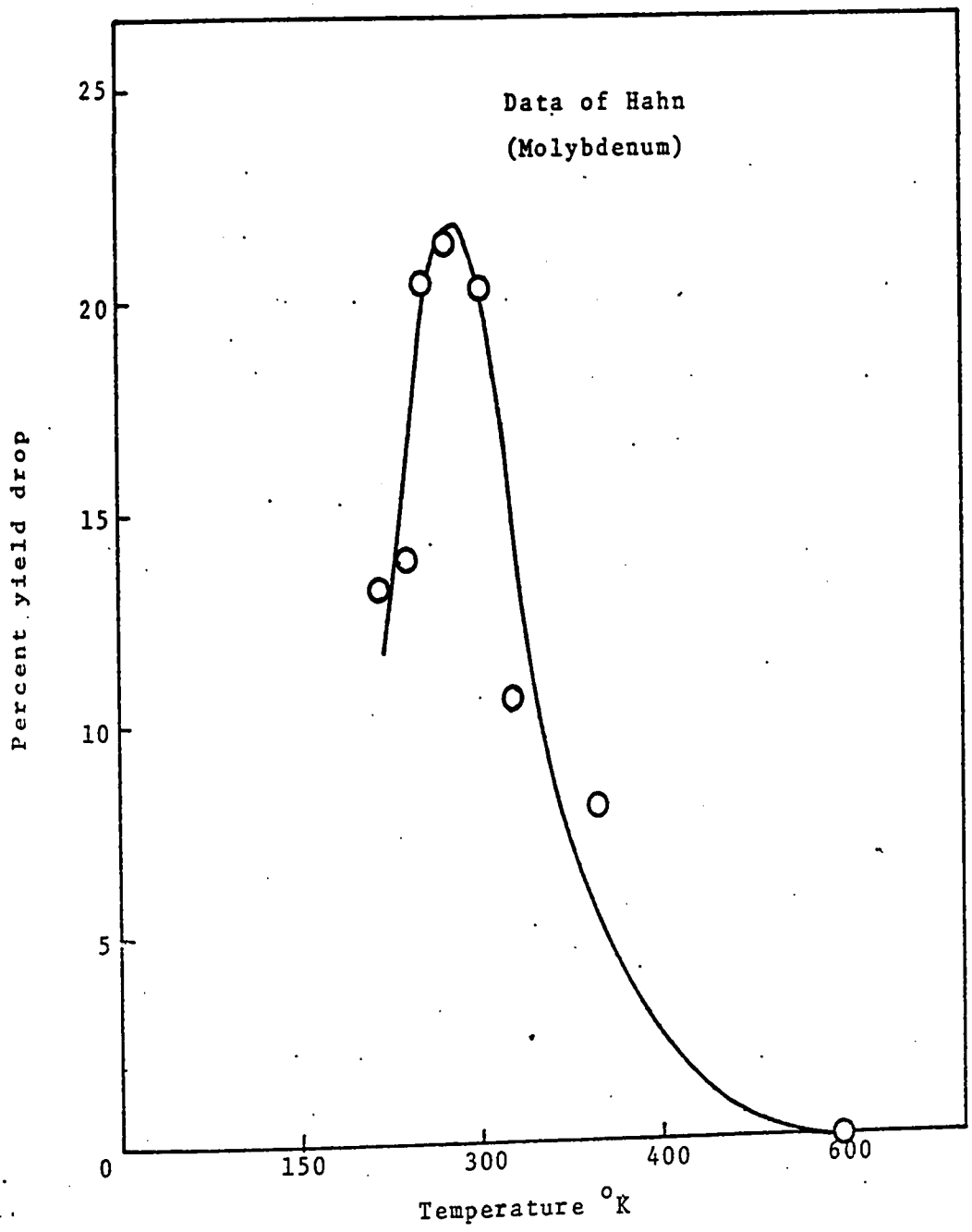

Fig. 2.7b The yield drop as a function of temperature measured in molybdenum (3)

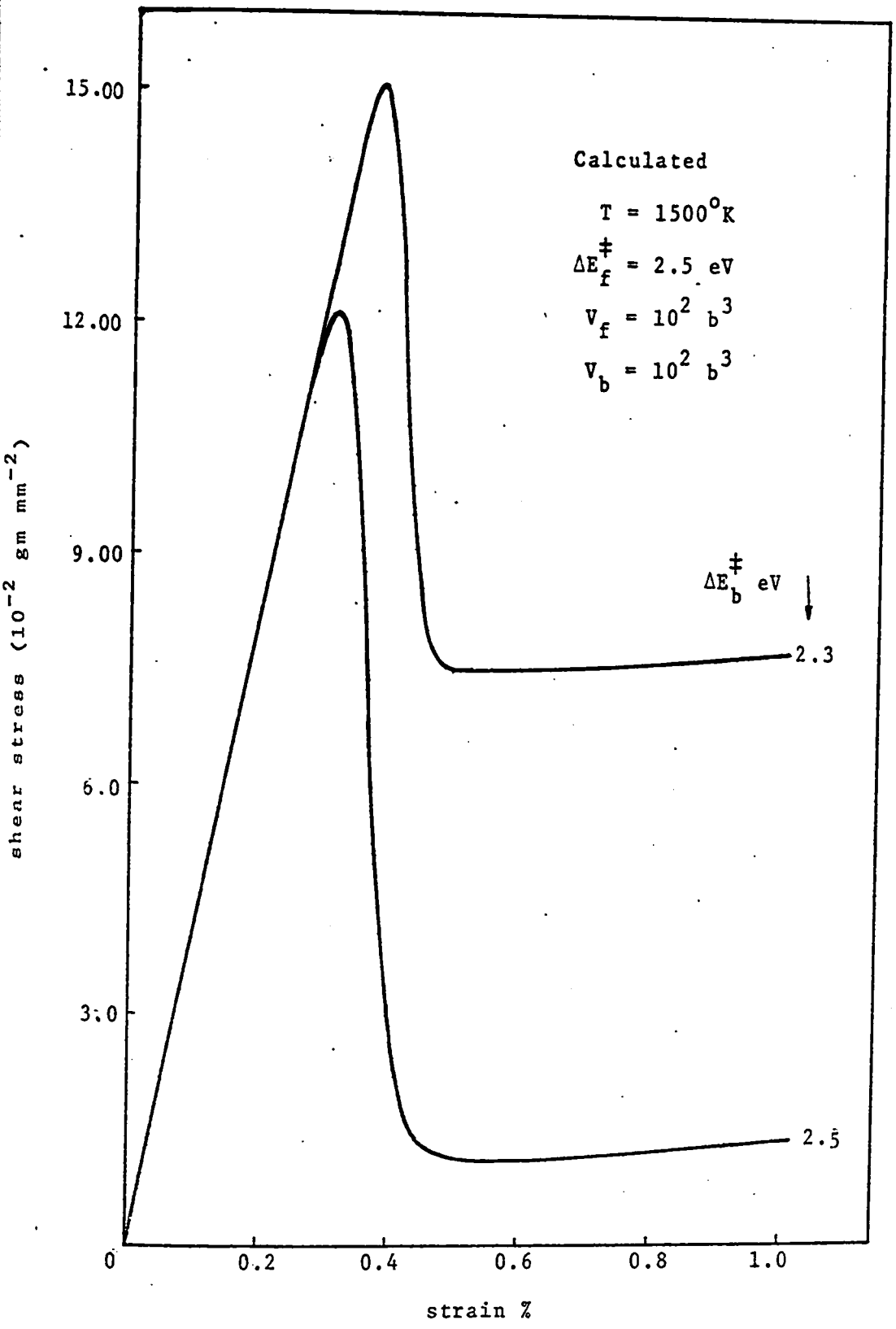

Fig. 2.8a Effect of the symmetry of the energy barrier on the calculated stress-strain curves

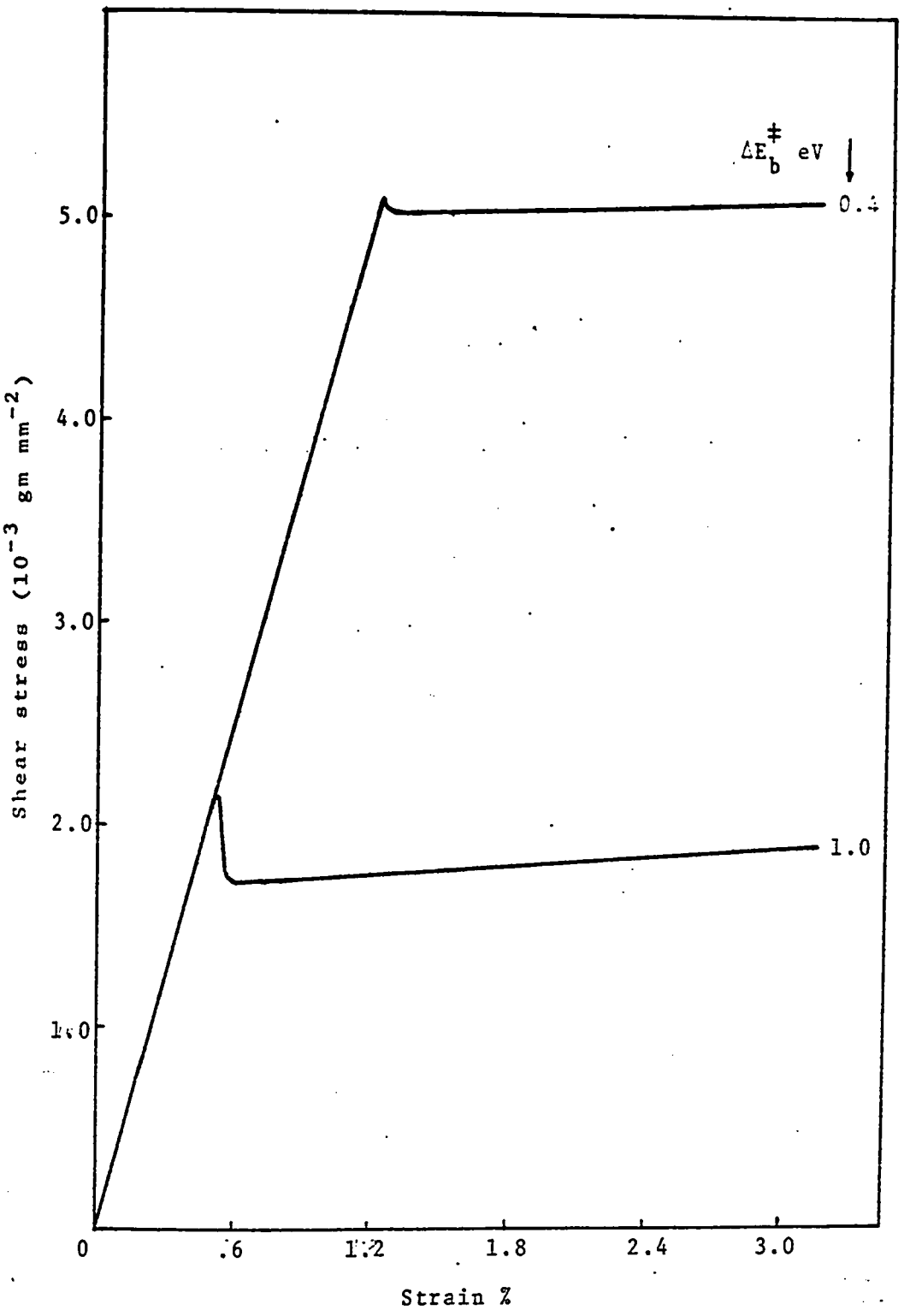

Fig. 2.8b Effect of the symmetry of the energy barrier on the calculated stress-strain curves

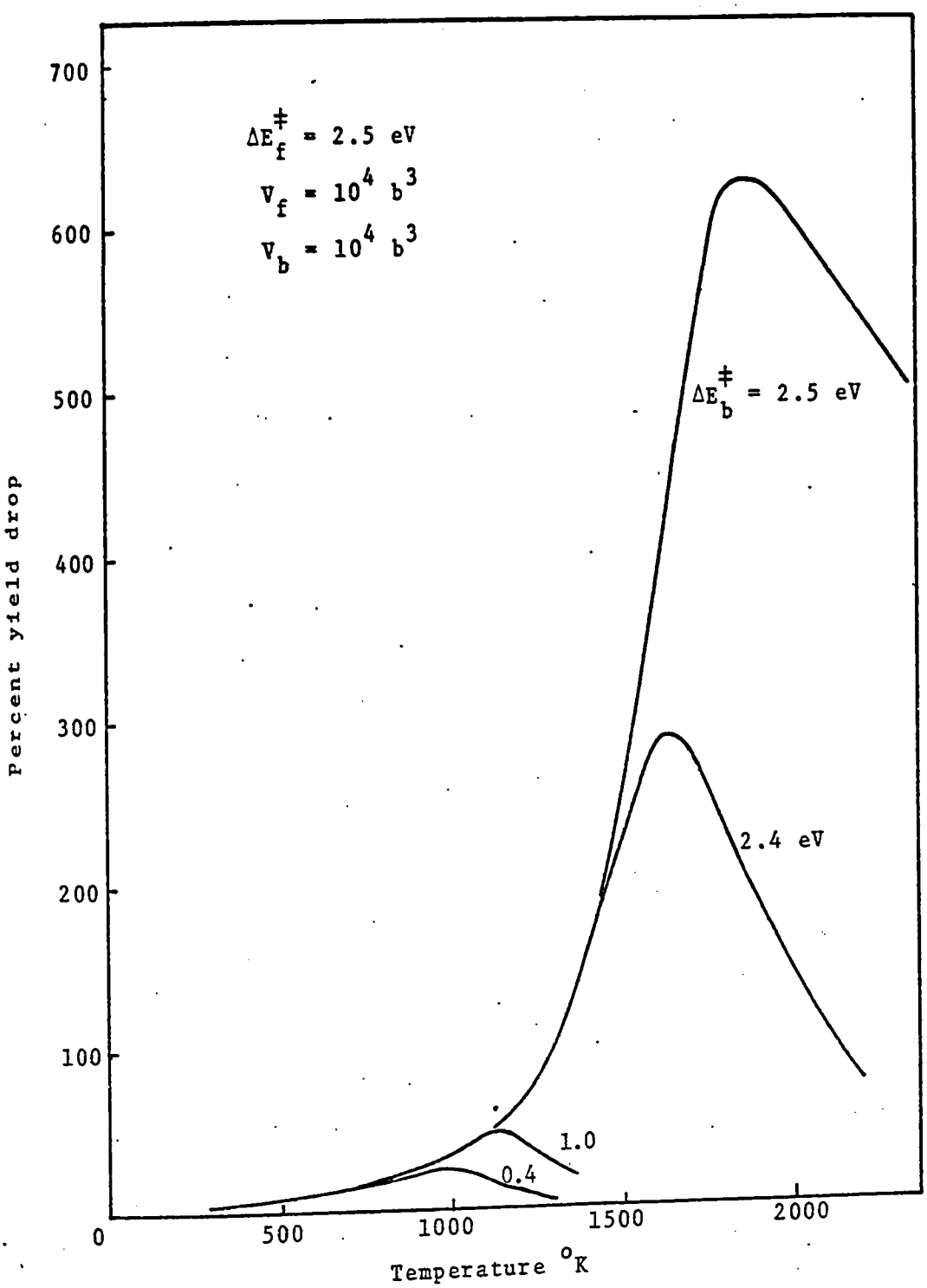

Fig. 2.9 Percent yield drop as a function of temperature for the various values of the backward activation energy

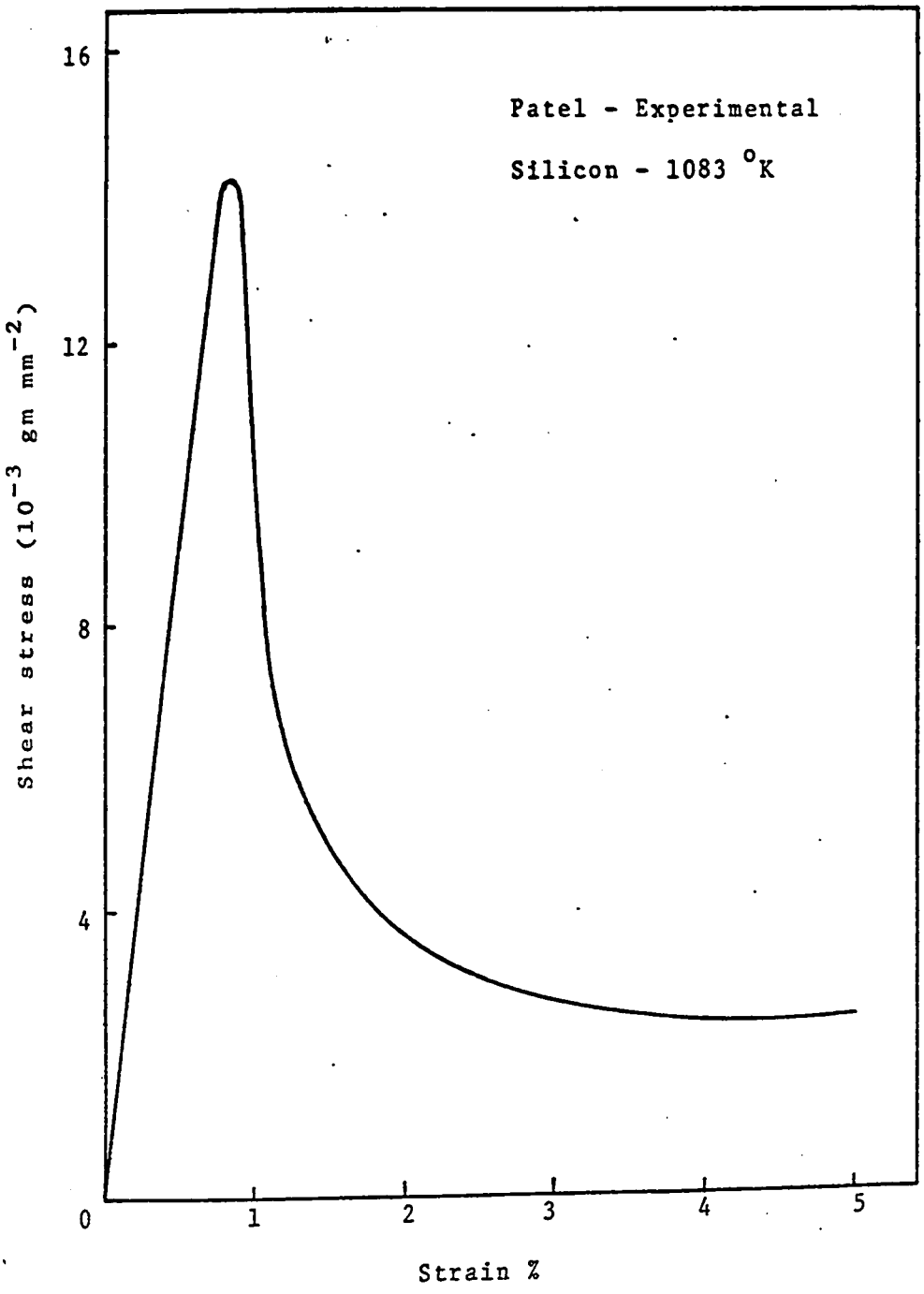

Fig. 2.10 Experimental stress-strain curve for Si single crystal (33)

on aluminium (Fig. 2.11) are in good agreement with the predicted behaviour.

Table 2.3 Typical Activation Parameters for Si and Al (11)

	$\Delta E_f^{\ddagger}$ eV	$\Delta E_b^{\ddagger}$ eV	V_f A^{o3}	V_b A^{o3}
Si	2.235	2.215	71	31.5
Al	0.585	0.0216	1400	28

While the effect of the backward activation energy on the yield stress is noticeable at high temperatures, because of the low applied stress, it makes only a negligible difference at low temperatures (Fig. 2.12).

B. The Effect of Forward Activation Energy

The stress required to move a dislocation depends on the energy level of the obstacle. More stress is required to overcome higher energy barriers and consequently the yield points will rise. The calculated upper and lower yield stresses are shown in Fig. (2.13) over a wide temperature range in which the value of the forward activation energy is varied up to 2.5 eV - the highest physically reasonable value. All other parameters were kept constant for the various curves.

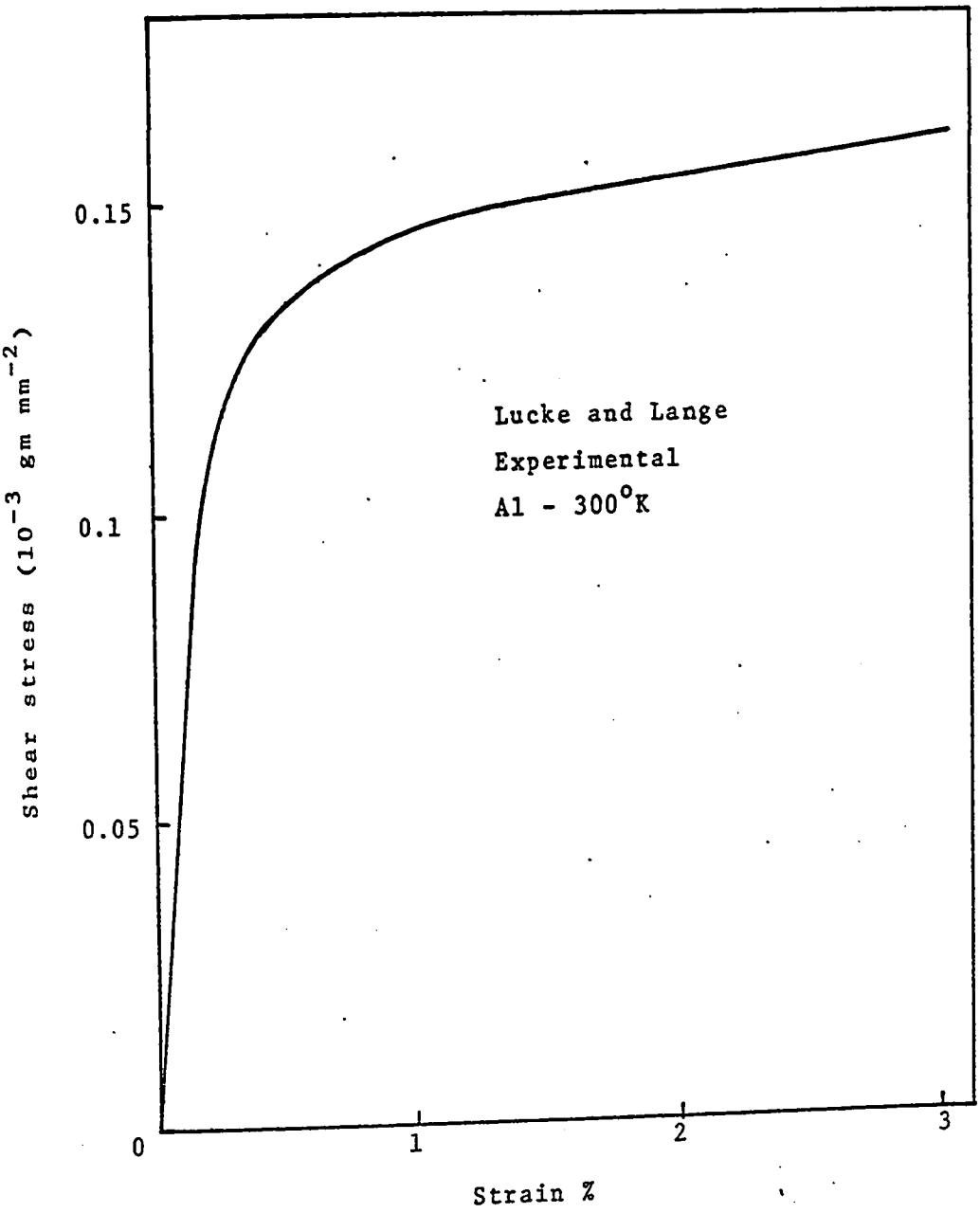

Fig. 2.11 Experimental stress-strain curve for Al single crystal (34)

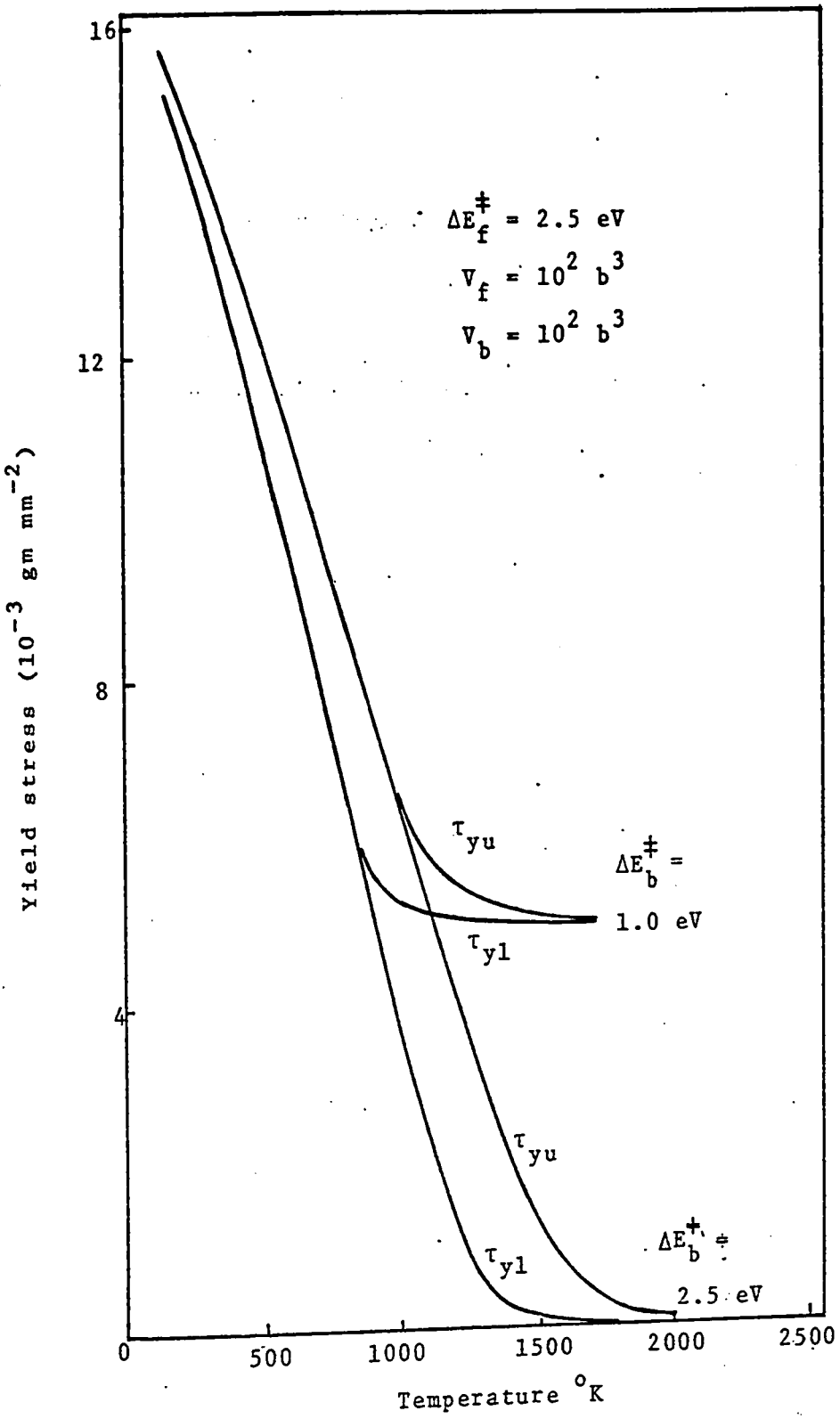

Fig. 2.12 The temperature dependence of the yield stresses for various values of the backward activation energy

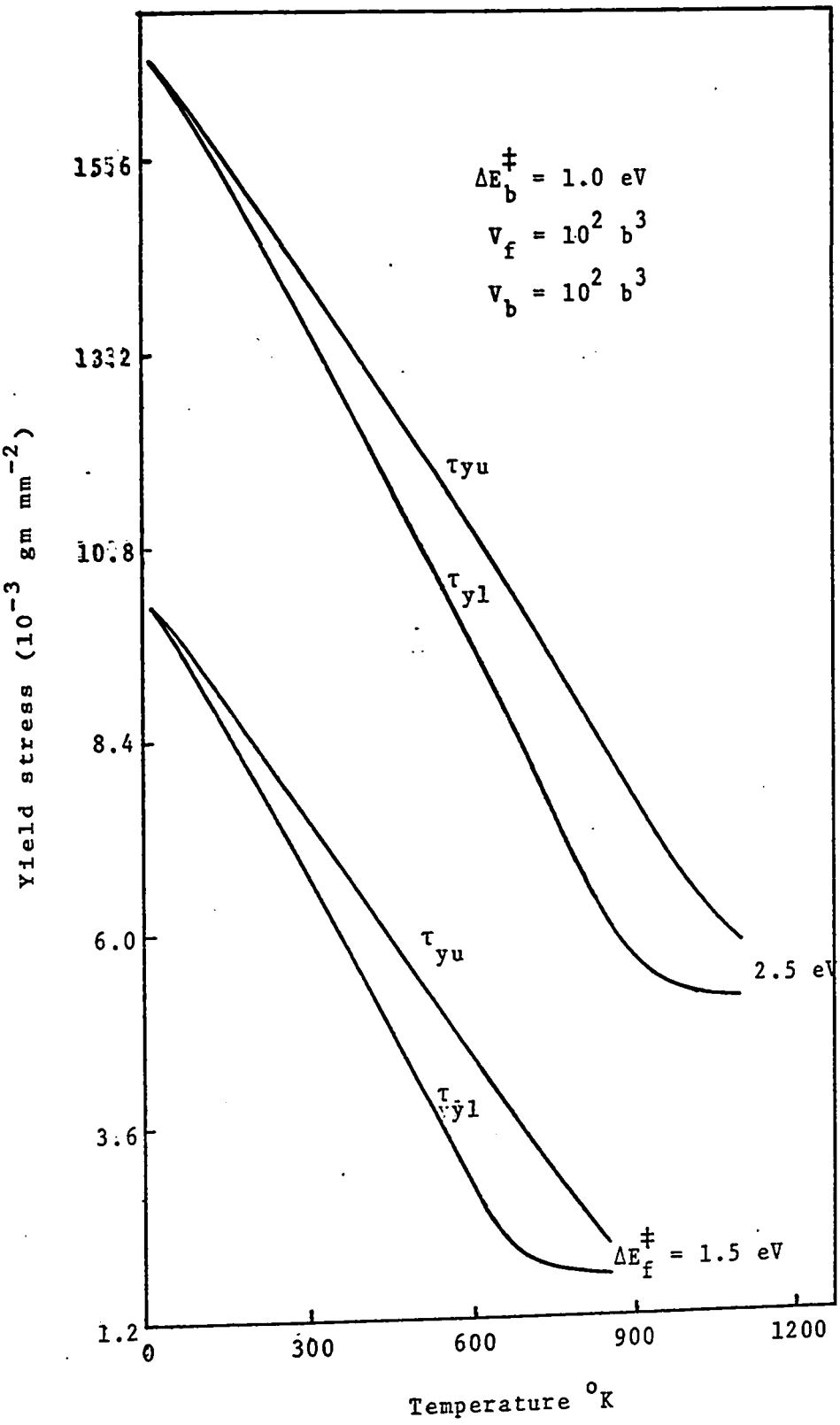

Fig. 2.13 The temperature dependence of the yield stresses calculated for various forward activation energies

The effect of inclusions is known to harden the materials by creating barriers due to the stressed regions around them. Experiments show that the resistance to flow increases with the concentration of impurities. Fig. (2.14) contains one such set of results (35). Assuming as a first approximation that the activation energy is proportional to the impurity concentration, the present analysis predicts a similar type of behaviour (Fig. 2.15).

The high energy barriers are inherent in certain materials due to the high Peierls-Nabarro energies (interatomic binding energy, Appendix Section 1). In these materials the yield stress is high and brittle fracture takes place at low temperatures. This behaviour is typical for materials with diamond cubic structures, such as, Ge, Si, C, InSb, etc., all of which deform plastically only at high temperatures.

The yield drop, as mentioned earlier, depends sensitively on the symmetry of the energy barrier. A material with high activation energy generally shows small yield drop at low temperatures. The yield drop becomes noticeable only at intermediate temperatures and drops again at high temperatures. This can be fully understood from the computed behaviour as illustrated in Fig. (2.16).

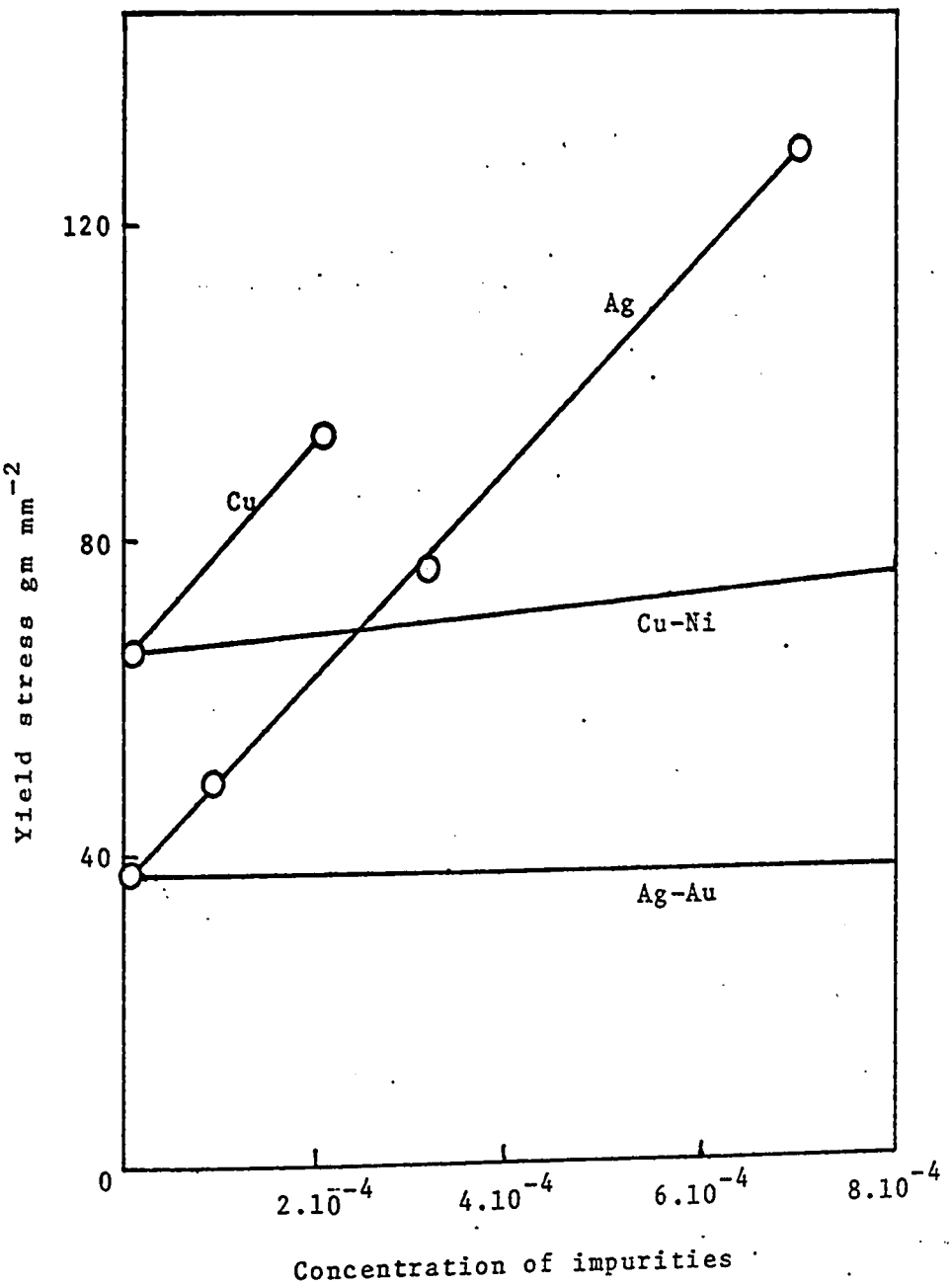

Fig. 2.14 The dependence of the yield stress of Cu and Ag at room temperature

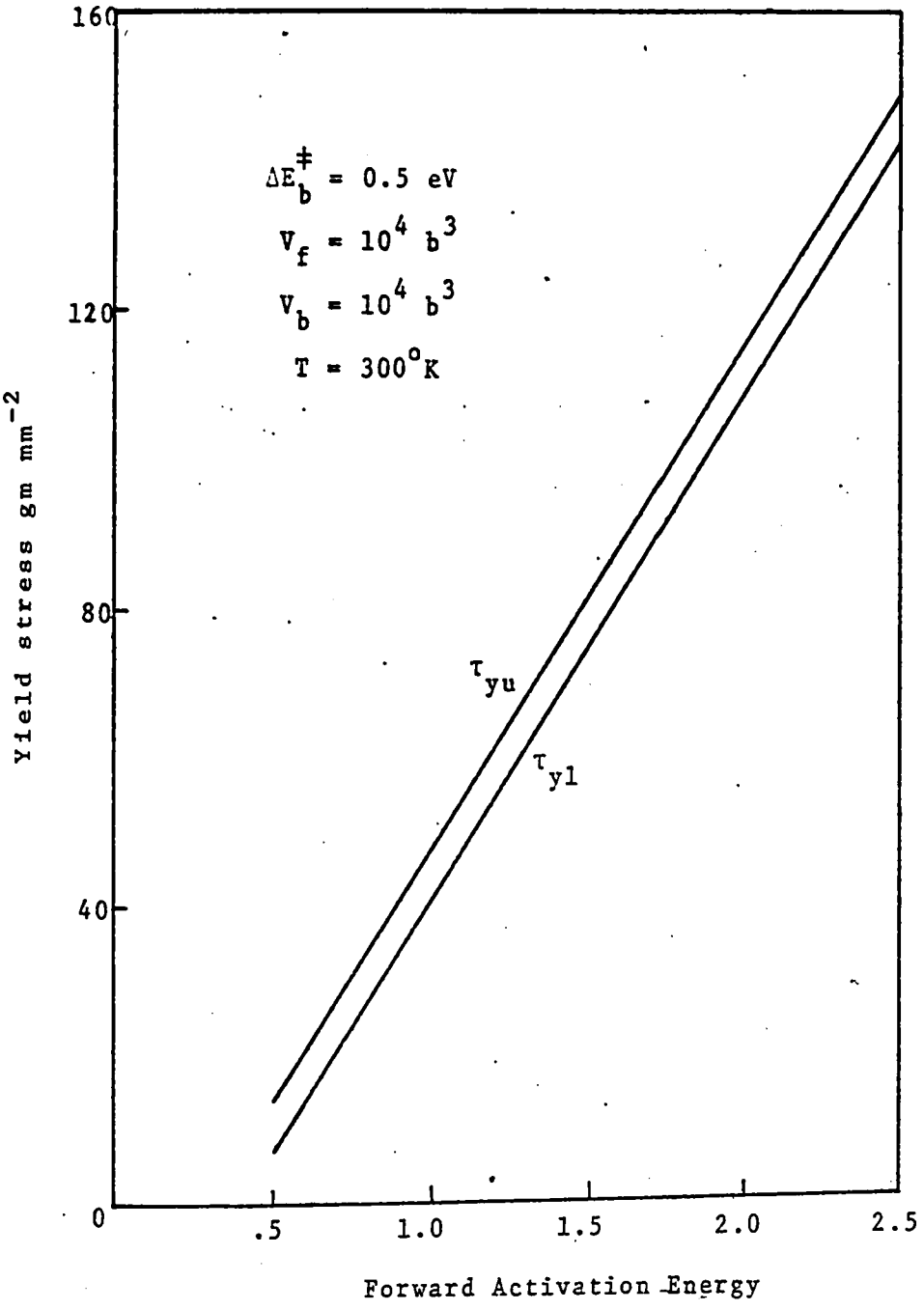

Fig. 2.15 Calculated curves show the effect of the forward activation energy on the yield stress

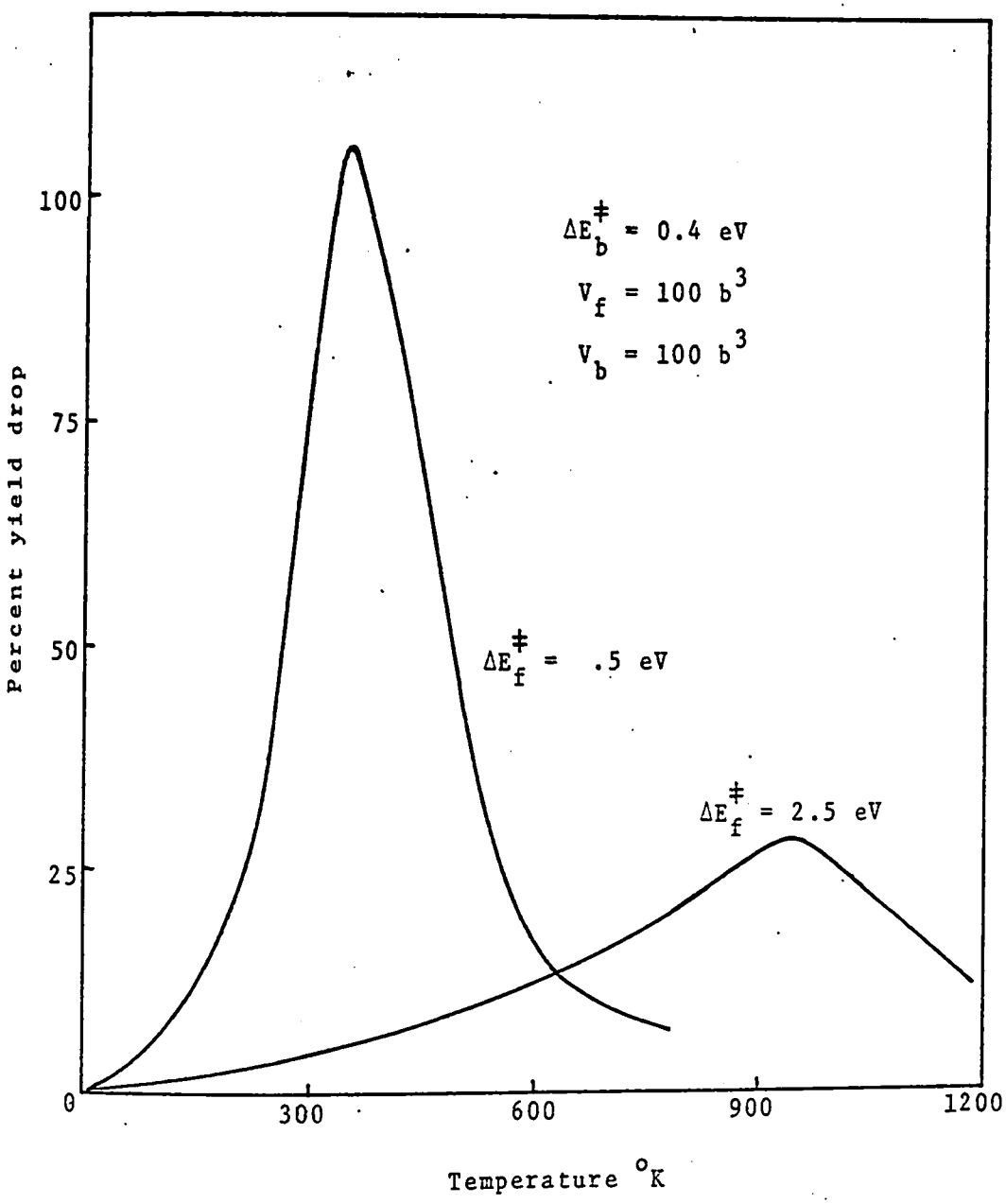

Fig. 2.16 Calculated values of the yield drop as a function of temperature for various values of the forward activation energy

C. The Effect of Forward Activation Volume

Thermally activated flow is very sensitive to the work contributed by the applied stress to the overcoming of the energy barrier. This work depends on the amount of atomic rearrangement required for the dislocation to reach the top of the barrier, which in turn is governed by the size of the atomic configuration forming the obstacle. The effects of small and large obstacles may, in consequence, be differentiated as follows.

The work performed by the applied stress is given by the expression $V \tau_{eff}$. The obstacles associated with small regions of lattice disturbance have low activation volumes and those with large regions of disturbance will have high activation volumes (Appendix). Experimental measurements by Byrne, Fine and Kelly (36) show that the smaller the obstacle size, the greater is the dependence of the flow stress on the temperature (Fig. 2.17). It follows from the present analysis (Fig. 2.18) that the yield points are very sensitive to temperature for low activation volumes - of the order of $1 - 100\ b^3$, while the sensitivity is relatively weak at $V_f > 10^3\ b^3$. The calculated behaviour vindicates Conrad's conclusions (37) as well, that the steep rise in yield stress is associated with the Peierls-Nabarro mechanism (Refer Appendix, Table 1).

While it has been found in some studies (11,13) that mechanisms with low activation volumes have high

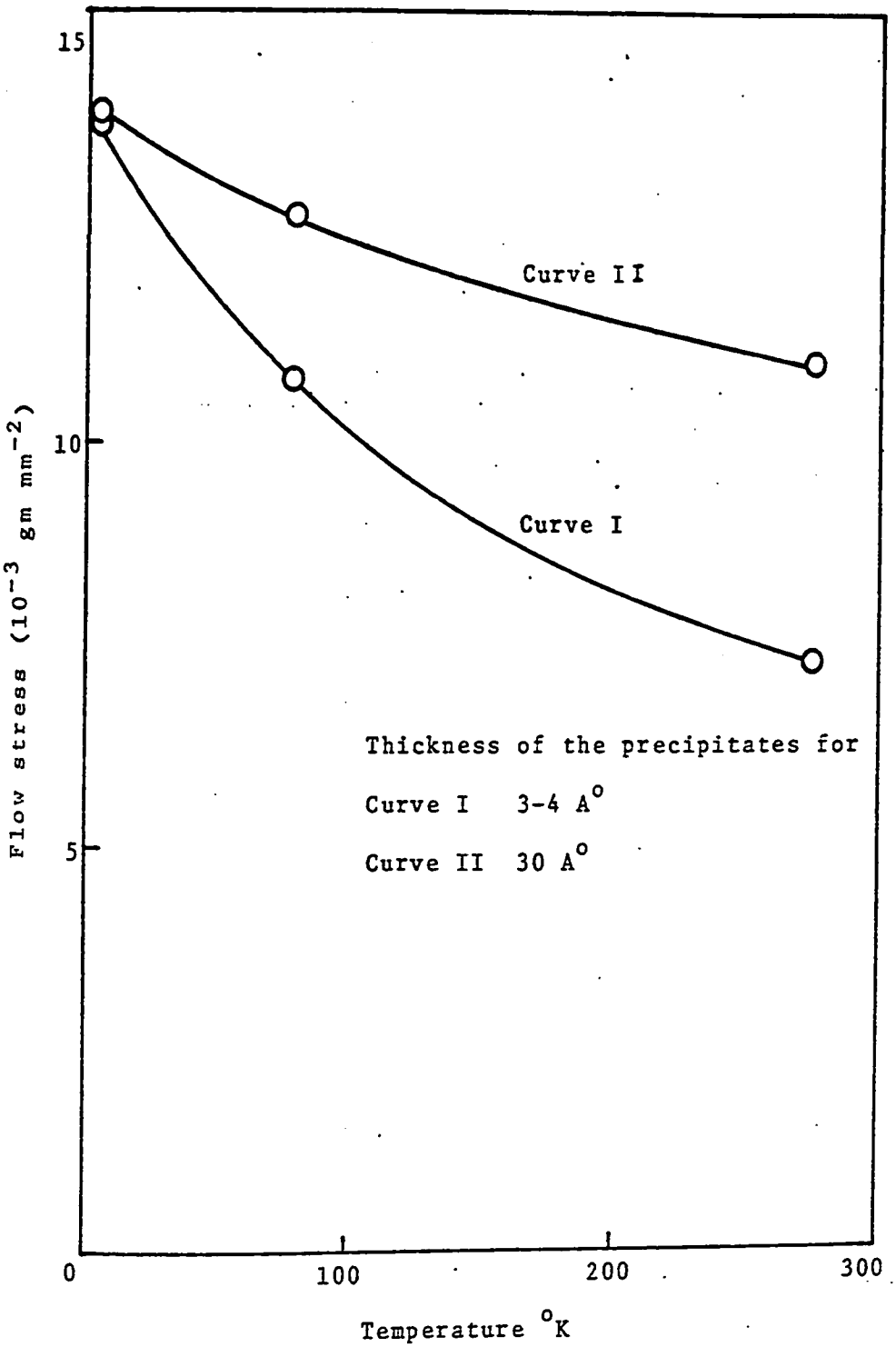

Fig. 2.17 The temperature dependence of the flow stress for a single crystal of an Al+3.85 % Cu alloy. The size of strained zone due to Cu precipitates for the Curve I is 3-4 A° and for Curve II it is some 30 A° thick

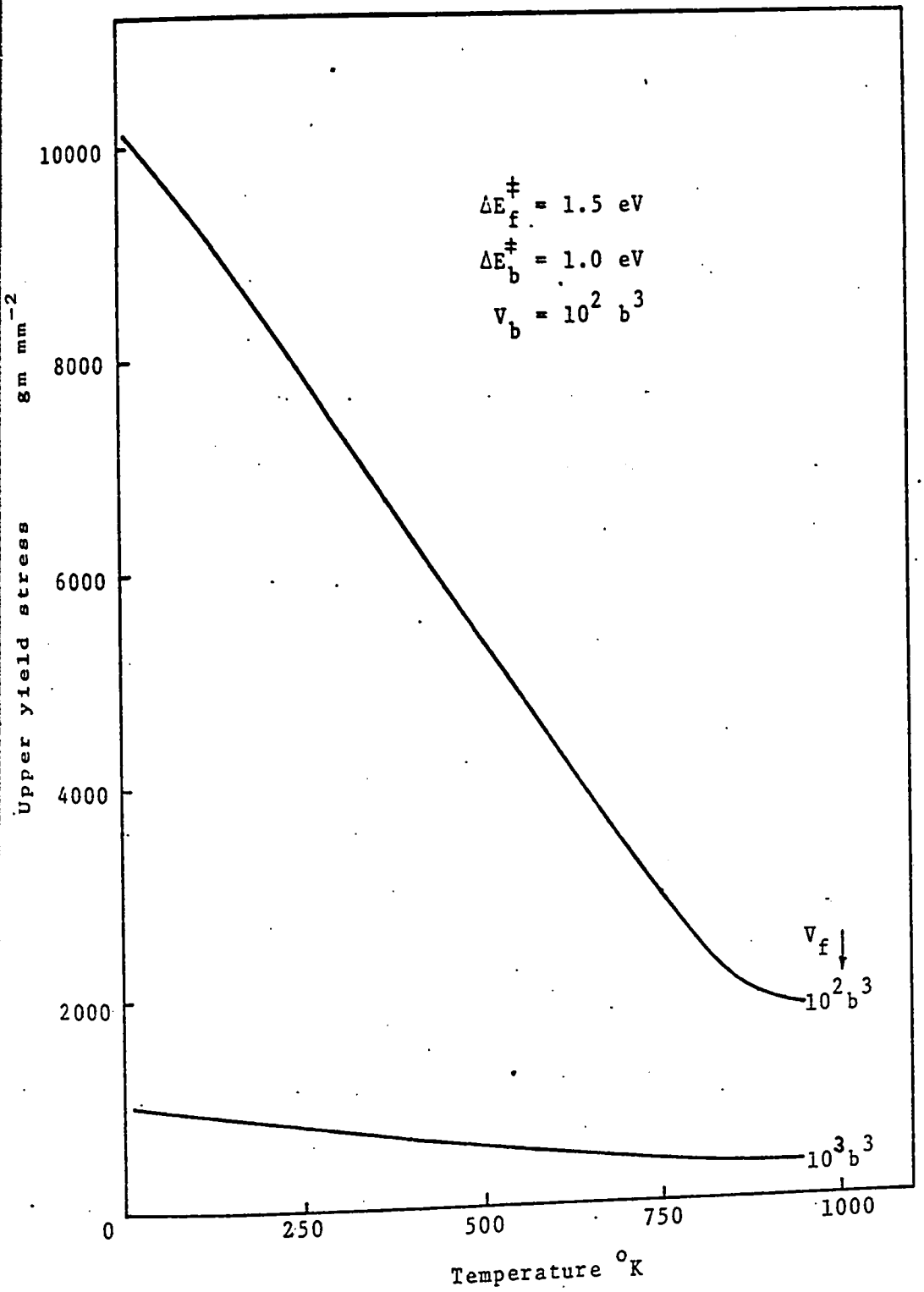

Fig. 2.18 The upper yield stress as a function of the temperature, calculated for the indicated range of forward activation volume

activation energies, the possibility of low activation volume to be associated with low activation energies cannot be ruled out entirely. For instance, a jog in the dislocation is an obstacle of the size of a few atoms (often the size is equal to 1 b^3). As suggested by Mott (38), the jog can move, under definite conditions, along the dislocation conservatively without creating vacancies. The process requires an energy less than that needed to form a vacancy. The yield stresses will, therefore, be lower for the conservative motion of jogs than when they move non-conservatively.

A calculation of the yield drop over a wide temperature range shows that it rises steeply and drops rapidly as well for low activation volumes (Fig. 2.19).

D. The Effect of Backward Activation Volume

As stated earlier, the effect of the backward activation parameters become noticeable only at high temperatures due to the low applied stresses. Fig. (2.20) illustrates that for low activation volume the yield stress is high. Computations show that the yield drop decreases with decreasing V_b (Fig. 2.21).

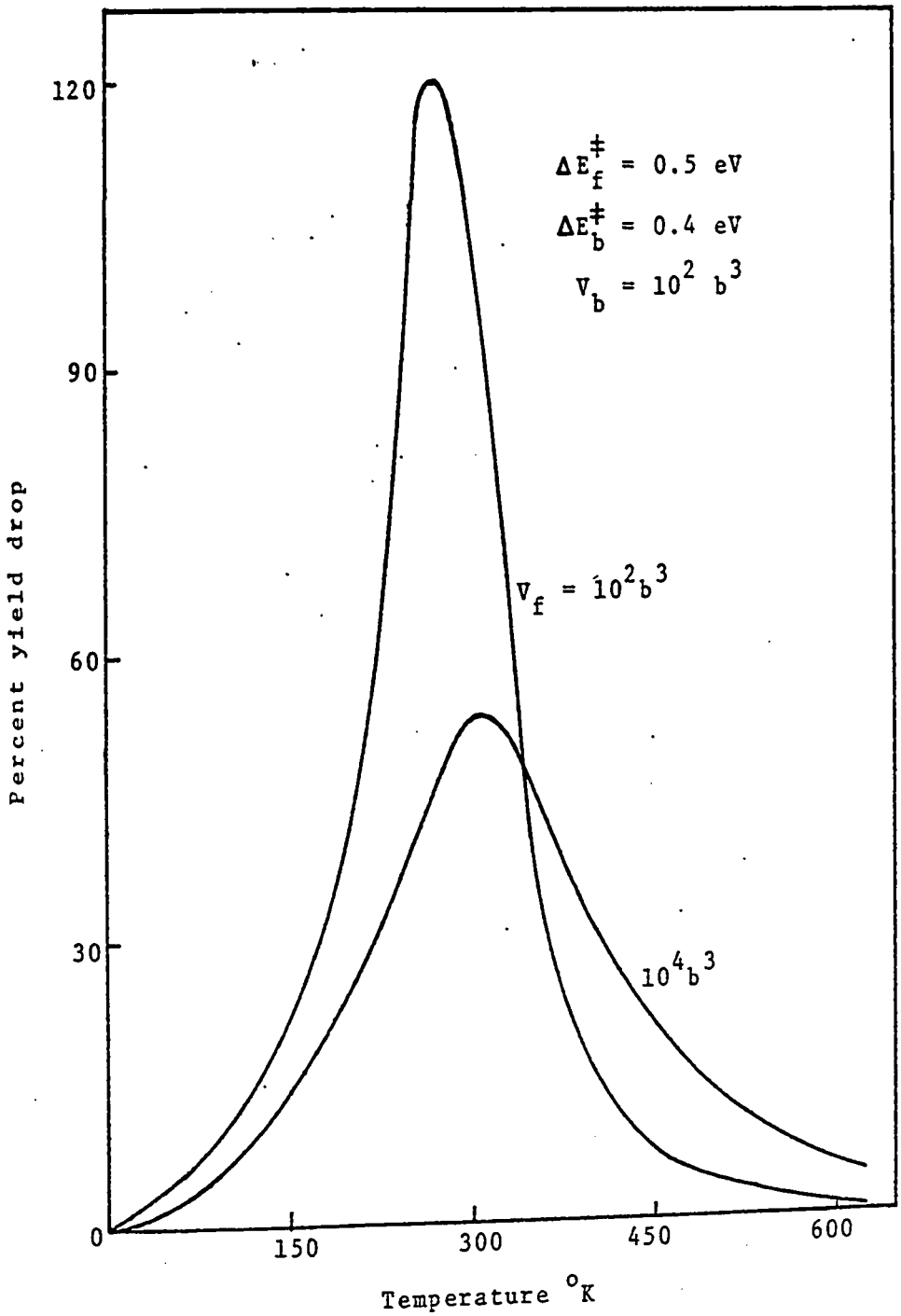

Fig. 2.19 Calculated values of the yield drop as a function of temperature for the various values of the forward activation volume

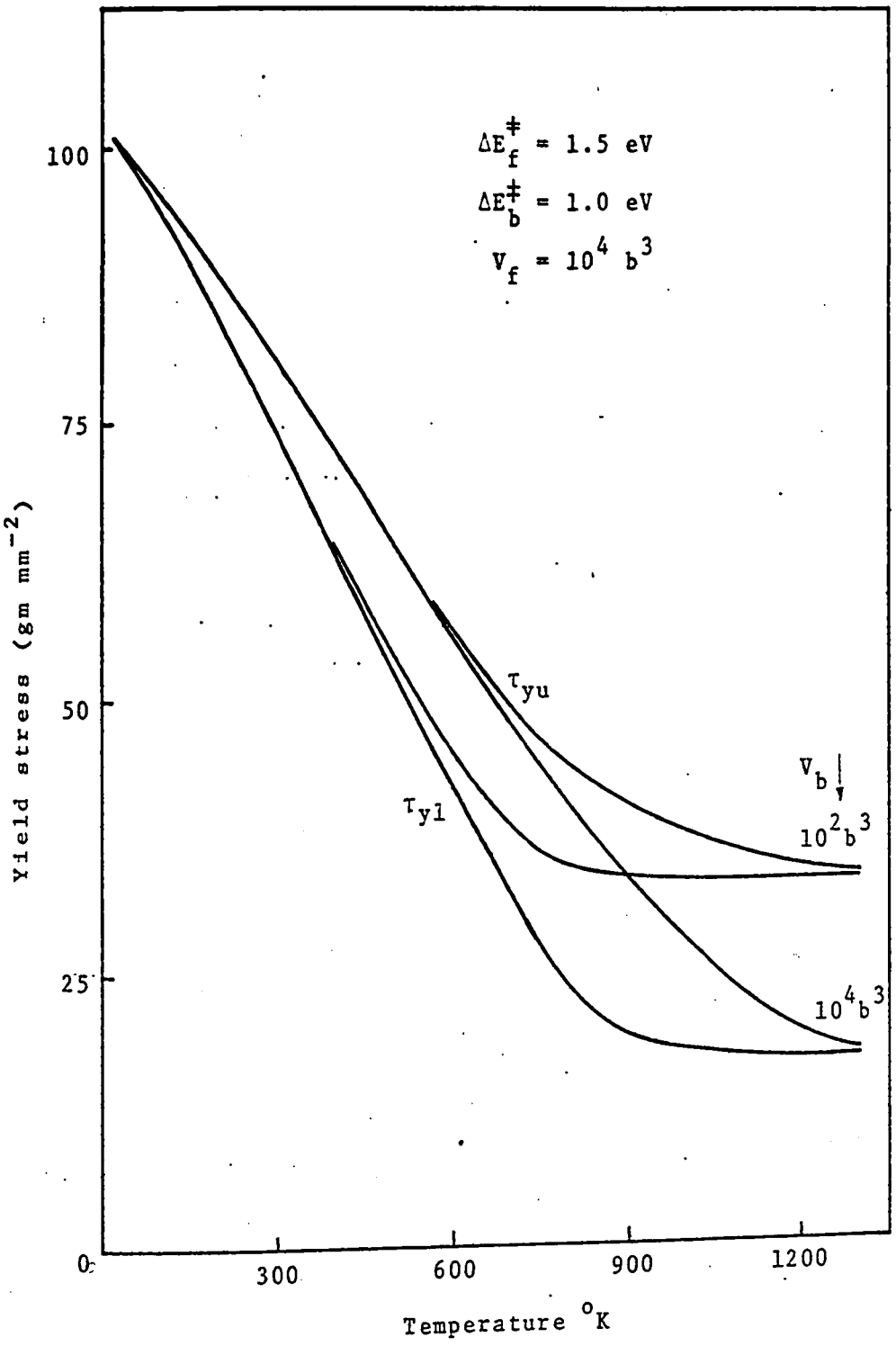

Fig. 2.20 The temperature dependence of the yield stresses for the indicated range of the backward activation volumes

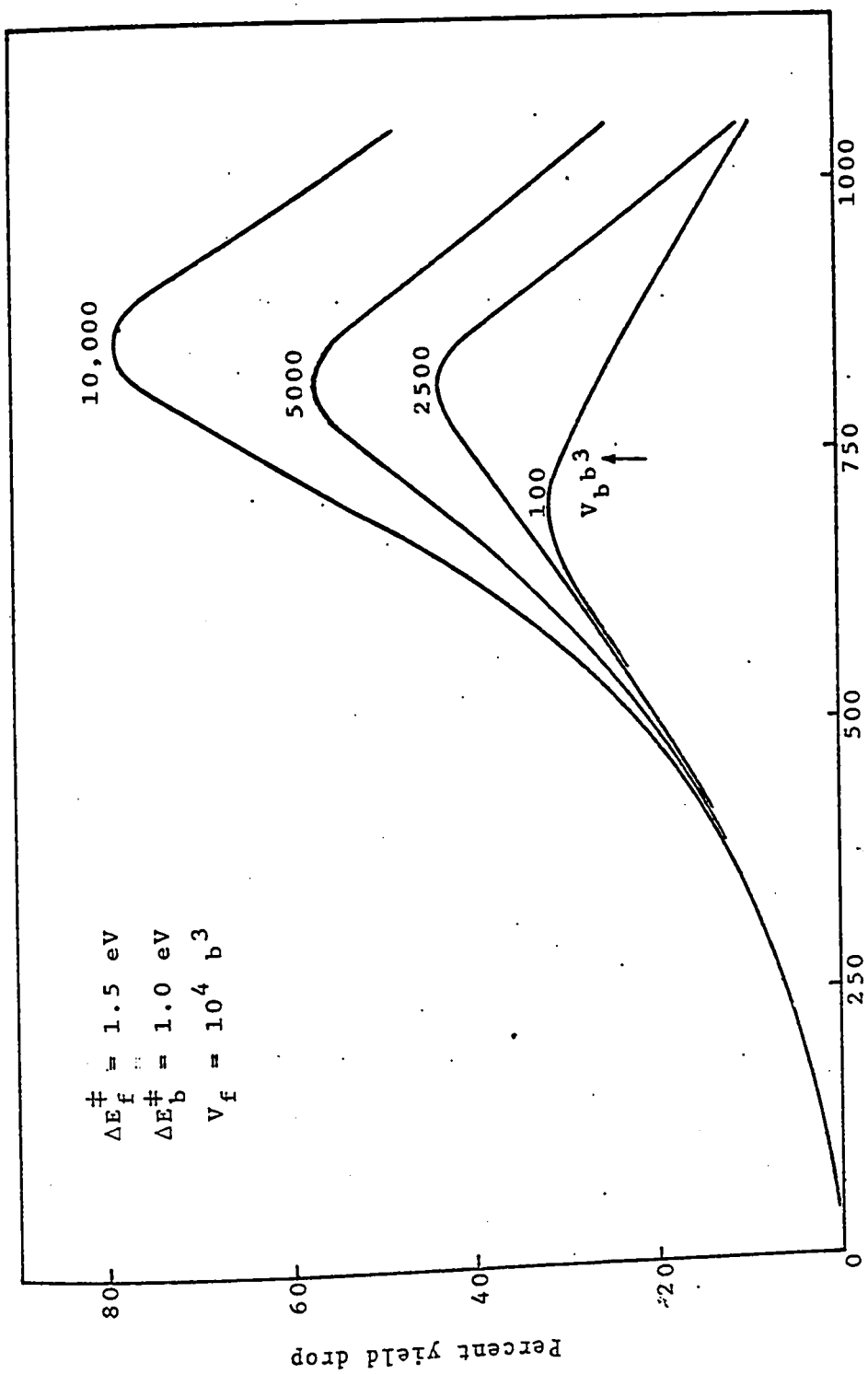

Fig. 2.21 The yield crop as a function of temperature for the indicated range of the backward activation volumes

2.4 The Analysis of Constant Stress Rate Test

Although the stress-strain relations are usually determined at constant strain rate, or more precisely, at constant crosshead velocity, the measurements can also be carried out under constant stress rate conditions. This mode of testing has received little attention so far and it is interesting to examine it because of the fact that loading at constant rates corresponds to some practical engineering situations. An example is the filling of a storage tank where the loading rate is constant. In addition, it has some definite advantages over the constant strain rate condition in materials testing as described below.

The first major advantage is its independence from the hardness characteristics of the machine. This may be illustrated by referring to Fig. (2.1). When the specimen is deformed at a constant strain rate, a load drop occurs at the yield. The extent of this drop was shown (2) to be dependent on the stiffness K' of the spring, representing the elastic response of the machine elements. With a flexible spring, the load on the specimen is unaffected and with a stiff spring, even small sudden elongation of the specimen would result in a large drop in the load (2). A study of the material behaviour in constant strain rate test will therefore require stiff machines and rapid load recording devices. In constant stress rate conditions, on the other hand, even when the specimen yields or elongates abruptly the load on the

elongating spring will be undisturbed. The experimental set-up required for this mode of testing would be simple and economical.

Secondly, the differential equation representing the constant stress rate behaviour leads to descriptions in the form of definite algebraic functions whereas only numerical solutions can be obtained for the corresponding equation of constant stress rate test. This will be derived in the following.

The Constant Stress Rate Equation

In constant stress rate tests, the condition to be imposed is

$$d\tau_a/dt = \dot{\tau} = \text{constant} \tag{2.12}$$

where τ_a is the stress applied at time t. Eqn. (2.3) when combined with condition (2.11) leads to the following differential equation.

$$\dot{\gamma}_p = \frac{d\gamma_p}{dt} = \alpha\beta(\rho_o + \beta\gamma_p)[\kappa_f \ell_f \frac{kT}{h} \frac{Q_f^{\ddagger}}{Q_f^r} \exp(-\frac{\Delta E_f^{\ddagger} - V_f(\dot{\tau}t - H\gamma_p)}{kT}) - \kappa_b \ell_b \frac{kT}{h} \frac{Q_b^{\ddagger}}{Q_b^r} \exp(-\frac{\Delta E_b^{\ddagger} + V_b(\dot{\tau}t - H\gamma_p)}{kT})] \tag{2.13}$$

which describes the time dependence of the plastic component of the strain. A stress-strain curve can be obtained from

this equation by numerical integration. It is to be emphasized however that algebraic solutions should be preferred, when feasible with reasonable approximations. Solutions of this form, besides making the calculation procedures easy, would facilitate the physical understanding of the process as well. The present investigation therefore aims to solve algebraically the above differential equation.

Two alternate conditions have been analyzed in the study. In the first, it is assumed for the time being that there is no work-hardening. The effect of work-hardening is introduced later.

Eqn. (2.13), in consequence, simplifies to

$$\frac{d\gamma_p}{dt} = \alpha b(\rho_o + \beta\gamma_p)[A_f' \exp(\frac{V_f \dot{\tau} t}{kT}) - A_b' \exp(-\frac{V_b \dot{\tau} t}{kT})]$$

where $$A_f' = \kappa_f \ell_f \frac{kT}{h} \frac{Q_f^{\ddagger}}{Q_f^r} \exp(-\frac{\Delta E_f^{\ddagger}}{kT})$$

and $$A_b' = \kappa_b \ell_b \frac{kT}{h} \frac{Q_b^{\ddagger}}{Q_b^r} \exp(-\frac{\Delta E_b^{\ddagger}}{kT})$$

Rearranging the terms and integrating, one gets

$$\int_o^{\gamma_p} \frac{d\gamma_p}{\rho_o + \beta\gamma_p} = \int_o^t \alpha b[A_f' \exp(\frac{V_f \dot{\tau} t}{kT}) - A_b' \exp(-\frac{V_b \dot{\tau} t}{kT})]\, dt$$

or

$$\frac{1}{\beta} \ln \left(1 + \frac{\beta}{\rho_o} \gamma_p\right) = \frac{\alpha b}{\dot{\tau}}\left[\frac{kT}{V_f} A_f' \left\{\exp\left(\frac{V_f \tau_a}{kT}\right) - 1\right\}\right.$$

$$\left. + \frac{kT}{V_b} A_b' \left\{\exp\left(-\frac{V_b \tau_a}{kT}\right) - 1\right\}\right] \qquad (2.14)$$

which expresses the plastic strain as

$$\gamma_p = \gamma_{po} \exp\left\{\frac{\alpha b \beta}{\dot{\tau}}\left[\frac{kT}{V_f} A_f' \left\{\exp\left(\frac{V_f \tau_a}{kT}\right) - 1\right\}\right.\right.$$

$$\left.\left. + \frac{kT}{V_b} A_b' \left\{\exp\left(-\frac{V_b \tau_a}{kT}\right) - 1\right\}\right]\right\} - \gamma_{po} \qquad (2.15)$$

where $\gamma_{po} = \rho_o/\beta$

The total strain, γ, is the sum of the plastic strain, γ_p, and the elastic strain, γ_e, therefore

$$\gamma = \gamma_e + \gamma_p$$

or
$$\gamma = \frac{\tau_a}{E} + \gamma_p \qquad (2.16)$$

A calculated stress-strain curve in the absence of work-hardening is shown dotted in Fig. (2.22). The behaviour is similar with the one that will be expected from section (2). The curve departs from the elastic slope at a stress much below the yield stress, turns over smoothly and then continues to rise slowly with increasing strain.

The dotted curve can now be modified to take into account the effect of work-hardening. Its linear dependence

expressed as, $\tau_i = H\gamma_p$, when added algebraically, leads to the solid curve of Fig. (2.22). The behaviour so obtained is typical of the yield region characteristics under constant stress rate conditions and can be compared with the experimental observations.

Stress-strain curves at temperatures ranging from $77^{\circ}K$ to $1100^{\circ}K$ for MgO single crystals were obtained by Pask and Copley (39) and the results are shown in Fig. (2.23). The crystals were tested in compression at a stress rate of 15 gm mm^{-2} sec^{-1} until fracture occurred. Within the yield region, these curves show a good qualitative agreement with those calculated from Eqn. (2.16), as illustrated by Fig. (2.24). The yield stress, defined as 0.2% offset, is plotted as a function of temperature in Fig. (2.25) for two different values of the activation volume. The behaviour is identical to the one obtained previously for constant strain rate conditions (Fig. 2.4). This is rather expected since the physical phenomenon of overcoming the energy barriers is the same for any plastic flow process. The rate of the process is determined principally by the mechanism controlling the deformational behaviour and consequently it can be predicted that the influence of the activation parameters on the yield stress would be the same as found in constant strain rate analysis, viz.,

i) the yield stress increases with an increase in the forward activation energy.

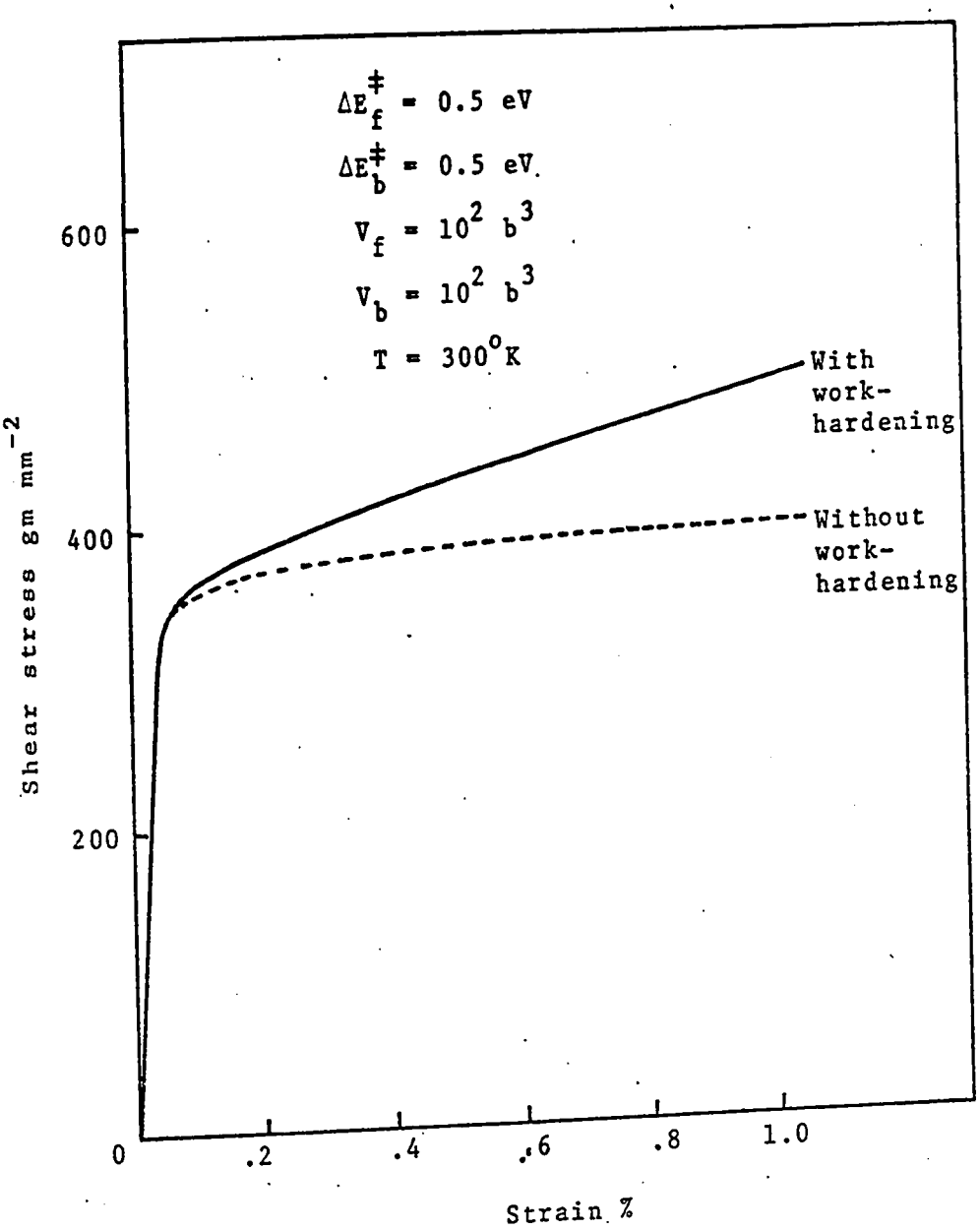

Fig. 2.22 Calculated stress-strain curve both with and without work-hardening

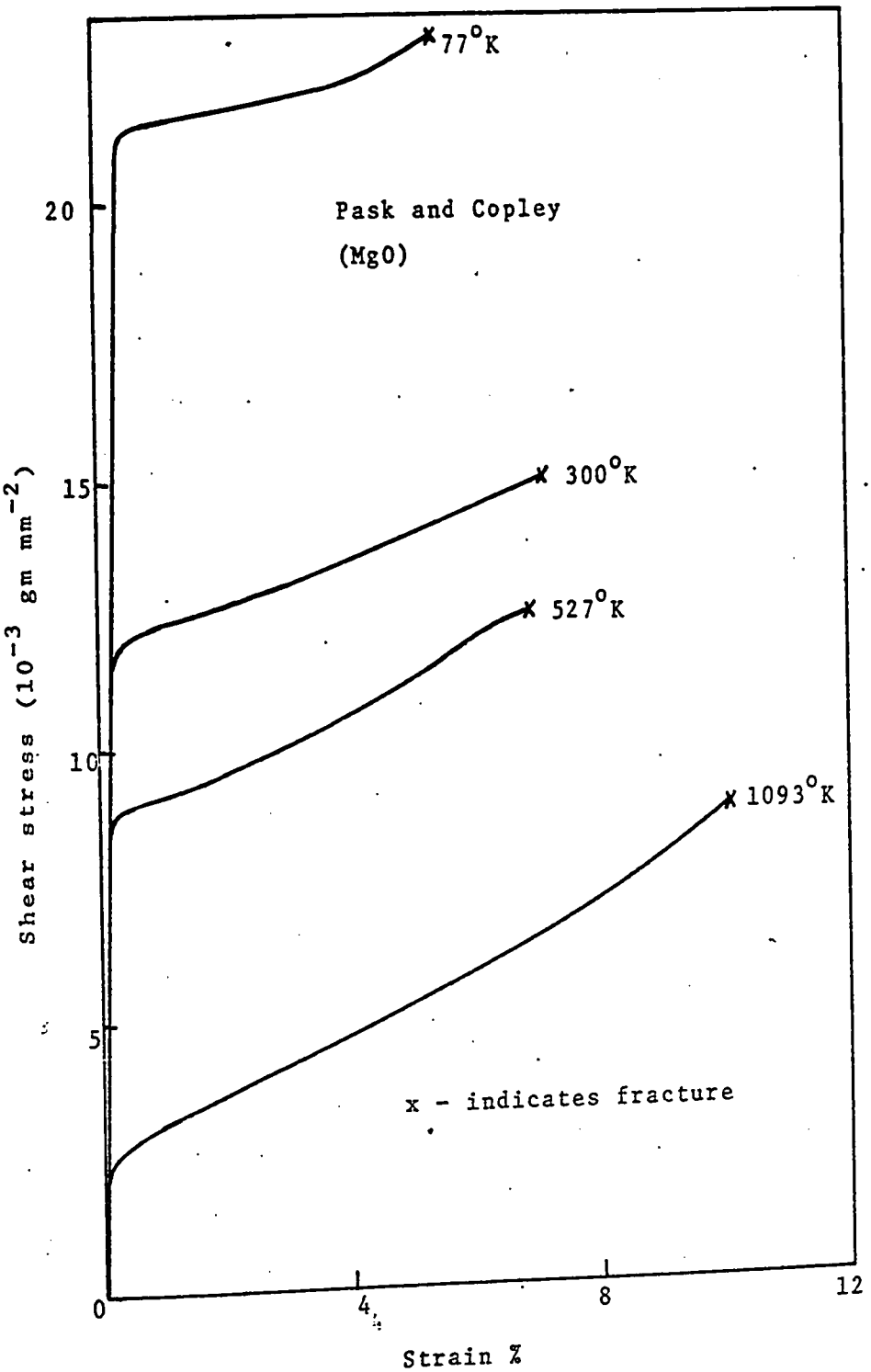

Fig. 2.23 Stress-strain curves at a range of temperatures for MgO single crystals tested at a stress rate of 15 gm mm^{-2} sec^{-1} (39)

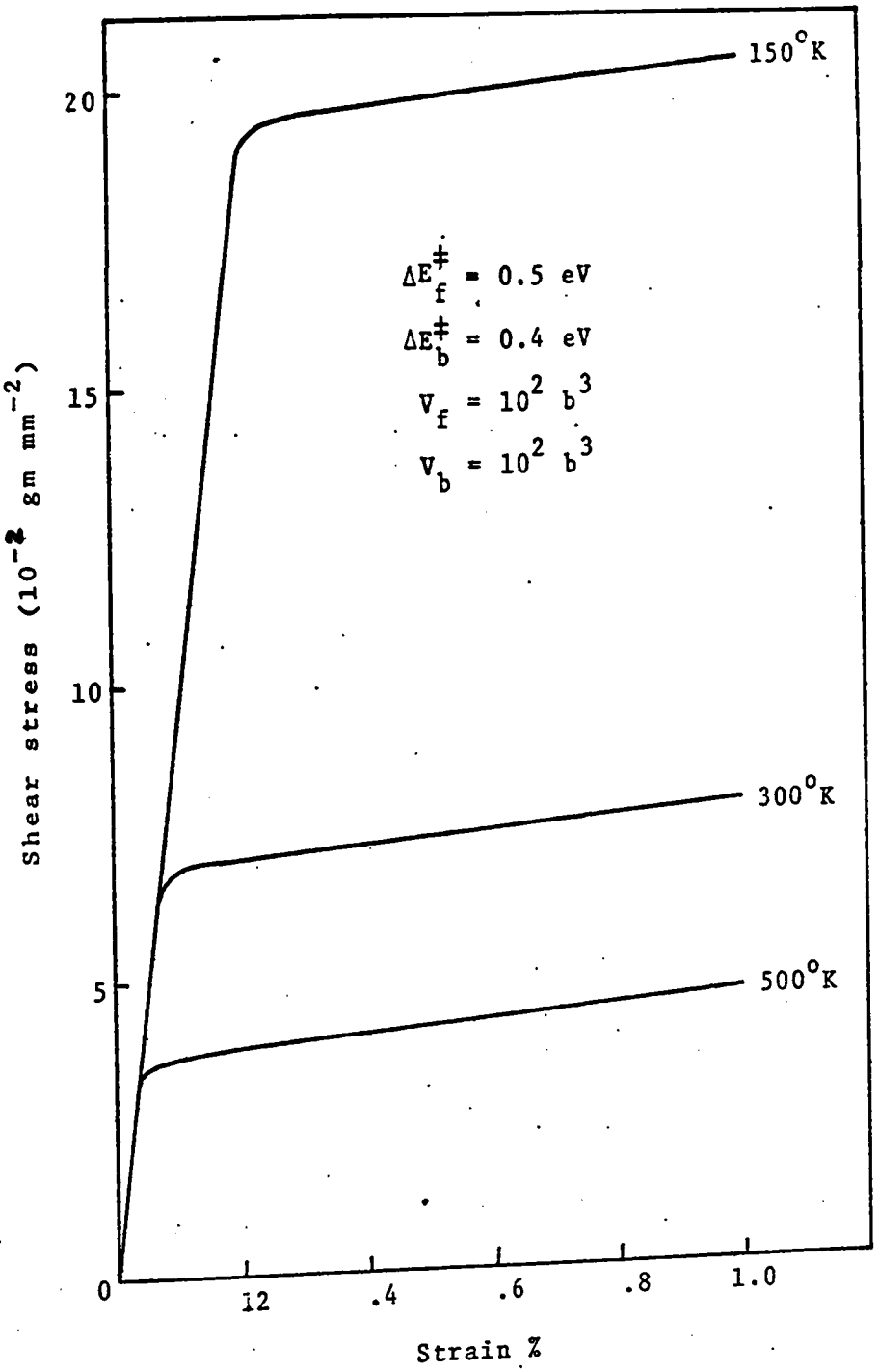

Fig. 2.24 The stress-strain curves calculated at a range of temperatures

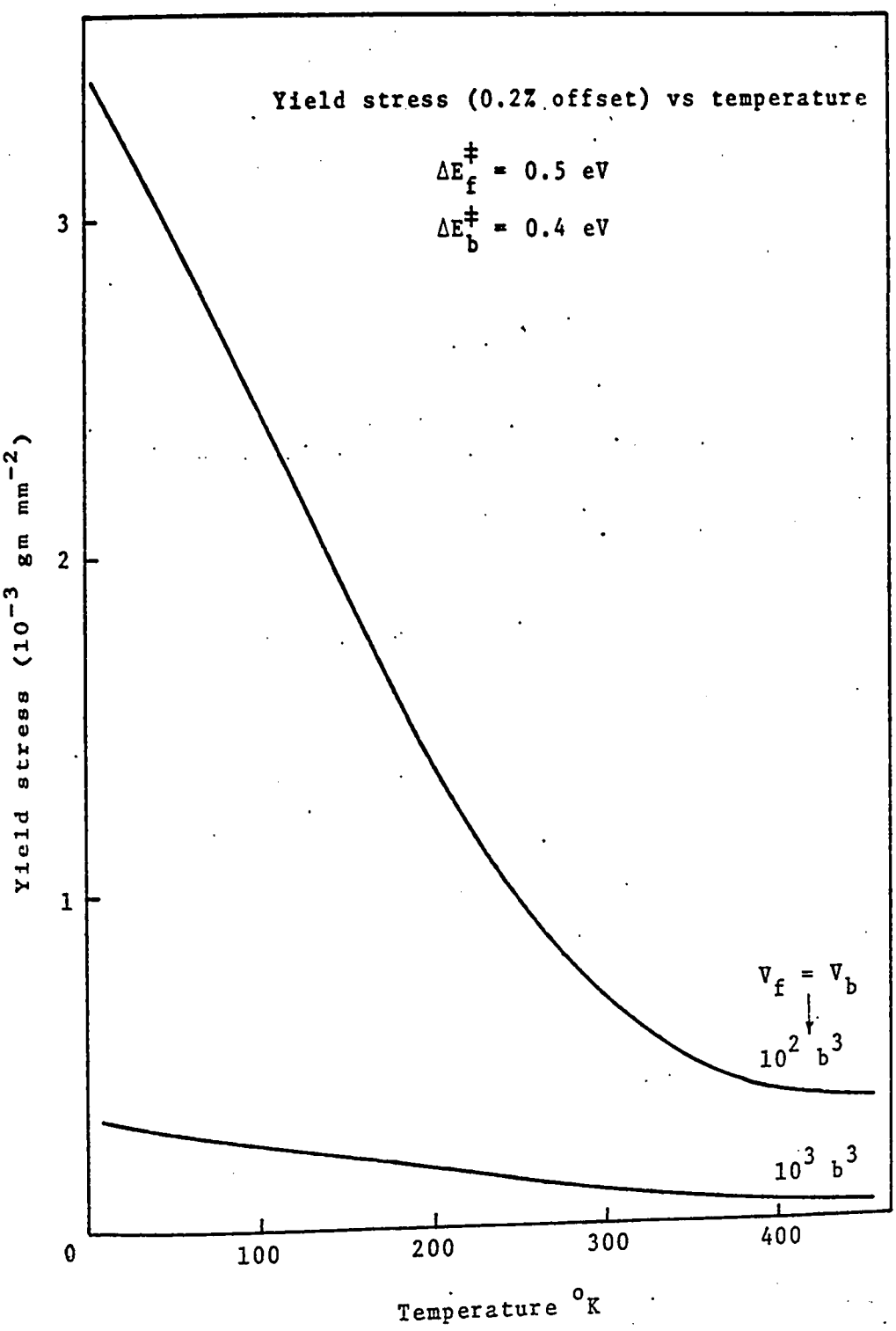

Fig. 2.25 The yield stress (0.2% offset) as a function of temperature for the indicated range of activation volumes

ii) the effect of temperature on the yield stress is significant for low forward activation volumes.

and iii) the yield stress increases with a decrease in the backward activation parameters, $\Delta E_b^{\ddagger}$ and V_b.

The Eqn. (2.15), expressing strain as a function of stress is, however, not adequate to calculate the dotted part of the curve beyond the yield point. It can be noticed from Fig. (2.22) that in this range, even a small change of stress would result in an appreciable change in the corresponding strain, and hence the above equation becomes less useful for the purpose of computations. This mathematical difficulty is overcome in the second approach where it is assumed that the backward movement of the dislocations is negligible. Eqn. (2.13), in effect, reduces to

$$\dot{\gamma}_p = \frac{d\gamma_p}{dt} = \alpha\, b\, \beta\, \gamma_p\, A_f' \exp\left(\frac{V_f(\tau t - H\gamma_p)}{kT}\right) \qquad (2.17)$$

in which the initial mobile dislocation density, ρ_o, is not accounted for, the effect of which will be introduced as follows.

Because the dislocation density is related to the strain by equation, $\rho_m = \beta\gamma_p$, when the condition $\rho_m = \rho_o$ is imposed, it becomes $\gamma_{po} = \rho_o/\beta$. Hence the condition that the mobile dislocations are initially present in the specimen is equivalent to specifying that the material of the specimen has been subjected to a pre-strain, of the magnitude γ_{po}.

Eqn. (2.17) can, therefore, be integrated as

$$\int_0^t \alpha\, b\, \beta\, A_f'\, \exp\left(\frac{V_f\, \dot{\tau} t}{kT}\right) dt = \int_{\gamma_{po}}^{\gamma_p} \frac{\exp\left(\frac{V_f\, H}{kT}\, \gamma_p\right)}{\gamma_p}\, d\gamma_p$$

Thus

$$\frac{\alpha\, b\, \beta\, A_f'\, kT}{\dot{\tau}\, V_f} \left[\exp\left(\frac{V_f\, \tau_a}{kT}\right) - 1\right]$$

$$= \ln\left(\frac{\gamma_p}{\gamma_{po}}\right) + \frac{V_f\, H}{kT}\, \frac{\gamma_p - \gamma_{po}}{1.1!} + \left(\frac{V_f\, H}{kT}\right)^2 \frac{\gamma_p^2 - \gamma_{po}^2}{2.2!} + \cdots$$

$$= \ln\left(\frac{\gamma_p}{\gamma_{po}}\right) + \sum_m \left(\frac{V_f\, H}{kT}\right)^m \frac{\gamma_p^m - \gamma_{po}^m}{m.m!}$$

which expresses stress as the following function of the strain

$$\tau_a = \frac{kT}{V_f} \ln\left[1 + \frac{\tau\, V_f}{\alpha\, b\, \beta\, kT\, A_f'} \left\{\ln\left(\frac{\gamma_p}{\gamma_{po}}\right) + \sum_m \left(\frac{V_f\, H}{kT}\right)^m \frac{\gamma_p^m - \gamma_{po}^m}{m.m!}\right\}\right] \quad (2.18)$$

This equation, due to the foregoing assumption, overestimates the dislocation velocity at high temperatures and low stresses. In the early stage of a tensile test, where the stress is small, the deformation behaviour is dominated by the elastic component of strain, and hence the error introduced in this range would be negligible. In the high stress and low temperature range, the backward movement of dislocations is small, therefore, this equation will be reasonably accurate.

Eqn. (2.18) can be utilized to study the effect on the yield behaviour by the following parameters

i) the initial density of mobile dislocations, ρ_o.

ii) the applied stress rate, $\dot{\tau}$.

iii) the dislocation multiplication rate, β.

and iv) the work-hardening rate, H.

2.5 Parametric Dependence of the Yield Behaviour

A. The Effect of Initial Mobile Dislocation Density

The number of dislocations initially present in the specimen was found (2,3) to have the greatest effect on the yield behaviour in constant strain rate tests. In constant stress rate conditions, the stress-strain curves obtained from Eqn. (2.18) exhibit an equally strong dependence on ρ_o, as shown in Fig. (2.26). The initial density has been varied in these calculations from 10^2 to 10^7 disl cm^{-2}, and the curves are shown displaced by the corresponding magnitude of the initial strain, γ_{po}. The figure illustrates that beyond the yield point, the various curves tend to merge with the one that corresponds to a minimum value of the initial mobile dislocation density.

B. The Effect of Stress Rate

Stress-strain curves were computed for a number of stress rates keeping all other parameters constant, and the results are shown in Fig. (2.27). The figure shows that the yield stress increases with the increasing rates of applied stress.

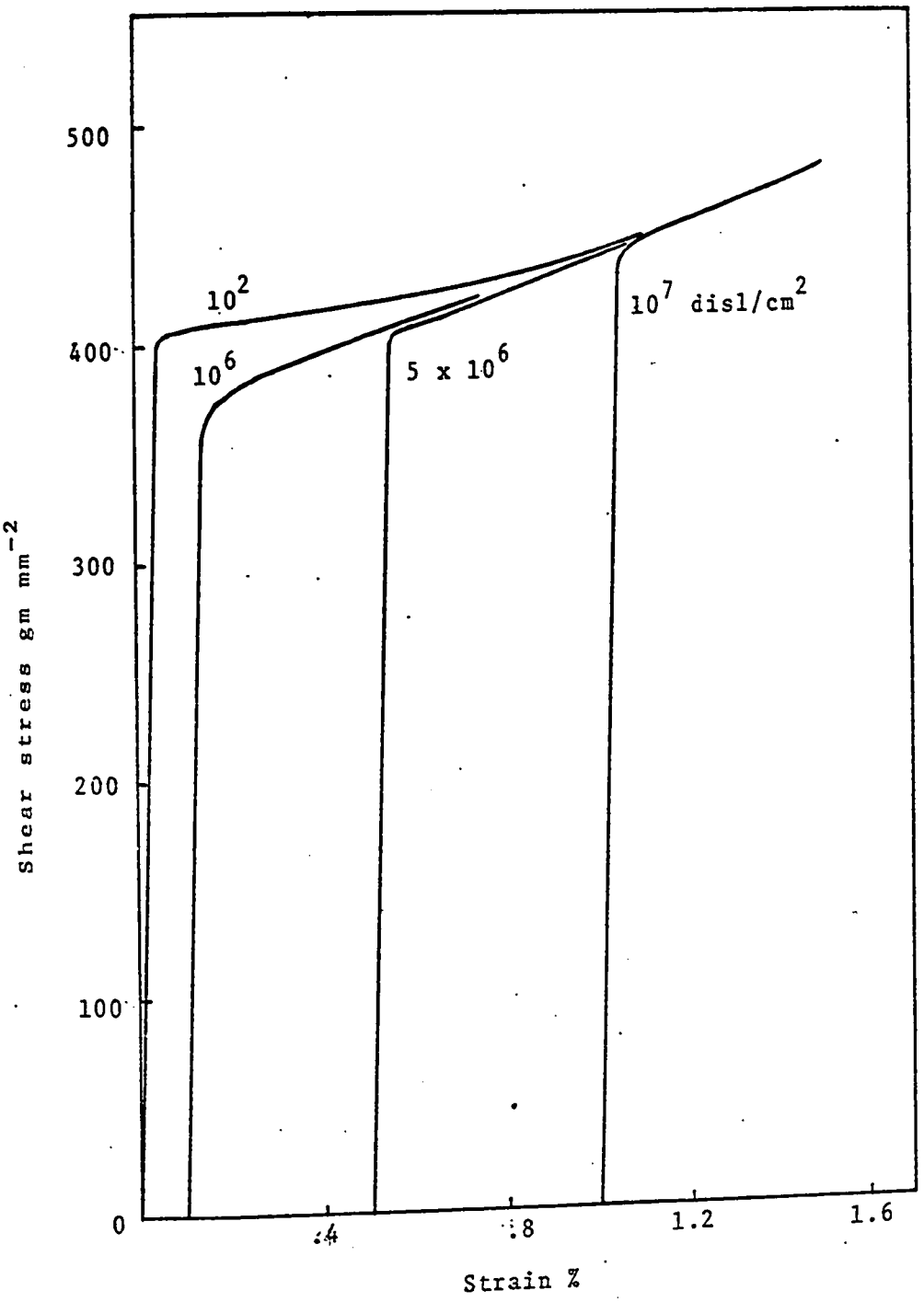

Fig. 2.26 The effect of the initial mobile dislocation density on the yield-point characteristics

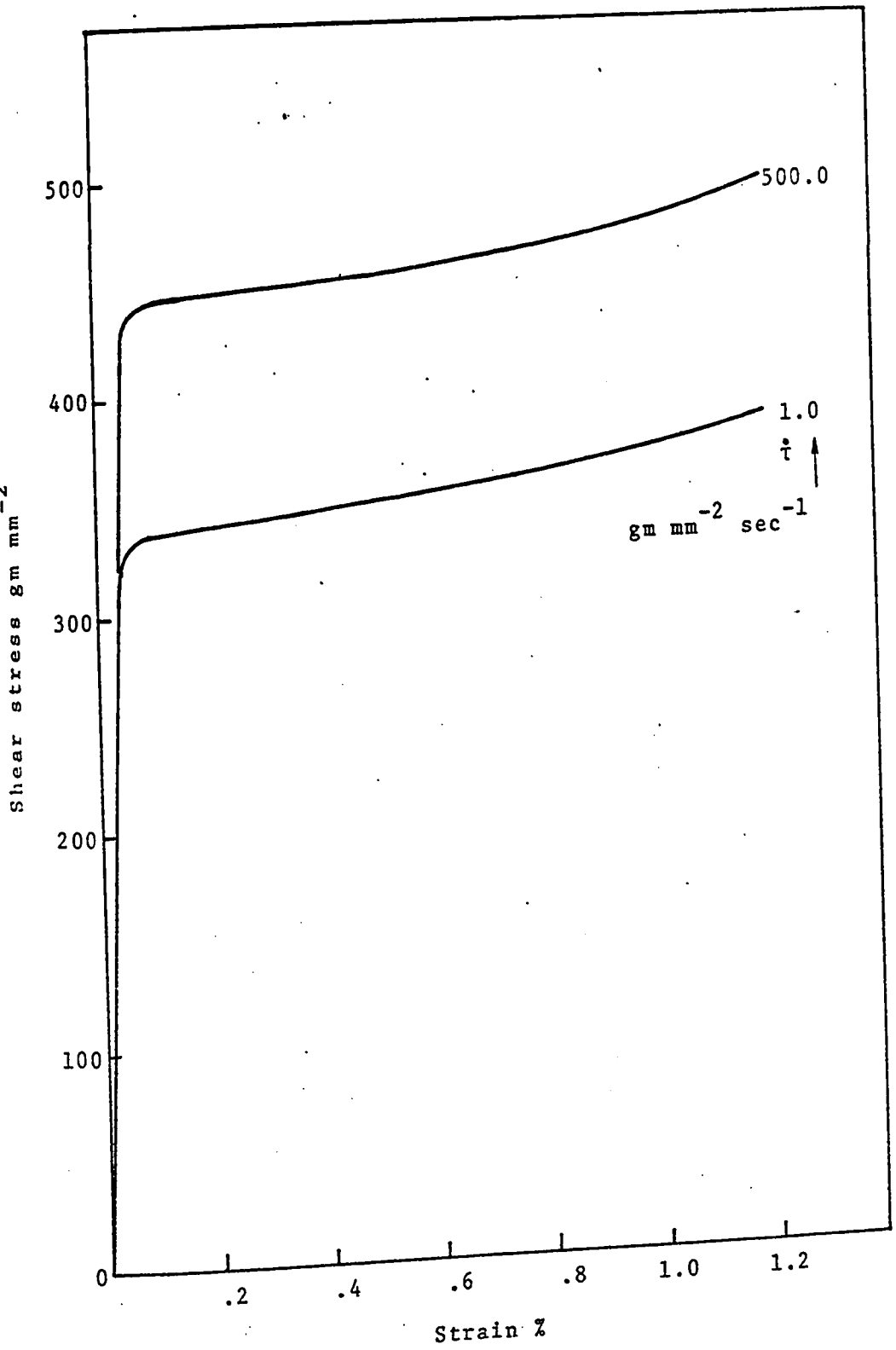

Fig. 2.27 The effect of the applied stress rate on the calculated stress-strain curves

At this stage, it should be mentioned that the creep tests are only a special case of constant stress rate tests where, theoretically, the applied rate of loading is zero. A typical set of creep curves, calculated from Eqn. (2.3), is plotted in Fig. (2.28) in which the strain and the time are represented along x and y axes respectively. The similarities between the curves in the above figures indicate that the constant stress rate tests could be correlated with the creep tests.

C. The Effect of Dislocation Multiplication Rate

The stress-strain curves shown in Fig. (2.29) were obtained from Eqn. (2.18) for two different values of the multiplication rates, β. The results show that the yield stress increases as β decreases.

This was the case when the dislocation density varies linearly with the strain. Some observations by Livingstone (40) indicate, however, that in copper the dislocation density is a quadratic function of the strain. Eqn. (2.13) when solved under these conditions, becomes

$$\tau_a = \frac{kT}{V_f} \ln \left[1 + \frac{\dot{\tau} V_f}{\alpha b \beta kT A_f'} \left[\frac{\exp\left(\frac{V_f H}{kT} \gamma_{po}\right)}{\gamma_{po}} - \frac{\exp\left(\frac{V_f H}{kT} \gamma_p\right)}{\gamma_p} + \frac{V_f H}{kT} \left\{ \ln \left(\frac{\gamma_p}{\gamma_{po}}\right) + \sum_m \left(\frac{V_f H}{kT}\right)^m \frac{\gamma_p^m - \gamma_{po}^m}{m.m!} \right\} \right] \right] \tag{2.19}$$

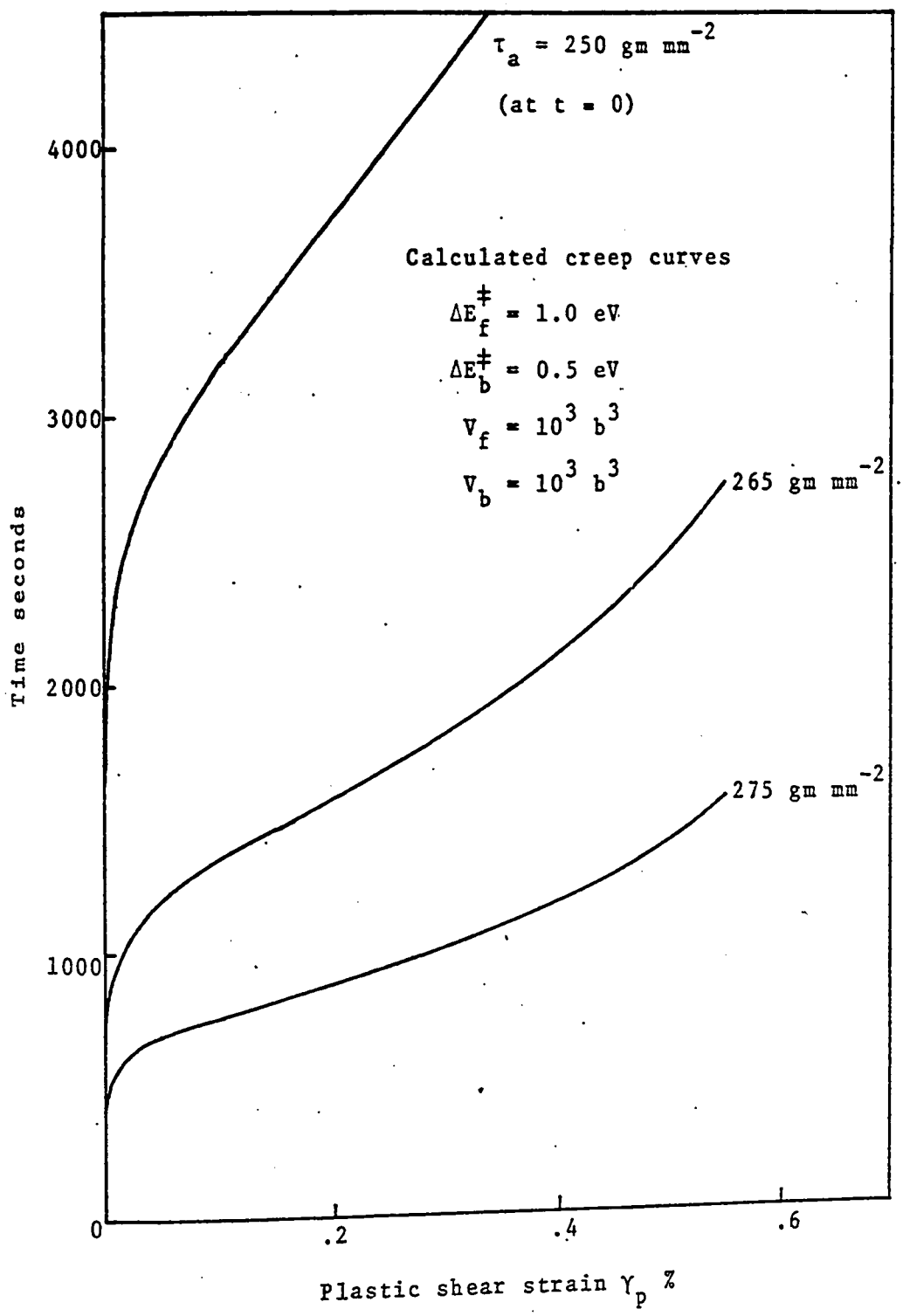

Fig. 2.28 Calculated creep curves plotted with its axes reversed than the usual ones

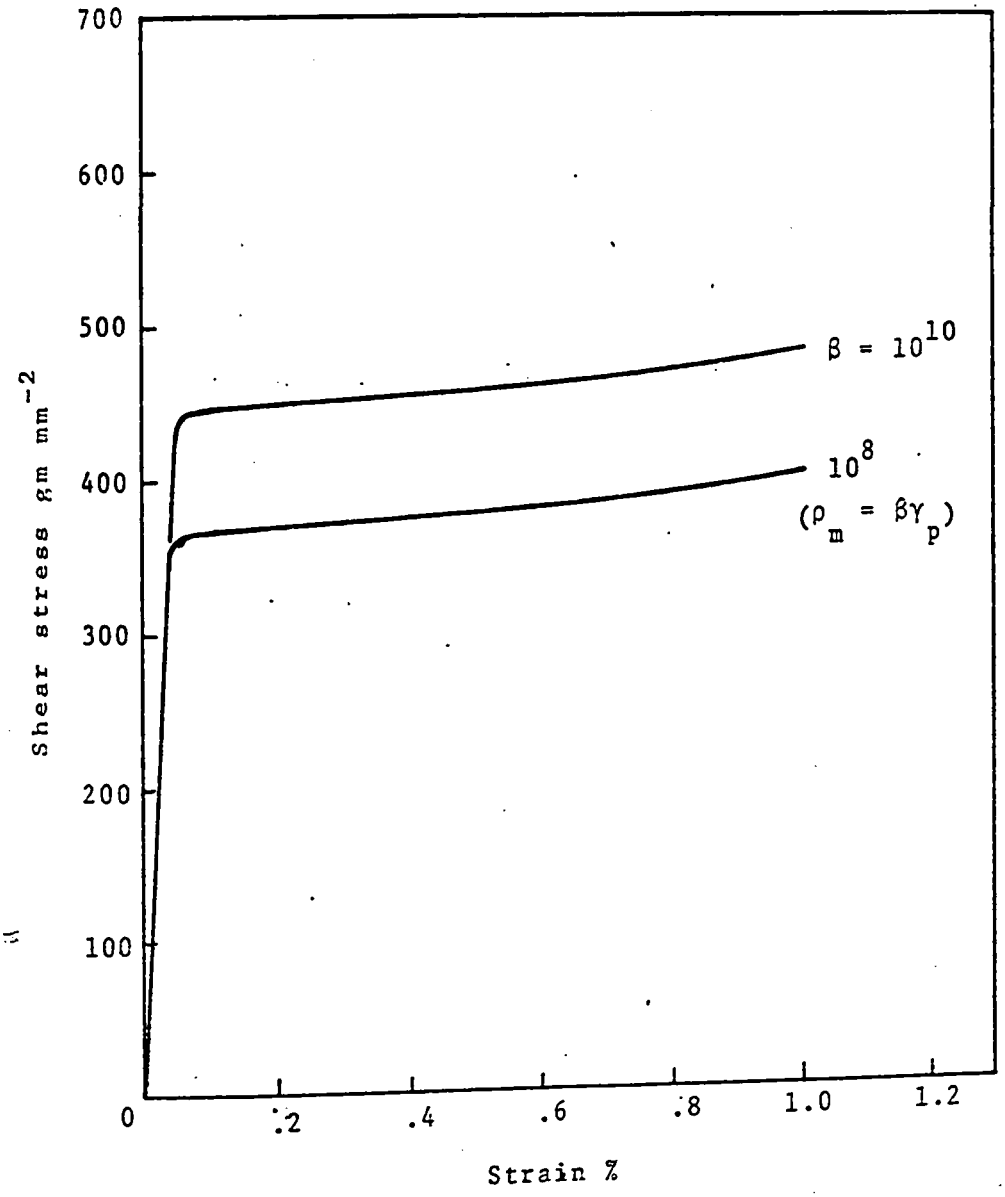

Fig. 2.29 The effect of the dislocation multiplication rate assuming that the dislocation density increases linearly with strain

The calculated behaviour for the linear as well as the quadratic dependences is shown in Fig. (2.30) where all other parameters were kept constant. The results show that the two curves have the same proportions, but the yield stress is higher when the dependence is quadratic than when it is linear.

D. The Effect of Work-Hardening Rate

The rate of deformation after yielding, indicated by the slope of a stress-strain curve in this region, depends on the work-hardening coefficient, H, as can be seen from Fig. (2.22). High work-hardening rates cause a considerable decrease in the deformation rate and the stress-strain curves ascend steeply as illustrated in Fig. (2.31). In the calculation of these curves, it is assumed that there are 10^2 disl cm^{-2} initially present in the specimen, and hence even at a high rate of work-hardening, there is a noticeable bend in the curve at the yield point. However, when ρ_o is also high, it is probable that such a bend will not result due to the slow rates of deformation.

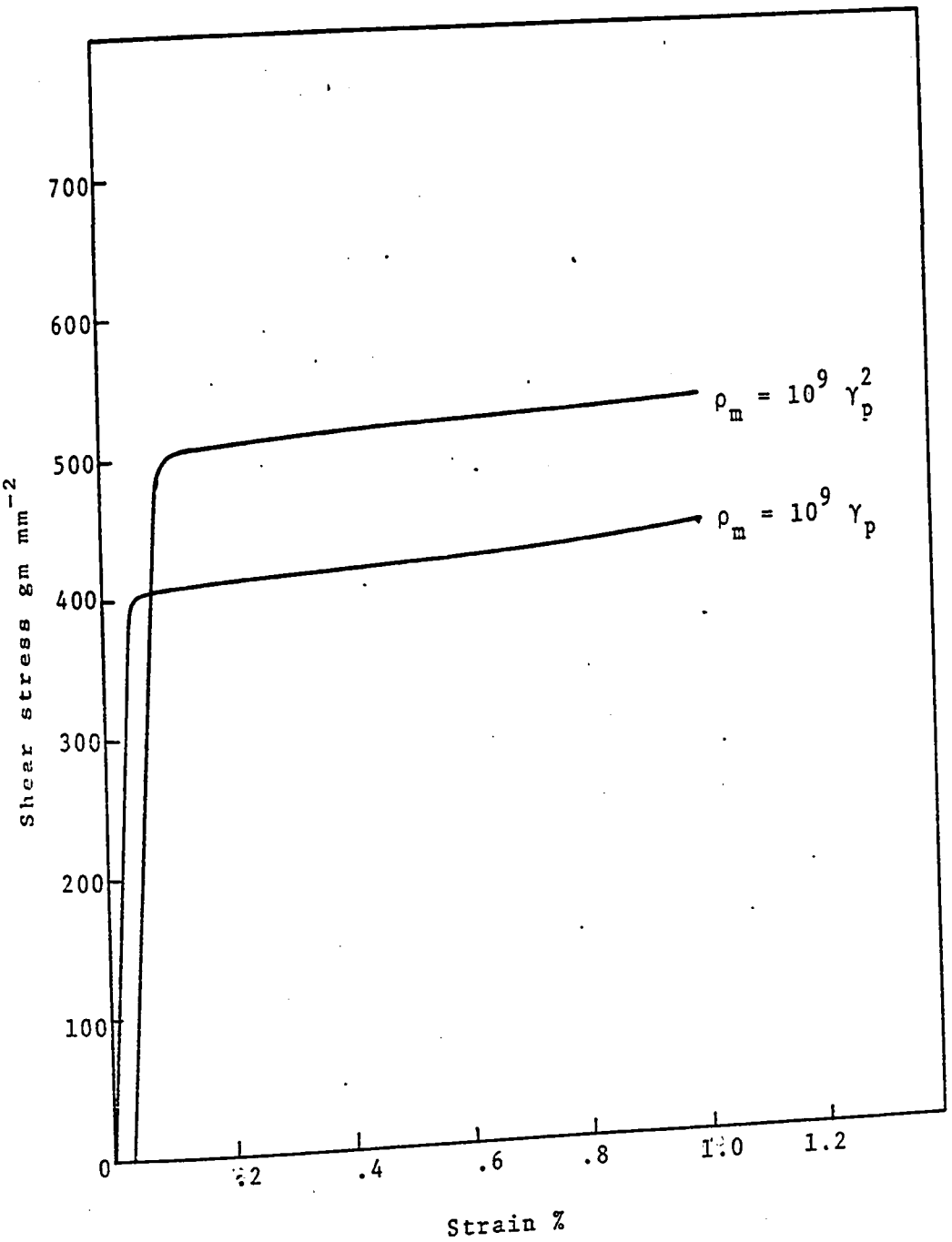

Fig. 2.30 Stress-strain curves calculated for a linear dependence and for a quadratic dependence of dislocation density on strain

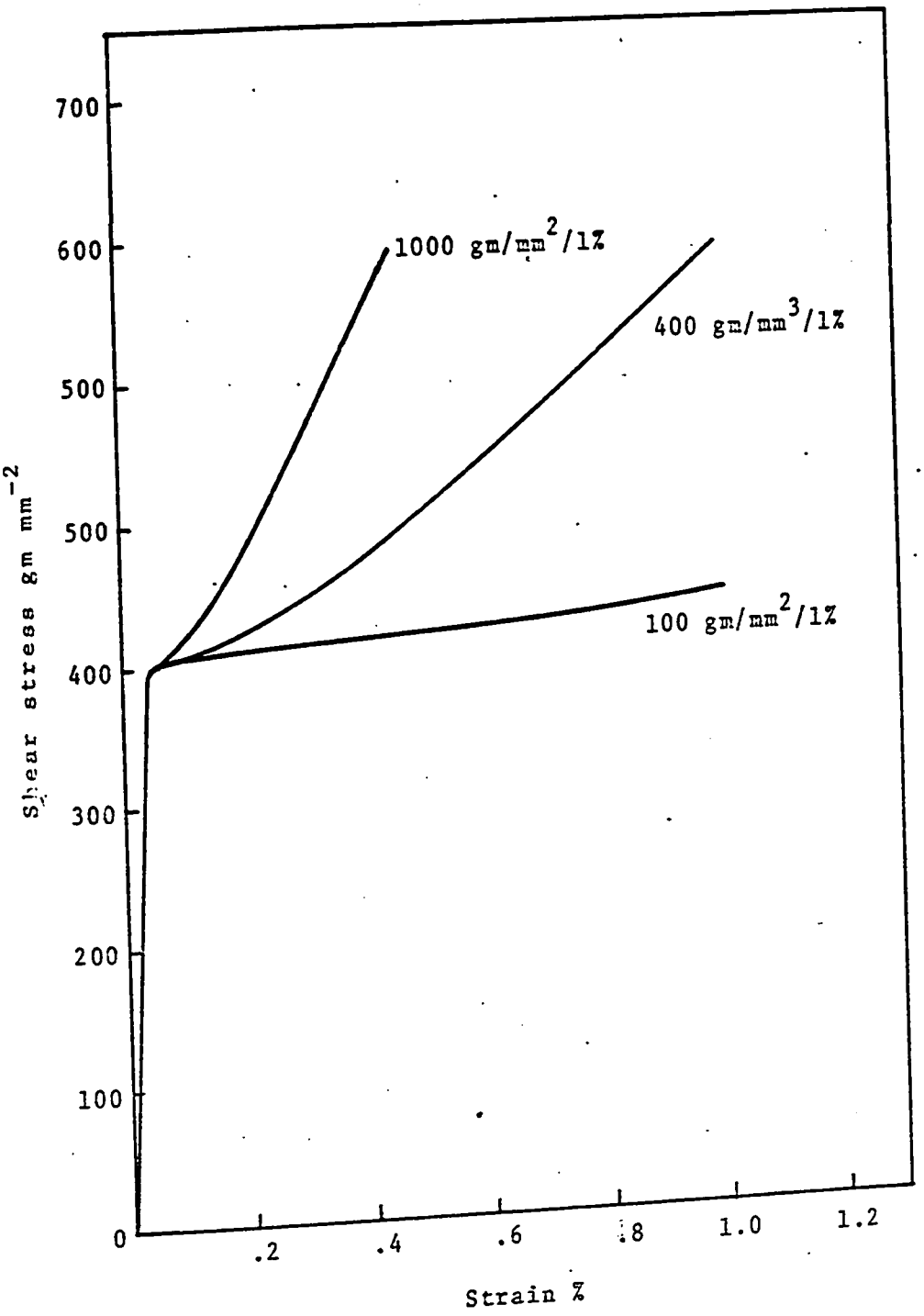

Fig. 2.31 Effect of the work-hardening rate on the calculated yield-point characteristics

CONCLUSIONS

The present investigation, utilizing a rigorous rate expression for the stress and the temperature dependence of dislocation velocity, provides a good understanding of the widely differing yield behaviour exhibited by various materials under the constant strain rate and the constant stress rate conditions. The following conclusions are drawn as a result of the foregoing analytical study.

A. Constant Strain Rate Analysis

1. The yield stress increases with increasing forward activation energy.
2. The yield stress is a sensitive function of the temperature when the forward activation volume is small and the temperature sensitivity is relatively weak at activation volumes greater than about $10^3\ b^3$.
3. The yield stress increases with a decrease in the backward activation parameters, $\Delta E_b^{\ddagger}$ and V_b.
4. The yield stress approaches a limiting value at absolute zero temperature.
5. The extent of rounding at the upper yield point is controlled by the amount of the yield drop.
6. The yield drop is maximum in the intermediate temperature range and vanishes both at very low and very high temperatures.
7. The symmetry of the energy barrier has a stronger effect on the yield drop than any of the other parameters. The yield drop is fully masked for a highly asymmetric barrier and becomes pronounced when it is symmetric.

B. Constant Stress Rate Analysis

1. The number of dislocations present initially in the specimen and the work-hardening rate, influence the shape of the stress-strain curves. Little difference is noticed when the applied stress rate and the dislocation multiplication rate are changed, or when the dependence of dislocation density on strain is assumed to be quadratic rather than linear.

2. The yield stress remains almost unaffected by the initial dislocation density and the work-hardening rate, but it increases when

   i) the applied stress rate is increased.

   ii) the dislocation multiplication rate is decreased.

   iii) the dependence of dislocation density on strain is quadratic rather than linear.

3. The constant stress rate test has definite advantages over other modes of testing, since

   i) it is independent of the machine characteristics.

   ii) the experimental set-up is simple.

   iii) its analysis leads to descriptions in the form of algebraic functions which greatly facilitates the computations.

APPENDIX

THERMALLY ACTIVATED DISLOCATION MECHANISMS

1. Peierls-Nabarro Mechanism (41)

In the periodic energy field of the crystal lattice, a dislocation line lies in the potential valleys between closed packed rows of atoms (Fig. 1). When the temperature is low or the interatomic binding energy is high, the motion of the dislocation is difficult even without other obstacles. Unless a straight dislocation in the energy valleys can move as a whole, which is energetically unfavourable, small dislocation segments have to be nucleated along the dislocation line. This is quite similar to the case of slip, in which a portion of a plane of atoms has to slip first, since a whole plane of atoms cannot slip all at once. A boundary is thus created between the slipped and unslipped areas, and as we now know, such a boundary is a dislocation. Continuation of slip then takes place by the motion of dislocations. Similarly, since a whole straight dislocation is not likely to move all at once, a portion of it has to move first, so that a junction is created between the moved and the unmoved segments. Such a junction is called a kink. Continuation of dislocation movement then takes place by the sideways motion of kinks. The nucleation of kink is the rate controlling step. Once the first kink is nucleated, the remainder of the

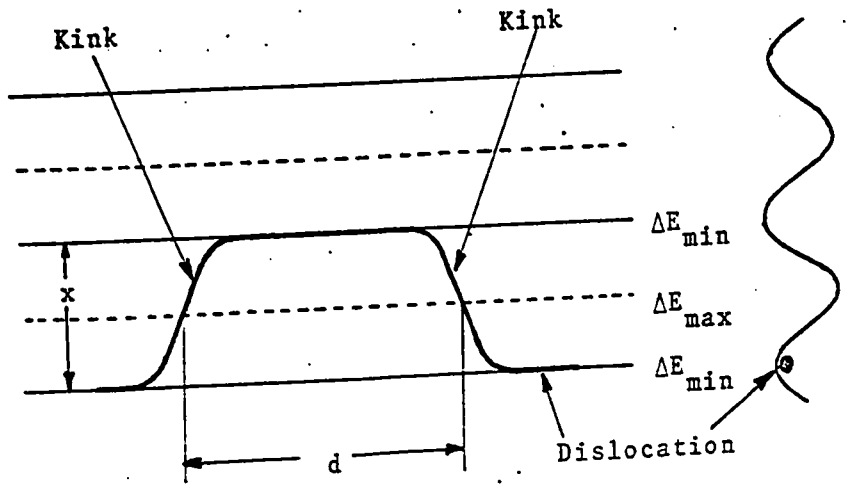

Fig. 1 Peierls-Nabarro mechanism for a dislocation to overcome the interatomic energy field

dislocation moves over the energy barriers as the kinks separate, under the influence of the applied stress and the line tension of the dislocation. The activation volume for the process would be about xbd where x is the distance between the equilibrium configurations and d is the separation of the two kinks (Fig. 1).

2. Cross Slip (42)

A dislocation in crystalline materials moves in specific directions and definite crystallographic planes; usually it is difficult for dislocation to leave the slip plane. Under certain conditions, however, a dislocation may find it easy to leave the original plane and move on another slip plane having a common slip direction. For example, in Fig. (2.a) consider two slip planes (111) and $(11\bar{1})$ having a line of intersection parallel to the slip direction $[\bar{1}10]$. A dislocation in one of these planes, if, has difficulty in slipping further it may surmount obstacles by gliding onto the second slip plane as shown in Fig. (2.b,c). In metals where there are many slip planes and slip directions, the phenomenon of cross slip occurs readily. The frequency of cross slip decreases as the temperature is lowered and therefore is a thermally activated process at normal temperature conditions. The activation volume is presumably about db^2 where d is the length of the dislocation anchored between two obstacles where the cross slip occurs (Fig. 2.c).

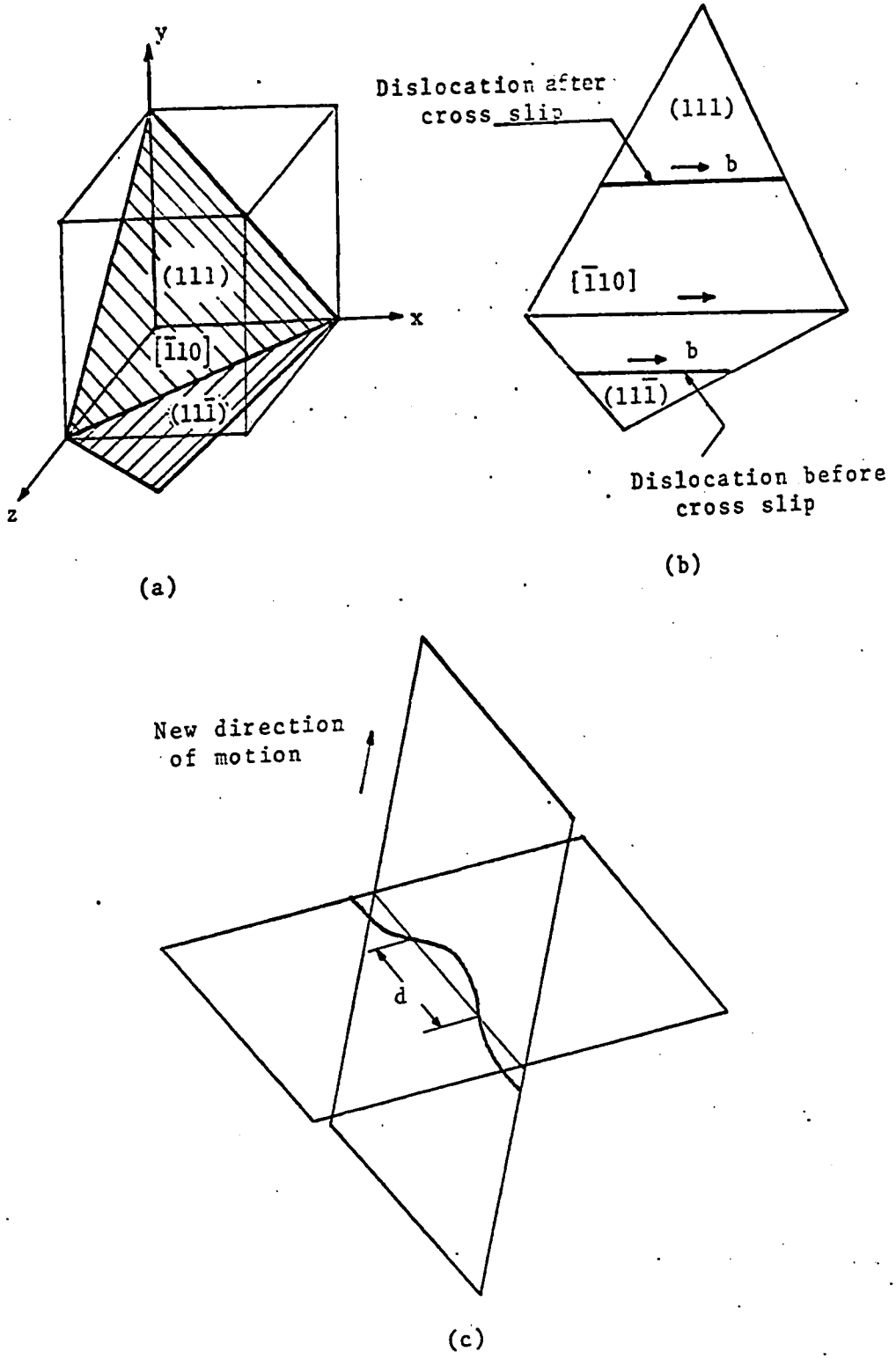

Fig. 2 The diagram illustrates the mechanism of cross slip

3. Intersection of Dislocations (43,35,44)

Barriers to a dislocation may arise when it encounters other dislocations intersecting the active slip plane. The dislocations threading through the active slip plane are often called forest dislocations. Fig. (3.a) illustrates the process of intersection of two dislocations. The intersection produces a jog, or an offset, in one of the dislocation lines. The phenomenon requires energy because the formation of a jog increases the length of a dislocation.

The intersection of forest dislocations by glide dislocations has been shown to be the rate controlling process in the low temperature deformation of several fcc metals (43, 44). The activation volume for the process is approximately given by xdb where x is the distance covered by the glide dislocation to overcome the barrier and d is the separation of forest dislocations (Fig. 3.b).

4. Climb (45)

If each of the atoms of a dislocation diffuses away or changes position with a vacancy, as shown in Fig. (4.a), the dislocation moves up by one atomic layer. The mechanism involved is called climb and is essentially a high temperature phenomenon. Movement of a dislocation in the downward direction can also occur if atoms are added to the dislocation, which creates vacancies, or, if interstitial atoms diffuse to the dislocation. A dislocation may thus 'upclimb' or

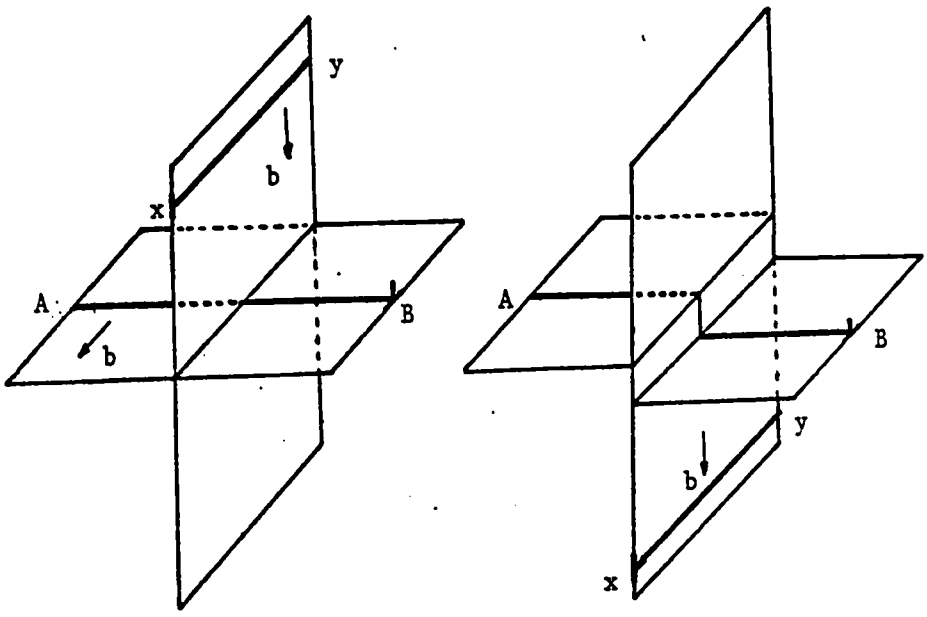

(a)

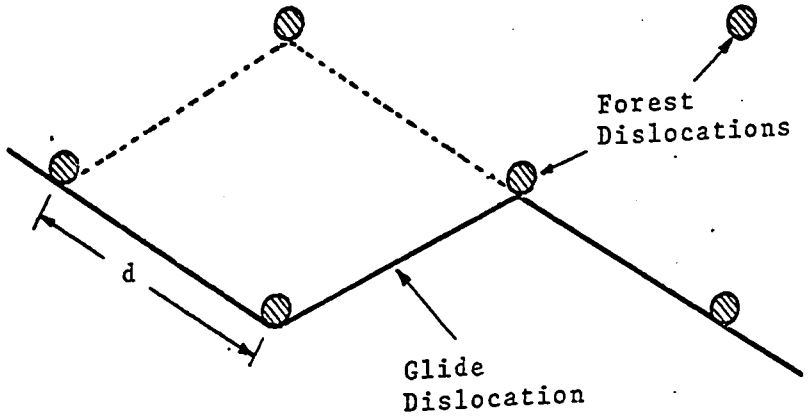

(b)

Fig. 3 Mechanism of intersection of forest dislocations by the glide dislocation

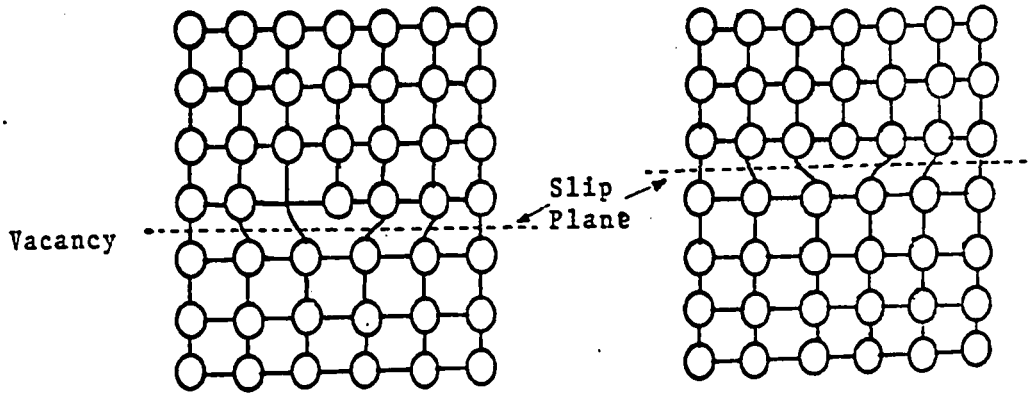

(a)

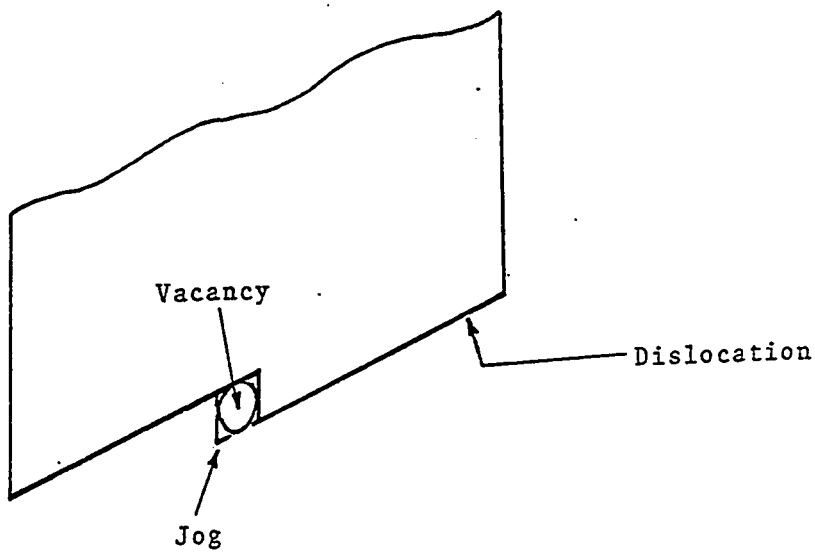

(b)

Fig. 4 Motion of the dislocation by climb

'downclimb' depending on the concentration of vacancies and interstitials in the crystal lattice. In either case the process involves mass transport by diffusion, and this motion of dislocation is referred to as a nonconservative motion.

Similarly to the motion of dislocation by forming a kink, if a dislocation cannot climb all at once, a small portion has to climb first. In consequence, a jog is created between the climbed and unclimbed segments of a dislocation (Fig. 4.b). Continuation of dislocation climb then takes place by the motion of jogs.

5. Non-conservative Motion of Jogs (42)

Jogs in dislocations may be produced by the intersection of dislocations, cross slip and climb. The difference between a kink and a jog is that a kink and its connecting segments lie in the same plane whereas the jog and its connecting segments lie in two or more slip planes. Under certain conditions, a jog and its two connecting segments can slip in their respective slip planes conservatively, but under other conditions the jog cannot slip with its segments. When the jog has to climb, the motion is nonconservative. To move a unit jog (one atom length) nonconservatively requires the energy needed to form and to move a vacancy. Point defects are thus created when jogs are forced to move along with the dislocation (Fig. 5). The applied stress causes the dislocation line to bow out between the jogs; the jogs then move forward under the action of the line tension of the dislocation

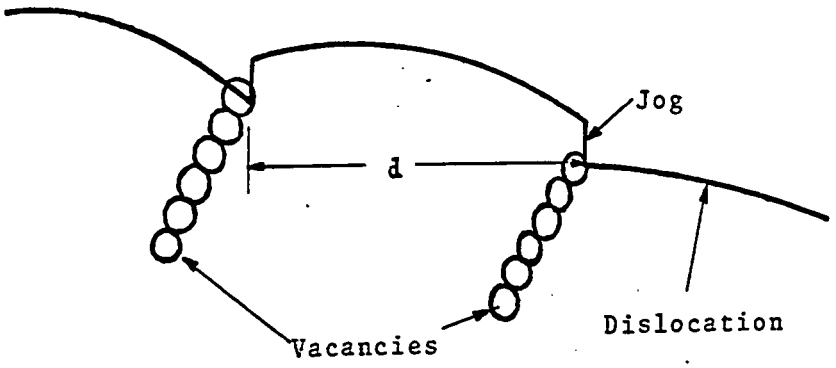

Fig. 5 Non-conservative motion of jogs

and create a point defect for every interatomic spacing moved. The activation volume will be about $d\ b^2$ where d is the distance between the jogs. The density of jogs would be expected to increase as a function of strain because of dislocation intersection.

TABLE 1 (46)

Typical Activation Volumes, V_f, for Various Mechanisms

Mechanism	Activation Volume, V_f
Overcoming of Peierls-Nabarro barrier	$10^1 - 10^2\ b^3$
Intersection of dislocations	$10^2 - 10^4\ b^3$
Non-conservative motion of jogs	$10^2 - 10^4\ b^3$
Cross slip	$10^1 - 10^2\ b^3$
Climb	$1\ b^3$

REFERENCES

1. W.G. Johnston and J.J. Gilman, J. Appl. Phys., 30, 129 (1959).
2. W.G. Johnston, J. Appl. Phys., 33, 2716 (1962).
3. G.T. Hahn, Acta Met., 10, 727 (1962).
4. A.H. Cottrell, Proc. Conf. Natn. Phys. Lab., Vol. 2, HMSO (1963).
5. J.J. Gilman and W.G. Johnston, Solid State Physics, edited by F. Seitz and D. Turnbull, Vol. 13, Academic Press (1962).
6. F.P.J. Rimrott, Engineering Journal, 14, 33 (1964).
7. A. Nadai, Theory of Flow and Fracture of Solids, McGraw-Hill (1951).
8. F.A. McClintock and A.S. Argon, Mechanical Behaviour of Materials, Addison-Wesley (1966).
9. E. Orowan, Proc. Phys. Soc., 52, 8 (1940).
10. D. Dew Hughes, IBM J. Research Development, 5, 279 (1961).
11. A.S. Krausz, Mater. Sci. Eng., 6, 260 (1970).
12. M. Berstein, Acta Met., 17, 249 (1969).
13. A.S. Krausz, Acta Met., 16, 897 (1968).
14. S. Glasstone, K.J. Laidler and H. Eyring, The Theory of Rate Processes, McGraw-Hill (1941).
15. T.L. Hill, An Introduction to Statistical Thermodynamics, Addison-Wesley (1960).

16. R.W. Rohde and C.H. Pitt, J. Appl. Phys., 33, 876 (1967).

17. H.G. Van Bueren, Imperfections in Crystals, North-Holland Publishing Company, Amsterdam (1960).

18. N. Krishna, M.A.Sc. Thesis, University of Ottawa, Ontario (1970).

19. A.S. Krausz, Mater. Sci. Eng., 4, 193 (1969).

20. S.J. Hahn, T. Ree and H. Eyring, Geol. Soc. Amer. Bull., 78, 773 (1967).

21. A.S. Krausz and H. Eyring, J. Appl. Phys., 42, 2382 (1971).

22. H. Eyring and G. Halsey, High Polymer Physics, edited by H.A. Robinson, Remsen Press Division (1948).

23. S. Katz, G. Halsey and H. Eyring, Textile Research J., 16, 382 (1946).

24. J.R. Patel and A.R. Chaudhuri, J. Appl. Phys., 33, 2736 (1962).

25. J.J. Gilman, Micromechanics of Flow in Solids, McGraw-Hill (1969).

26. G. Halsey, H.J. White and H. Eyring, Textile Research J., 15, 295 (1945).

27. R.E. Smallman, Modern Physical Metallurgy, Butterworths (1970).

28. P.J. Worthington, Acta Met., 15, 1795 (1967).

29. C.A. Pampillo and A.E. Vidoz, Acta Met., 14, 313 (1966).

30. J.B. Lean, Aust. J. Phys., 13, 359 (1960).

31. J. Heslop and N.J. Petch, Phil. Mag., 1, 866 (1956).

32. E. Orowan, Z. Physik, 89, 612 (1934).

33. J.R. Patel, Discuss. Faraday Soc., 38, 201 (1964).

34. K. Lucke and H. Lange, Z. Metallkunde, 43, 55 (1952).

35. A. Seeger, Dislocations and Mechanical Properties of Crystals, Wiley (1957).

36. J.G. Byrne, M.E. Fine and A. Kelly, Phil. Mag., 6, 1119 (1961).

37. H. Conrad, Proc. Conf. Nat. Phys. Lab., Vol. 2, HMSO (1963).

38. N.F. Mott, Trans. Metall. Soc., AIME, 218, 962 (1960).

39. J.A. Pask and S.M. Copley, Modern Ceramics, edited by J.E. Hove and W.C. Riley, Wiley (1965).

40. J.D. Livingstone, Acta Met., 10, 229 (1962).

41. J.E. Dorn and S. Rajnak, Trans. AIME, 230, 1052 (1964).

42. J. Friedel, Dislocations, Addison-Wesley, Mass. (1964).

43. J.S. Basinski, Phil. Mag., 4, 393 (1959).

44. S.K. Mitra, P.W. Osborne and J.E. Dorn, Trans. AIME, 221, 1206 (1961).

45. N.F. Mott, Phil. Mag., 43, 1151 (1952).

46. H. Conrad, J. Metals, 16, 582 (1964).